



TECHNISCHE  
UNIVERSITÄT  
WIEN

Vienna University of Technology

## Diplomarbeit

# **Pour Point Measurements and Thermal History of Crude Oils**

ausgeführt am  
Institut für Angewandte Physik  
Der Technischen Universität Wien

unter Anleitung von  
**Ao. Univ. Prof. Dr. Martin Gröschl**

durch  
**Martin Vietauer**  
Matr. Nr. 0425305

Wien, Mai 2011

---

(Martin Vietauer)

# **Affidavit**

Herewith I declare in the lieu of oath that this thesis is entirely of my own work using only literature cited at the end of this volume.

---

(Martin Vietauer)

Vienna, May 2011

# Kurzfassung

In dieser Diplomarbeit wurde der Einfluss der "thermischen Vorgeschichte" von Rohölen auf deren Pour Point (Stockpunkt) erforscht. Mit thermischer Vorgeschichte (thermal history) ist die Fähigkeit von Rohöl gemeint, sich an die thermische Vorbehandlung zu "erinnern", was das Heizen auf verschiedene Temperaturen für unterschiedliche Zeiten und die Verwendung diverser Kühlraten zur Pour Point Bestimmung beinhaltet. Die Pour Points wurden mit einem automatischen Pour Point Tester gemessen. Während Kristallisationsprozesse, die Kristallmenge und die Kristallform mit einem Transmissionsmikroskop, welches auch einen Polarisationsfilter für Messungen mit gekreuzter Polarisation hat, bestimmt wurden. Zusätzlich wurde die Kristallstruktur mit einem Rasterelektronenmikroskop beobachtet.

Die Behandlung der Rohöle vor den Pour Point Messungen umfasste das Heizen auf Temperaturen zwischen 25 °C und 85 °C. Für die Mikroskopmessungen wurden nur Proben ohne Vorbehandlung und mit zwei verschiedenen Vorheiztemperaturen vorbereitet, welche 55 °C und 85 °C waren.

Die Pour Point Messungen von Rohölen mit verschiedenen Kühlraten durch einen Pour Point Tester sind nicht möglich. Deshalb wurde in dieser Arbeit eine Methode entwickelt, um den Pour Point mit einem Rheometer zu messen, somit können auch Pour Points mit unterschiedlicher Kühlrate gemessen werden.

Um den Pour Point eines Rohöls zu bestimmen, müssen Oszillationsversuche durchgeführt werden, weil Rohöle an ihrem Pour Point als viskoelastische Feststoffe angesehen werden können und sich deshalb nicht wie Newton'sche Flüssigkeiten verhalten. Trotz dieser Bezeichnung, ist ein Fließen an deren Pour Point aufgrund des scherverdünnenden Verhaltens unterhalb der Wachsbildungstemperatur (Wax Appearance Temperature), immer noch möglich, wenn eine ausreichend hohe Scherspannung anliegt. Das bedeutet in dem für Pour Point Messungen interessantem Bereich sind viele Kristalle in der Rohölprobe vorhanden, weshalb ein Platte-Platte Messsystem für das Rheometer verwendet wurde.

Durch Berücksichtigung der Erkenntnisse dieser Diplomarbeit in Feldanwendungen, könnte sich ein beachtliches Einsparungspotential ergeben, beispielsweise durch die reduzierten Wartungsarbeiten in Pipelines oder Öltanks aufgrund der geringeren Paraffinablagerungen.

# Abstract

In this thesis the influence of thermal history on the pour point and the crystal structure of crude oils is investigated. Thermal history refers to the ability of crude oils to "remember" their thermal treatment, which includes heating to different temperatures for various times and the use of diverse cooling rates for the pour point determination. The pour points were measured with an automatic pour point tester, while the crystallization processes, the amount of crystals and the crystal shapes were determined with a transmission microscope which also has a polarization filter for crossed polar measurements. Additionally the crystal structure was observed with a scanning electron microscope.

The treatment of the crude oils before the pour point measurements involved heating to temperatures between 25 °C and 85 °C. For the microscope experiments only samples without pretreatment and with two different pretreatment temperatures were prepared, they were 55 °C and 85 °C.

The measurement of the pour point of crude oils with different cooling rates is not possible using the pour point tester. Therefore a method to measure pour points with a rheometer was developed in this work with which pour points at various cooling rates can be measured.

To measure a pour point of a crude oil, oscillation tests have to be performed since crude oils can be considered as viscoelastic solids in the temperature range around the pour point and hence do not behave as Newtonian fluids. Even though they can flow at their pour point if a high enough shear stress is applied because of the shear thinning behavior of crude oils under their WAT (wax appearance temperature). That means in the area which is interesting for pour point measurements a lot of crystals have formed in the crude oil sample, therefore a plate-plate measuring system was used for the rheometer.

The findings of this thesis can help to save a lot of money due to the reduction of maintenance jobs, e.g. in pipelines and storage tanks, if they are taken into account at field applications.

# Table of contents

Affidavit .....	2
Kurzfassung .....	3
Abstract .....	4
<b>1 Introduction.....</b>	<b>8</b>
<b>2 Composition of Crude Oils .....</b>	<b>10</b>
2.1 Saturated Hydrocarbons .....	10
2.1.1 Alkanes or Paraffins .....	10
2.1.2 Cycloalkanes or Naphthenes.....	11
2.2 Unsaturated Hydrocarbons .....	11
2.2.1 Aromatic Hydrocarbons .....	11
2.3 Characterization of Paraffin Wax .....	12
2.3.1 System according to van Nes & van Westen, 1951.....	12
2.3.2 System according to Tissot & Welte, 1984 .....	12
<b>3 Crystallization of Paraffin in Crude Oils .....</b>	<b>14</b>
3.1 Wax Appearance Temperature (WAT) .....	14
3.1.1 Cross Polarized Microscopy (CPM).....	14
3.1.2 Differential Scanning Calorimetry (DSC) .....	15
3.1.3 Solid Detection System (SDS).....	17
3.1.4 Near-Infrared (NIR) Scattering .....	18
3.1.5 Filter Plugging .....	19
3.1.6 Viscometry .....	20
3.2 Wax Crystallization Mechanisms .....	22
3.2.1 Nucleation .....	22
3.2.2 Crystal Growth.....	26
3.2.3 Agglomeration .....	27
3.3 Factors Influencing Wax Precipitation.....	28
3.3.1 Flow Rate and Surface Properties of Tubes.....	28
3.3.2 Oil Composition .....	29
3.3.3 Pressure .....	29
3.3.4 Temperature Difference and Cooling Rate .....	30
<b>4 Pour Point of Crude Oils.....</b>	<b>33</b>
4.1 Methods to determine the Pour Point .....	33
4.1.1 Manual (Tilt) Method – ASTM D 5853 .....	33
4.1.2 Automatic (Rotational) Method – ASTM D 5985.....	35
<b>5 Thermal History of Crude Oils.....</b>	<b>37</b>
5.1 Influence of Temperature on Wax Precipitation .....	37
5.2 Influence of Cooling Rate on Wax Structure .....	38
<b>6 Problems due to Wax Dissipation.....</b>	<b>40</b>
6.1 Formation Damages .....	40
6.2 Paraffin Deposition in Storage Tanks .....	41

6.3	Pressure Losses .....	41
<b>7</b>	<b>Methods of Wax Reduction/Removing .....</b>	<b>43</b>
7.1	Chemical Methods .....	43
7.1.1	Pour Point Depressants .....	43
7.1.2	Wax Dispersants .....	44
7.1.3	Paraffin Solvents .....	45
7.2	Electromagnetic and Magnetic Methods .....	45
7.3	Mechanical Methods .....	46
7.3.1	Pigging .....	46
7.3.2	Scraping .....	47
7.4	Microbial Methods.....	48
7.5	Thermal Methods.....	48
7.5.1	Hot Oiling .....	48
7.5.2	Downhole Heater.....	49
7.5.3	Thermal Insulation.....	50
7.6	Thermochemical Methods.....	50
7.7	Ultrasonic Waves.....	51
<b>8</b>	<b>Rheology Fundamentals .....</b>	<b>53</b>
8.1	Viscosity.....	53
8.1.1	Two Plates Model.....	53
8.1.2	Newtonian Fluids.....	54
8.1.3	Non-Newtonian Fluids .....	55
8.2	Rheological Models .....	56
8.2.1	Ideal Viscous Behavior .....	56
8.2.2	Ideal Elastic Behavior .....	57
8.2.3	Viscoelastic Behavior .....	58
8.3	Rheometers .....	60
8.3.1	Rheometer Measurement Systems .....	60
8.3.2	Rotational Tests .....	62
8.3.3	Oscillation Tests .....	62
<b>9</b>	<b>Thermal History Experiments.....</b>	<b>67</b>
9.1	Pour Point Measurements .....	67
9.1.1	Experimental Setup/ The Pour Point Tester (PPT).....	67
9.1.2	Different Heat Pretreatment/PPT Starting Temperatures .....	70
9.1.3	Thermal History Measurements of 4 Crude Oils.....	73
9.2	Microscopical Measurements .....	81
9.2.1	Transmission Microscope (TM)/CPM .....	81
9.2.2	Scanning Electron Microscope (SEM).....	86
9.2.3	Comparison between TM and SEM Pictures.....	89
<b>10</b>	<b>Influence of Cooling Rates on the PP .....</b>	<b>92</b>
10.1	Experimental Setup .....	92
10.1.1	Selection of the Measuring Method/System .....	92
10.2	Oscillation Tests .....	93
10.2.1	Selection of the Proper Parameters .....	93
10.2.2	Pour Point Measurements.....	94

<b>11 Conclusion and Recommendations</b> .....	<b>100</b>
<b>12 Future Prospects</b> .....	<b>102</b>
<b>Nomenclature</b> .....	<b>103</b>
<b>Glossary</b> .....	<b>105</b>
<b>List of Figures</b> .....	<b>106</b>
<b>References</b> .....	<b>110</b>
<b>Acknowledgements</b> .....	<b>113</b>
<b>Appendix</b> .....	<b>114</b>
A1 Results of the Thermal History Measurements .....	114
A2 Transmission Microscope Photographs .....	119
A3 Scanning Electron Microscope Pictures .....	122
A4 Gas Chromatography Diagrams .....	125
A5 Data Sheet Rheometer .....	127
A6 Data Sheet Measuring System PP50 .....	128

# 1 Introduction

The problem of paraffin wax depositions is present in every branch of oil industry. Wax depositions can cause high costs in form of losses of production, shutdowns of wells and pipelines and even damage of used equipment.

Paraffin crystallization is followed by wax precipitation which first occurs when the reservoir conditions of crude oils change, the most common reasons for such changes are reduced temperatures and reduced pressures during production. This can already happen downhole in the wellbore where the wax can plug the pores of the formation and the perforations of the tubing. The precipitated wax affects every piece of equipment the crude oils pass on their way to the refinery, this includes tubings, pumps, pipelines, storage tanks etc.

There are two very important temperatures which are used to classify oils and if they are known, they can help to take the necessary precautions early enough to save resources and prevent equipment from damage. These temperatures are the wax appearance temperature (WAT) and the pour point. Wax problems always occur when the temperature of the crude oils drops below the WAT. The pour point tells at which temperature a crude oil stops to flow and solidifies, hence this value is of great interest for offshore production and wells in colder regions where the temperature often drops below 0 °C.

Therefore the OMV, with whose aid this work was done, has started a project with the goal to gain better understanding of paraffin crystallization processes which are highly dependent on the thermal pretreatment of the crude oils and consequently lead to big variations in the pour point due to different thermal pretreatment.



# I Theoretical Part

## 2 Composition of Crude Oils

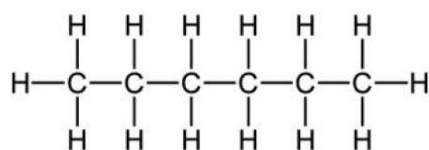
Crude oils are basically mixtures of hydrocarbons, nitrogen, sulfur, oxygen, resins, asphaltenes and metallic components in very small amounts. A bigger part of the nitrogen, sulfur and oxygen are bound to resins and asphaltenes. Therefore, they are called polar NSO-compounds. But usually the biggest and hence the most important part consists of hydrocarbons, which mainly belong to three groups, the alkanes, the cycloalkanes and the aromatic hydrocarbons. The first two of these three groups are saturated hydrocarbons, which means they are single bonded. Unsaturated hydrocarbons have one or more double (alkenes) or triple (alkynes, acetylenes) bonds between the carbon atoms. Molecules with cyclic multiple unsaturated bonds are mostly aromatic hydrocarbons [1] [2] [3].

### 2.1 Saturated Hydrocarbons

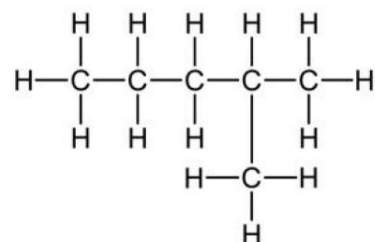
#### 2.1.1 Alkanes or Paraffins

These so-called acyclic alkanes are classified in normal (n) and branched (iso) alkanes. Normal alkanes are mostly prevalent and can reach lengths up to  $C_{40}$  and more. The main part normally is around  $C_6$ - $C_8$  but decreases above  $C_{10}$ . Branched alkanes have usually about the same carbon chain length as normal alkanes. They consist of a long carbon chain and hydrogen atoms which are linked to this backbone, see Fig. 2.1. Therefore the general formula for alkanes is  $C_nH_{2n+2}$  [1] [2] [3].

Because of the saturated bonding, reactions can only take place after cracking of carbon-carbon or carbon-hydrogen bonds. This is also indicated with the term paraffin<sup>1</sup>, the former name for alkane (lat. parum = little and affinis = willing) [2] [3].



n-Hexane  
(n-paraffins)



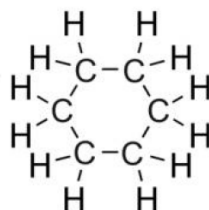
Isohexane  
(isoparaffins)

Fig. 2.1: Structure formulas of examples of alkanes [4]

<sup>1</sup> According to popular literature alkane will be referred to as paraffin from here.

### 2.1.2 Cycloalkanes or Naphthenes

Cycloalkanes are saturated cyclic hydrocarbons which consist of at least one ring containing solely carbon atoms. This leads to the common formula  $C_nH_{2n}$ . Cycloalkanes with one or more rings generally exist in crude oils, but their occurrence decreases with the number of the rings. Like the alkanes, the cycloalkanes show a very low reactivity and can thus be used as solvents. In nature only cyclopentan-, -hexan and -heptan are found in crude oils [1] [2] [3].



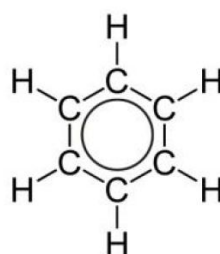
Cyclohexane  
(naphthenes)

Fig. 2.2: Structure formula of a cycloalkane [4]

## 2.2 Unsaturated Hydrocarbons

### 2.2.1 Aromatic Hydrocarbons

Originally aromatic compounds were known as fragrant (lat.: aroma = fragrancy) substances. The most common aromatic hydrocarbon is benzene, it has six carbon atoms located in a hexagonal circle and six hydrogen atoms, which means its formula is  $C_6H_6$ . Since every carbon atom has four electrons to share the remaining six electrons (one from each carbon atom) are delocalized between the carbon atoms, which is illustrated with the circle in Fig. 2.3 [2] [3].



Benzene  
(aromatics)

Fig. 2.3: Structure formula of an aromatic hydrocarbon [4]

## 2.3 Characterization of Paraffin Wax

One of the oldest and even today widely-used systems to categorize crude oil is the compound type system. There exist two different approaches to this system.

### 2.3.1 System according to van Nes & van Westen, 1951

The goal of this system is the differentiation of oil either on a paraffin or an asphalt basis, because some oils use to precipitate paraffin waxes during cooling and others do not.

Paraffin precipitates out of paraffinic part of the crude oil under normal circumstances, while asphaltene deposits from the naphthenic fraction of the crude oil. The main fractions for crude oils are displayed in Fig. 2.4. This diagram shows that also mixed base crude oils exist [5].

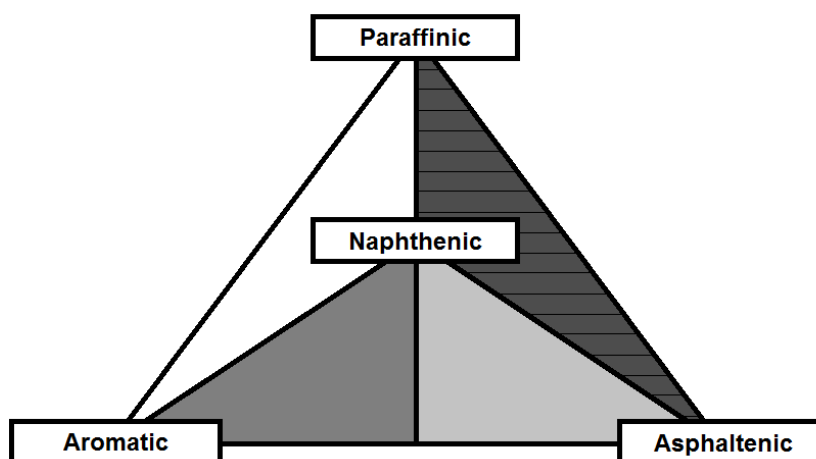


Fig. 2.4: Composition Diagram for Crude Oils (facsimile) [5]

### 2.3.2 System according to Tissot & Welte, 1984

This system classifies crude oils on the basis of relative fractions of acyclic alkanes, cycloalkanes and combined aromatic hydrocarbons plus NSO-compounds. The triangle-diagram of this classification is illustrated in Fig. 2.5.

Resulting from this it is possible to differentiate between the following main classes of crude oils: [1]

- a) paraffinic oils, containing mostly acyclic alkanes with  $< 1\%$  S
- b) paraffinic-naphthenic oils, containing mostly acyclic alkanes and cycloalkanes with  $< 1\%$  S
- c) aromatic-intermediate oils, with  $> 50\%$  aromatic hydrocarbons and typically  $> 1\%$  S

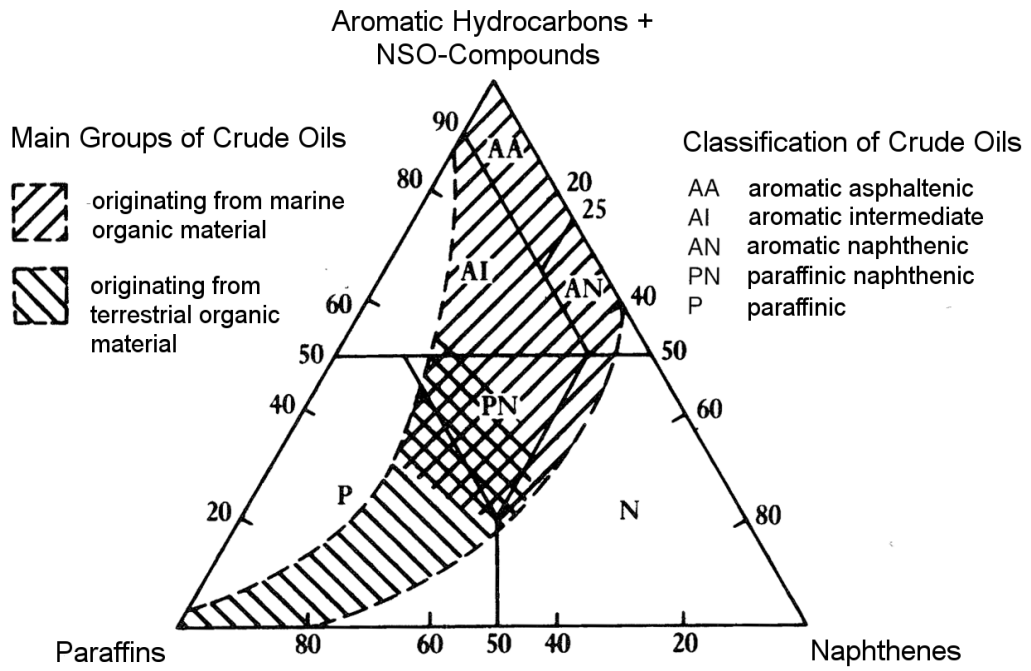


Fig. 2.5: Classification scheme of crude oils (facsimile) [1]

## 3 Crystallization of Paraffin in Crude Oils

The main constituents of macrocrystalline waxes are n-paraffins, they form clearly defined needle-shaped crystals. The branched-chain paraffins on the other hand make up the major part of the microcrystalline waxes. The long, straight-chain naphthenic and aromatic paraffins add to the microcrystalline waxes as well. The solubility of paraffin waxes is very sensitive to temperature changes. That means temperature variability affects wax crystallization. Paraffin waxes remain as soluble constituents of crude oils under most reservoir conditions under a state of equilibrium. When the equilibrium is disturbed by such factors as change in temperature or pressure, paraffin may crystallize and hence precipitate. Volatile light ends act as naturally occurring solvents, therefore paraffin can also precipitate due to loss of these volatile light ends. The waxes formed from alkane hydrocarbons have carbon atom numbers from  $C_{18}$  to  $C_{36}$  and those formed from naphthenic hydrocarbons have carbon atom numbers from  $C_{30}$  to  $C_{60}$  [6] [7].

### 3.1 Wax Appearance Temperature (WAT)

Wax constituents in a waxy crude oil start to separate from the liquid phase and hence begin to crystallize visible, if the crude oil is cooled under the wax appearance temperature (WAT) or wax precipitation temperature (WPT), traditionally known as "cloud point". That means below this temperature, deposition problems are likely to arise [8] [9]. The true WAT is defined as the temperature at which the first crystal of paraffin is formed in a fluid. Unfortunately the true WAT is probably not accessible experimentally and alone wouldn't be a good indication of the hazardous potential of crude oils anyway.

There are several methods available to determine the WAT and it is known that each measuring technique will provide a different WAT. The simplest way to observe wax crystals is to use a common microscope, but this method can only be applied to transparent oils. For dark oils more complex methods have to be used. Anyhow, some of these techniques seem to be more accurate than others [10]. Several of these measuring methods are described below.

#### 3.1.1 Cross Polarized Microscopy (CPM)

The functional principle of the CPM is to illuminate the specimen from below with polarized light and the plane of polarization of the transmitted light is rotated by wax crystals contrary to liquid hydrocarbons, because crystalline materials with noncubic geometry are optically anisotropic. To use this characteristic of paraffin wax the light source is combined with an IR-filter and a polarizer underneath the temperature controlled hot stage which contains the specimen. Above the hot stage are an analyzer and a video camera, for a schematic drawing see Fig. 3.1. To determine the WAT the

sample is heated so that all crystals are melted. Hence the crude oil has to be cooled to measure the WAT.

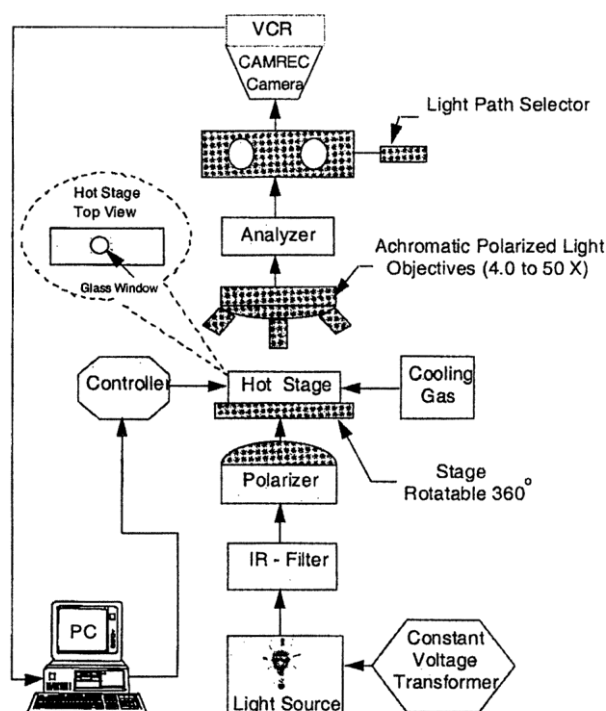


Fig. 3.1: CPM schematic drawing [11]

As long as no crystals have formed, the analyzer absorbs the polarized light, because the direction of polarization is orthogonal to the polarization of the analyzer. But due to the cooling, wax crystals appear and rotate the plane of polarization, thus the paraffin wax can be seen as bright spots in the previous black field, because the light with the rotated direction of polarization is transmitted through the analyzer. With this method crystals of a size from 0.5 to 1  $\mu\text{m}$  can be detected [9] [10] [11].

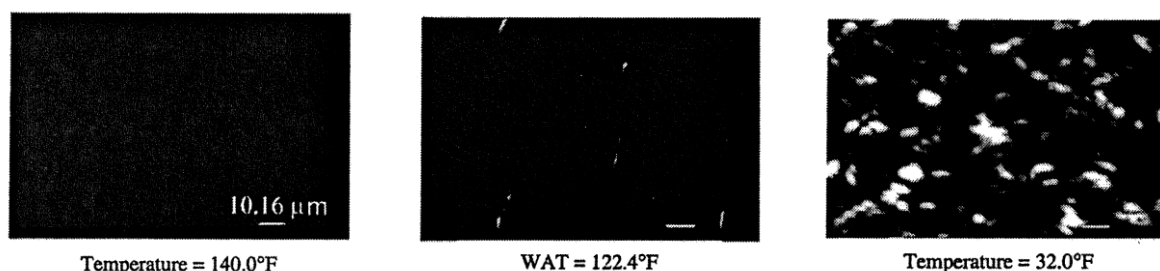


Fig. 3.2: A crude oil sample observed at different temperatures with a CPM [11]

### 3.1.2 Differential Scanning Calorimetry (DSC)

This thermal method is very popular, it determines the WAT via the high enthalpies of the crystallizing paraffin because if a substance undergoes a phase change from liquid to solid (freezing) heat energy is released, and the other way round (melting

needs heat energy). The DSC records the energy change due to the phase transformation from liquid to solid. The heat measured by the DSC is converted into mass which is described by the following equation

$$\Delta mH_i = cM_iT_{m,i} \quad (3.1)$$

$\Delta mH_i$  = the molar melting heat in [J mol<sup>-1</sup>] for a given n-alkane  $i$

$M_i$  = the molecular weight in [g mol<sup>-1</sup>]

$T_{m,i}$  = the melting temperature in [K]

$c$  = 0.6111; this value was used by Martos [12]

Such a device is designed in the following way, two brackets are placed symmetrically in an oven, one is containing the specimen and the other a reference sample. The latter does not show any thermal reaction in the used temperature range. The temperature ramp is chosen so that the temperature of the reference sample changes linear with time. The temperature of the specimen, of the reference sample and simultaneously the temperature difference between them are measured using a thermocouple element, and their time response is also recorded. If an exothermic reaction (e.g. crystallization) occurs in the specimen, its temperature will be higher or lower than the temperature of the reference sample [3] [10] [13].

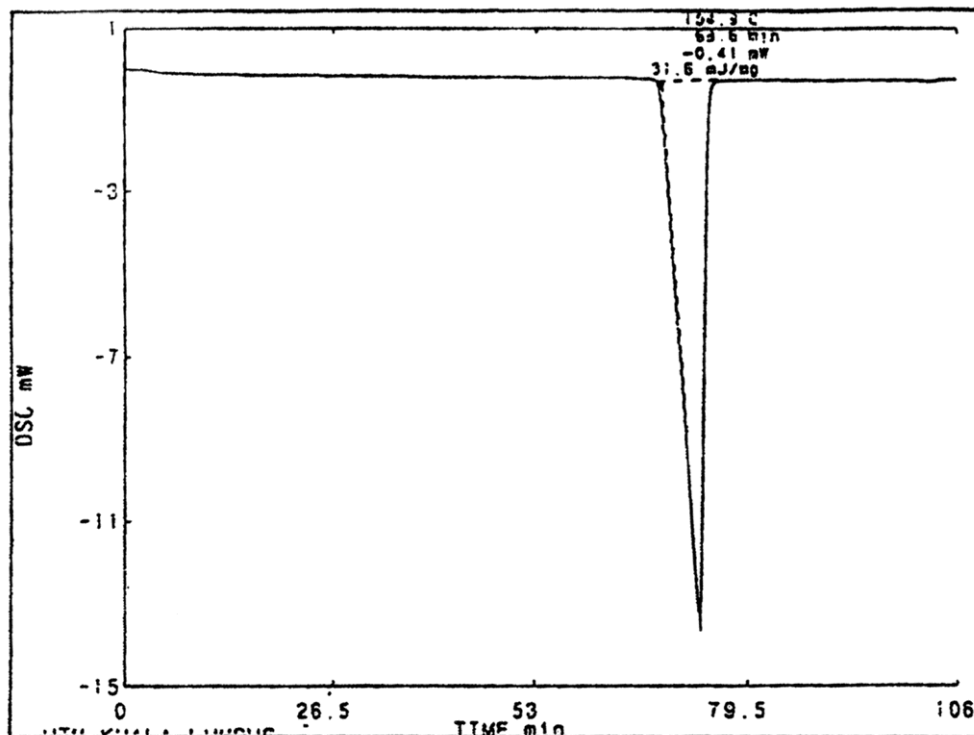


Fig. 3.3: Typical DSC curve (heat power vs. time) [13]



### 3.1.3 Solid Detection System (SDS)

The CPM detects paraffin crystals at the nucleation stage with a size around  $1\ \mu\text{m}$ , WATs determined by this technique are called onsets of wax crystallization temperatures (OWCT). The SDS method on the other hand can only measure paraffins at the early stage of crystal growth, which are about  $10\ \mu\text{m}$  in size. These WATs are also known as critical wax deposition temperatures (CWDT).

As pictured in Fig. 3.4 the SDS device consists of a light source (laser), a detector and a high pressure, volume and temperature (PVT) cell, which is mounted between the light source and the detector. This cell is a cylinder made of Pyrex glass that contains the specimen, it has a shell made of steel with vertical glass plates to observe the Pyrex cylinder and the sample. Both, volume and pressure of the inner cell as well as the differential pressure between the steel shell and the Pyrex cylinder are controlled by a variable volume displacement pump. For temperature control the PVT cell is mounted in an oven with controllable temperature. The apparatus used by Hammami and Raines [11] can be operated with a maximum pressure of 1034 bar and a maximum temperature of  $182\ ^\circ\text{C}$ . A wide range of pressure is very useful because of the big influence of the pressure on crystallization [4]. The system is controlled by a software, which records the power of the transmitted light (PTL) among other things. The WAT is reached when the crystals are big enough (ca.  $10\ \mu\text{m}$ ) so that a dramatic drop in the PTL occurs, as shown in Fig. 3.5 [11].

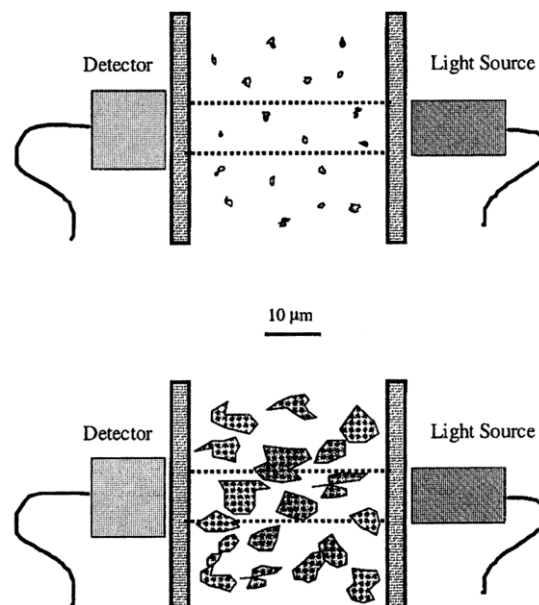


Fig. 3.4: SDS Configuration [11]

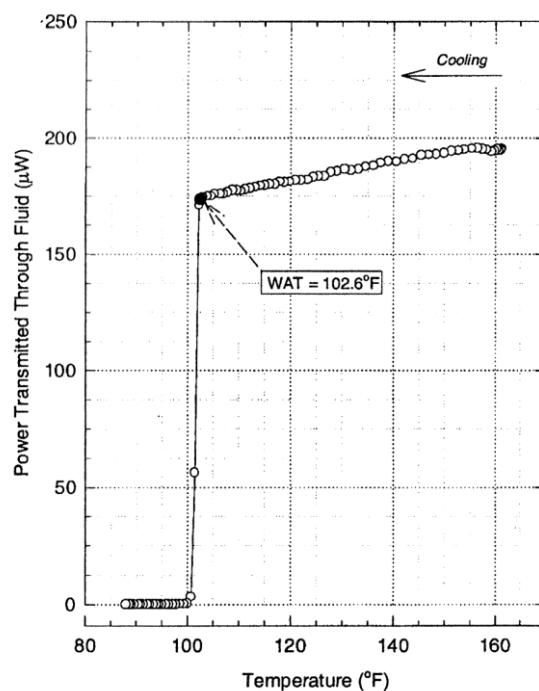


Fig. 3.5: Typical PTL curve [11]

### 3.1.4 Near-Infrared (NIR) Scattering

Unlike most other techniques this one is able to determine the WAT of live oils<sup>2</sup> at high pressure. Theoretically NIR attenuation measurements with a wavelength of 1100 nm can detect crystallites smaller than 55 nm, which is one order of magnitude smaller than the lower limit of the CPM method (0.5  $\mu\text{m}$ ). The determination of the WAT of dark crude oils is very complicated, because it is necessary to specify the radiation attenuation originating from the precipitated wax crystals and from the mother oil. The NIR scattering technique yields comparable WAT results to the CPM method. A big disadvantage of the CPM is the fact that it is very difficult to optically differentiate between wax crystals and other e.g. nonorganic crystals. The NIR wavelength region ranges from 780 to 2526 nm. Characteristic NIR absorbance bands come from methylenic, alkenic and aromatic C-H stretching vibrations but also from O-H and N-H vibrations.

Due to the phenomenon of light scattering from colloidal systems it is possible to gain information about these systems with NIR. The particle size and the wavelength ( $\lambda$ ) of the used NIR-light have an impact on the scattering of the same light. In such an incident oscillating electromagnetic radiation a particle behaves itself as a single oscillating electric dipole and emits (scattered) electromagnetic radiation in all directions. In the range of the Rayleigh limit ( $r/\lambda \leq 0.05$ ) scattering as well as absorption processes add to the light attenuation separately and are written as two independent parts of the total particle cross section.

<sup>2</sup> Live oil is containing gas and is under high pressure. Gas-free oil is also known as dead oil. For this work only the latter kind has been used.

$$\sigma_{tot} = \sigma_{sc} + \sigma_{abs} \quad (3.2)$$

The more paraffin crystals form in the crude oil the stronger gets the light attenuation. The WAT is determined by detection of this light attenuation or optical density (OD), see Fig. 3.6.

$$OD = \log\left(\frac{I_0}{I}\right) = 0.434N\sigma_{tot} \quad (3.3)$$

$I_0$  = intensity of the incident light

$I$  = intensity of the transmitted light

$N$  = number of particles in the crude oil

For condensates and gases the NIR technique provides higher WAT than the CPM while it is the other way round for dark crude oils [14].

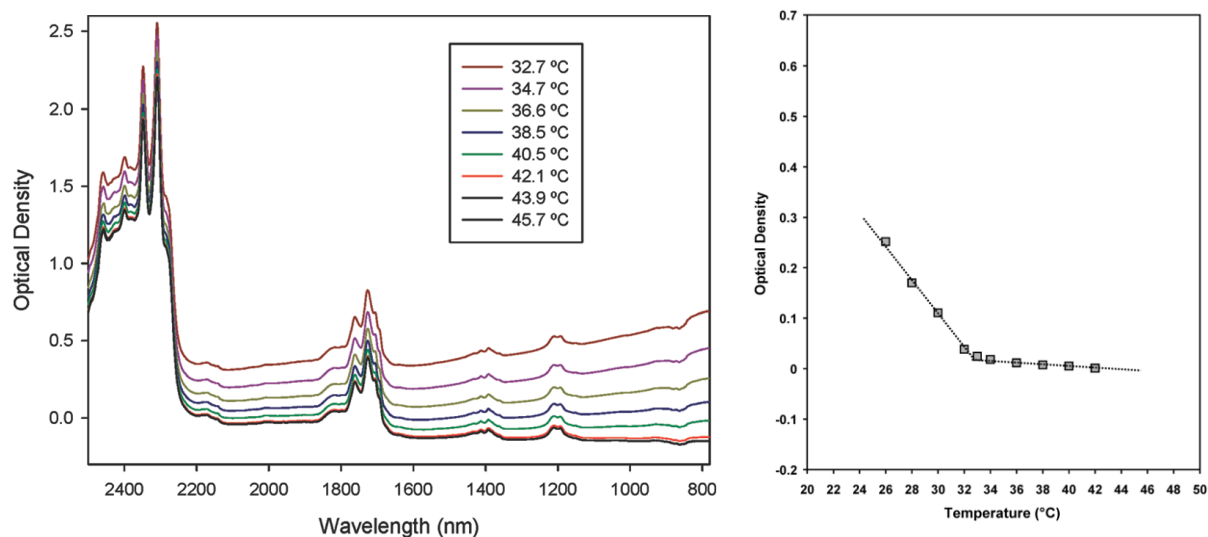


**Fig. 3.6:** Left: NIR spectra of a waxy gas condensate; right: changes in optical density of an oil at a wavelength of 1100 nm, the WAT is  $33 \pm 1$  °C [14]

### 3.1.5 Filter Plugging

Like the NIR this technique is also applicable to live oils and to dead oils at high and at low pressures. Using this technique the oil flows through a temperature controlled flow loop. During the entire measurement the pressure drop is measured across an in-the-flow-loop built-in filter with  $0.5 \mu\text{m}$  mesh size. Normally such filters are used at very low flow rates ( $\leq 0.5 \text{ cm}^3/\text{min}$ ), because high flow rates and so high shear stresses would hinder the wax deposition on the filter. That means filter plugging WATs are dependent on the flow rate, because a specific quantity of wax crystals larger than  $0.5 \mu\text{m}$  has to form on the filter before it plugs. High flow and hence high shear rates will restrain the crystal growth and therefore reduce the WAT. The

Carman-Kozeny equation associates the pressure drop  $\Delta P$  with porosity  $\varepsilon$  and the solids concentration  $\omega_s$  [10].

$$\Delta P \propto \varepsilon^{-3} \propto \omega_s^3 \quad (3.4)$$

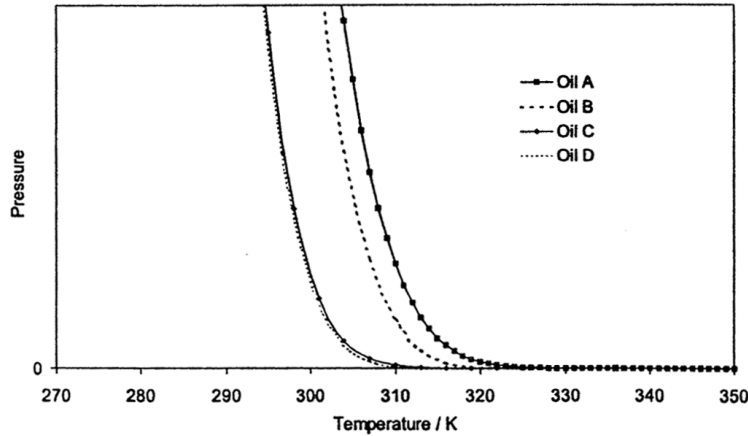


Fig. 3.7: Pressure drop across a filter plugged by several oils [10]

### 3.1.6 Viscometry

Another method to determine the WAT is to measure the viscosity (see section 8.1) of the crude oil. At temperatures above the WAT crude oils have a Newtonian behavior which means the viscosity is shear rate independent and the temperature dependence can be expressed by a simple exponential Arrhenius or Guzman-Andrade type equation.

$$\mu = Ae^{E_a/RT} \quad (3.5)$$

$\mu$  = Newtonian dynamic viscosity

$A$  = constant dependent on the entropy of activation of flow

$E_a$  = activation energy of viscous flow

$R$  = universal gas constant

$T$  = absolute temperature

Over limited temperature ranges  $A$  and  $E_a$  are assumed to be constant.

If the crude oil is cooled down paraffin starts to crystallize, and the rheological properties of the measured crude oil change to non-Newtonian or more specific to shear thinning behavior in the case of crude oils. Below this non-Newtonian limit,  $\mu$  has to be replaced by the shear rate dependent viscosity  $\eta$ , and the previously as constant assumed variables  $A$  and  $E_a$  become shear rate dependent as well. According to the fact, that crude oils behave as Newtonian fluids, as described in equation (3.5), till paraffin starts to crystallize there are two possible ways to determine the WAT, both are using the relation between the logarithmic Newtonian dynamic viscosity  $\ln \mu$  and the reciprocal temperature  $1/T$ , the slope of  $\ln \mu$  against  $1/T$  is equal to  $E_a/R$ . The

first way to determine the WAT uses the fact that due to wax crystallization  $E_a$  increases and therefore the slope gets larger. The outcome of this is a break in the viscosity curve is defined as WAT and can be seen in Fig. 3.8 (b). In the second method the Newtonian part of the viscosity is fitted via equation (3.5) over a temperature range of preferable 40 °C or more. The first temperature which deviates from the Arrhenius fit is the WAT. An example of such a curve is pictured in Fig. 3.8 (a) and (c), the WAT lies around  $3.48/K^{-1} \cdot 10^{-3}$ . Which one of these two methods is used doesn't make a big difference, because the reproducibility and accuracy of the WAT determination depends mostly on how obvious the deviation of the experimental curve from the Arrhenius fit is. Due to the shear thinning behavior of crude oils there should not be used high shear rates. Even though it was observed, that cooling rate and thermal history highly influence the viscosity of crude oils it was not found, that one of these or both factors had a significantly impact on the WAT [13].

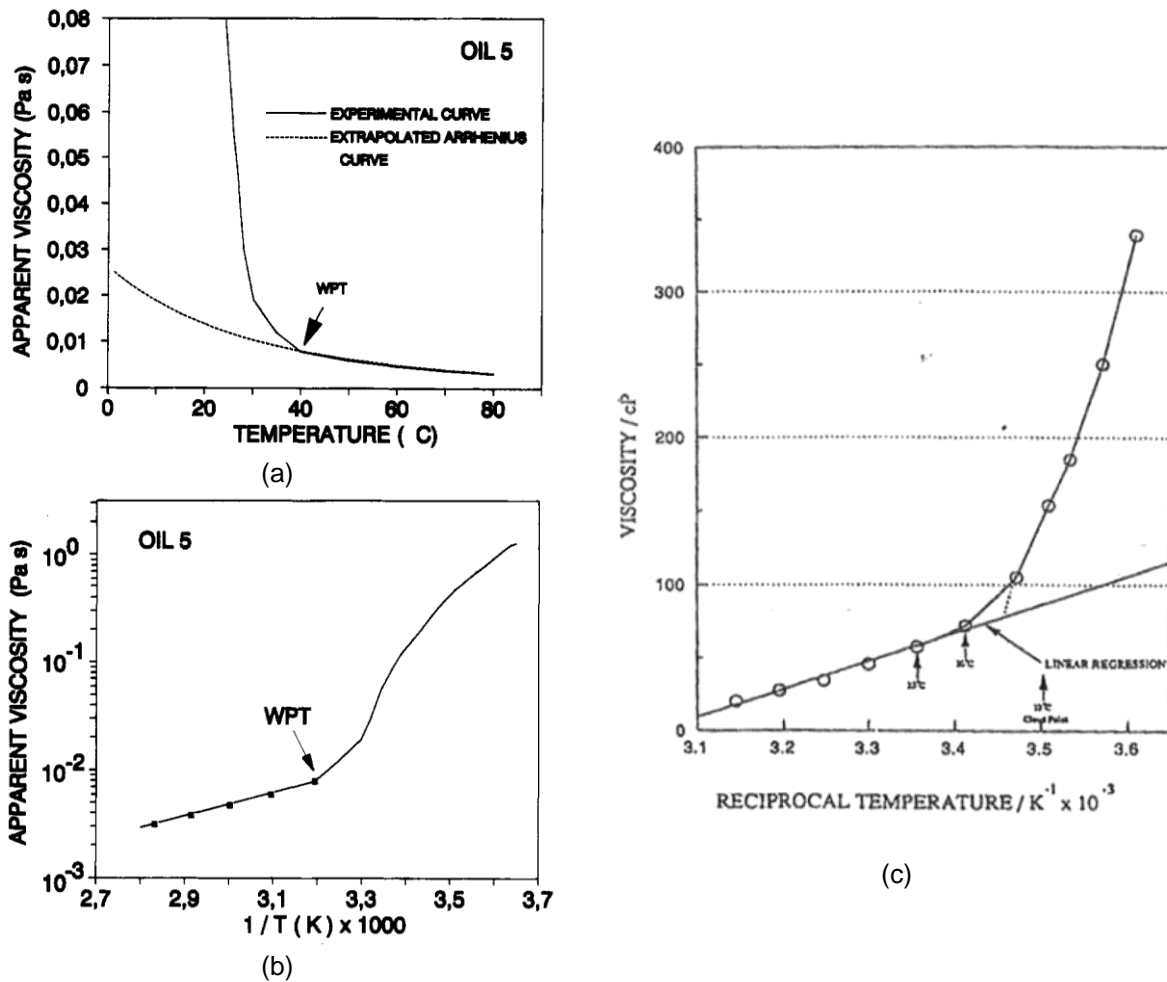


Fig. 3.8: Determination of the WAT from a viscosity-temperature curve via Arrhenius fit: (a) linear viscosity-temperature plot, (b) logarithmic viscosity-reciprocal temperature plot showing the deviation of the viscosity from linearity [13] (c) viscosity-reciprocal temperature, close-up of the deviation from linearity [9]

Since every WAT determination method yields another WAT value it is obvious that the crystallization processes depend on the measuring method and of course on the sample container geometry [4]. Another difference between the measuring tech-

niques is the stage of crystallization, so the CPM and the NIR method measure crystals at the nucleation stage (3.2.1) while DSC, SDS, filter plugging and viscometry do not detect any crystallization until the stage of growth (3.2.2).

## 3.2 Wax Crystallization Mechanisms

Since paraffin waxes cause significant problems in production, transportation and storage of crude oils, it is a big concern to understand the formation of wax crystals. Therefore the three wax crystallization mechanisms are described in this subsection, nucleation, crystal growth and agglomeration.

### 3.2.1 Nucleation

When paraffin molecules are mixed in a solvent, they have interactions with the solvent molecules and form an isotropic medium, wherein the heavy paraffins are dissolved by the light hydrocarbons. The interaction between the paraffin molecules increases with decreasing temperature, because with lower temperature the molecules are slower and less agile, therefore they stay closer together. A crystal nucleus is formed by combination of paraffin molecules, when the intermolecular forces of attraction become greater than solvent-paraffin interactions. The following empiric equation for nucleation defines the nucleation enthalpy ( $\Delta G$ ) [15]

$$\Delta G(n^*) = \frac{A\sigma^3}{(kT \ln \beta)^2} \quad (3.6)$$

$n^*$  = critical number of molecules in the nucleus

$A$  = geometric constant depending on the nucleus morphology

$\sigma$  = specific energy of the crystal-solution interfacial surface

$k$  = Boltzmann constant

$T$  = temperature in [°C]

$\beta$  = supersaturation =  $X_s/X_c$

$X_s$  = molar fraction of solute in the saturated solution at the saturation temperature

$X_c$  = molar fraction of solute at the crystallization temperature

There are two different nucleation mechanisms, homogeneous and heterogeneous nucleation. The initial state of each of those mechanisms is a random allocation of the minority component B (in this case paraffin) in the majority component A (in this case the solvent) as displayed in Fig. 3.9. This is a supersaturated solution of B in A. Depending on the temperature the formation of a chemical disposition is very fast or very slow.

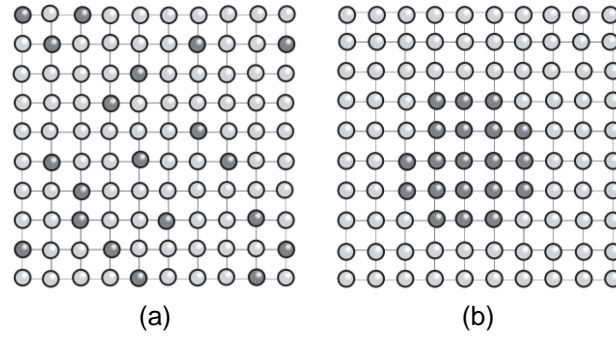


**Fig. 3.9:** Formation of a chemical disposition in a mixture of two components, A (bright) and B (dark). (a) Disordered allocation of the two components. (b) Formation of a disposition of the minority component B [16]

### 3.2.1.1 Homogenous Nucleation

For a spherical chemical disposition with constant radius  $r$ , constant temperature  $T$  and constant pressure  $p$ , the difference of the free enthalpy  $G$  between the supersaturated solution of  $n$  particles and the chemical disposition which contains  $n$  particles reads as follows

$$\Delta G_n = \frac{4}{3} \pi r^3 \cdot (G_{vol} - G_{sol}) + 4\pi r^2 \cdot \sigma_{AB} \quad (3.7)$$

The first term contains the energy gain at the changeover from  $n$  solved particles to an  $n$ -particle aggregate, whereas  $G_{vol}$  is the free enthalpy of the solution and  $G_{sol}$  is the free enthalpy of the chemical disposition. In the case of a supersaturated solution this term is always negative, this means that the free enthalpy of the solution is bigger than from the disposition. The second term describes the interface between A and B which is created due to the formation of the disposition,  $\sigma_{AB} [J/m^2]$  is the interfacial energy.

As can be seen in equation (3.7) and in Fig. 3.10 the free enthalpy  $\Delta G_n$  has a maximum with the critical radius

$$r^* = -\frac{2\sigma_{AB}}{(G_{vol} - G_{sol})} \quad (3.8)$$

Inserting (3.8) in (3.7) yields the activation barrier for the nucleation

$$\Delta G_n^* = \frac{16\pi\sigma_{AB}^3}{3 \cdot (G_{vol} - G_{sol})^2} \quad (3.9)$$

If the chemical disposition has a radius  $r < r^*$ , a further decrease of  $r$  because of particle loss results in the reduction of  $\Delta G_n$ , this kind of dispositions are called subcritical or instable. For  $r > r^*$  a growing  $r$  due to the addition of particles also leads to a decrease of  $\Delta G_n$ , such dispositions are named supercritical or stable (see Fig. 3.11).

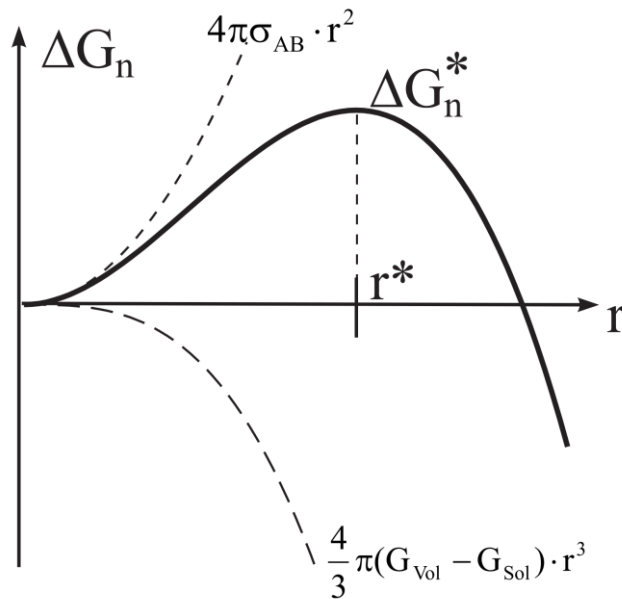


Fig. 3.10: Free enthalpy of a spherical chemical disposition [16]

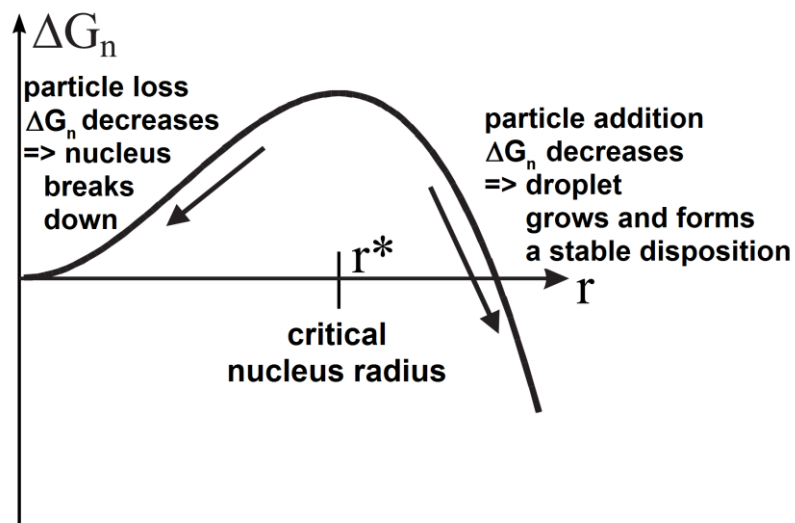


Fig. 3.11: Definition critical nucleus (facsimile) [16]

The number of  $n$ -particle dispositions  $N_n$  which form out of a supersaturated solution with  $N$  particles results to

$$N_n = N \cdot e^{\left(\frac{-\Delta G_n}{k_B T}\right)} \quad (3.10)$$

From equation (3.10) we know that the number of stable dispositions ( $\Delta G_n < 0$ ) decreases with increasing temperature ( $T$ ) and the number instable dispositions ( $\Delta G_n > 0$ ) increases with increasing temperature. With higher temperature the parti-



cles of the minority component cross each other more often but due to the higher particle mobility the so-formed dispositions are instable.

A system with homogenous nucleation has no defects or impurities, hence the disposition density only depends on  $\Delta G_n^*$  and  $r^*$  at constant temperature. Under these ideal conditions not very high disposition densities occur because of the too low supersaturation for high  $G_{vol} - G_{sol}$  values. Homogenous nucleation is barely observed in volume by reason of high  $G_n^*$  and  $r^*$  due to low  $G_{vol} - G_{sol}$  values, as can be seen in the equations (3.8) and (3.9) [16].

### 3.2.1.2 Heterogeneous Nucleation

The situation described above changes significantly if the binary system has impurities. One of these possible impurities is a grain boundary between two crystallites of the material A, which is displayed in Fig. 3.12. At this grain boundary a ball scraper shaped disposition with the radius  $r$  has formed. How much the value of  $\Delta G_n^*$  is varied depends on how well the interface is wetted by the component B.

$$\Delta G_n^* = \frac{16\pi\sigma_{AB}^3}{3 \cdot (G_{vol} - G_{sol})^2} \cdot \frac{2 - 3\cos\theta + \cos^3\theta}{8} \quad (3.11)$$

The value of the contact angle  $\theta$  is defined by the interface energies  $\sigma_{AA}$  and  $\sigma_{AB}$ , which is pictured in Fig. 3.12. The grain boundary is wetted much better the smaller  $\theta$  gets and therefore the activation energy also gets smaller according to equation (3.11) because the contact angle dependent factor tends to zero for  $\theta \rightarrow 0$ .

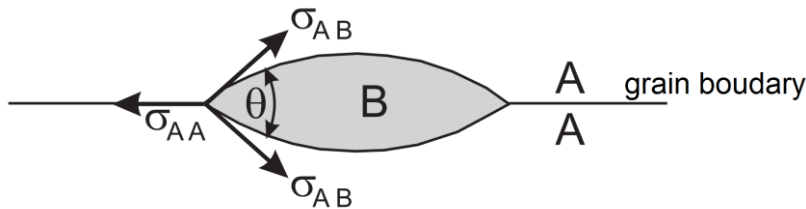


**Fig. 3.12:** Heterogeneous nucleation of a disposition consisting of the component B between two crystallites of the component A (facsimile) [16]

Equation (3.11) also shows that impurities like e.g. grain boundaries, impurities from trace elements, clustering of voids or the surface of the majority component (the surface of the solvent in the case of crude oil  $\rightarrow$  wax precipitation on the pipe wall) result in a significant reduction of the activation energy for the formation of critical nuclei. This leads to an important increase of the disposition density. Thus dispositions preferentially form at impurities, hence the heterogeneous nucleation is the most common in crude oils, because the many impurities like asphaltenes, formation fines, clay, salt, corrosion products and the surface of the pipe act as nucleating materials.

To defer between homogeneous and heterogeneous nucleation the behavior of the disposition density has to be observed over time with constant temperature. In the case of heterogeneous nucleation all critical nuclei have formed after a short period

of time, and then the disposition density remains constant. Considering homogenous nucleation on the other hand new nuclei form constantly and hence the disposition density increases over the time until all solved material reaches a stable disposition and finally becomes constant. Both cases can be seen in Fig. 3.13 [11] [16].

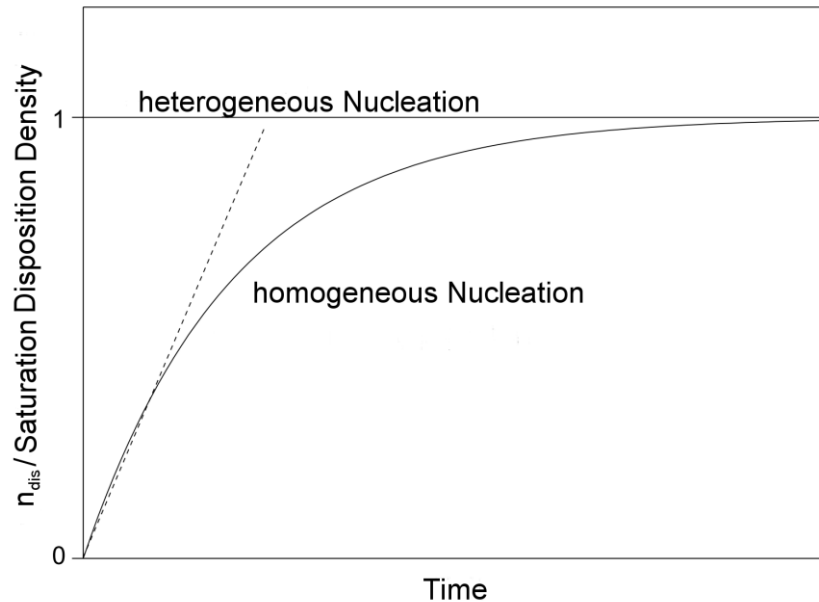


**Fig. 3.13:** *Disposition density over time (normalized to the saturation disposition density) (facsimile) [16]*

### 3.2.2 Crystal Growth

Once the nuclei are formed and the temperature stays below the WAT, other molecules add to the nuclei and a lamellar structure grows [11].

Crystal growth occurs where the surface energy of cohesion between the crystals and the free paraffin is at the maximum. This mechanism is fastest on lateral faces, it increases strongly with supersaturation. Paraffins can crystallize in mono- or multi-molecular layers and the zigzag shaped chains are arranged parallel to each other within these layers, so that the terminal methyl ( $\text{CH}_3$ ) groups are in parallel planes which are perpendicular or oblique to the chain axes.

There exist four different unit cells in paraffin crystals:

1. Monoclinic
2. Triclinic
3. Orthorhombic
4. Hexagonal

For the slower growth in thickness two theories have been postulated, the first and earlier of the two says that a nucleus deposited on a crystal face initiates a second layer across the first one. The outcome of this is a very thin pyramidal structure as pictured in Fig. 3.14. The second and newer theory includes the role that impurities

play in the growth process of a layer. These impurities form edges and new paraffin crystals add to them as described before in section 3.2.1. This leads to spiral-shaped growth also called "screw dislocation" (see Fig. 3.15), which seems to be the most frequent crystal growth process and has been observed in multiple microphotographic analyses [15].

Paraffin crystallizes basically in the following three morphologies: [15]

1. Platelets or lamellae which are rhombic, this form occurs particularly due to low cooling
2. Needles appear because of rapid cooling and impurities in the n-paraffins.
3. In complex media other forms of crystals often are observed like dendrites which are very irregularly stacked lamellae, long crystals, parallelepipedic or pyramidal blocks.

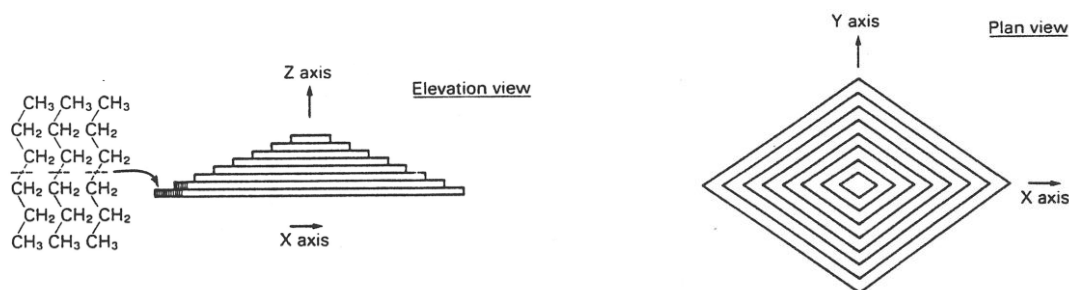


Fig. 3.14: Crystal growth in stacked layers [15]

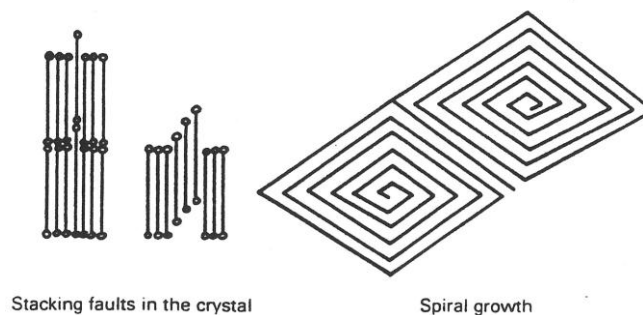


Fig. 3.15: Crystal growth in spirals [15]

### 3.2.3 Agglomeration

When cooled under the WAT the size of the crystals in the crude oil increases greatly and hence strongly influences the rheological properties of the solution, the bigger the crystals become, the higher the viscosity gets. If cooled down further, the crystals agglomerate into particles, which precipitate or form a rigid lattice and the higher the amount of liquid oil entrapped in the lattice is, the tougher the oil gets till it reaches the pour point (see Chapter 4). There are crude oils in which more than 80 % of the liquid fraction is enclosed in the crystal lattice [5] [15].

### 3.3 Factors Influencing Wax Precipitation

As described above under reservoir conditions paraffin is in solution. If this equilibrium is disturbed by anything like e.g. temperature, pressure change or the loss of volatile components, nucleation starts and wax crystals are formed. The most important factors influencing the further crystallization are described below.

#### 3.3.1 Flow Rate and Surface Properties of Tubes

The wax deposition increases with the flow rate if it stays in the laminar range, this can be explained with the fact that with higher flow rates more particles for crystallization and deposition at the surface are available. When the flow rate exceeds a specific threshold value, the flow becomes turbulent. In a turbulent flow the shear rates are very high thus it is more likely that deposited particles are removed again, that means with increasing turbulent flow rates the wax deposition decrease. The flow behavior of a flowing fluid is described by the "Reynolds Number".

Wax deposits at high flow rates are harder and more compact than others formed at low flow rates, hence those wax crystals and crystal clusters with strong cohesion between them and firm attachment to the surface are not removed by the turbulent flow on the contrary to those with weak cohesion which are flushed away (see Fig. 3.16).

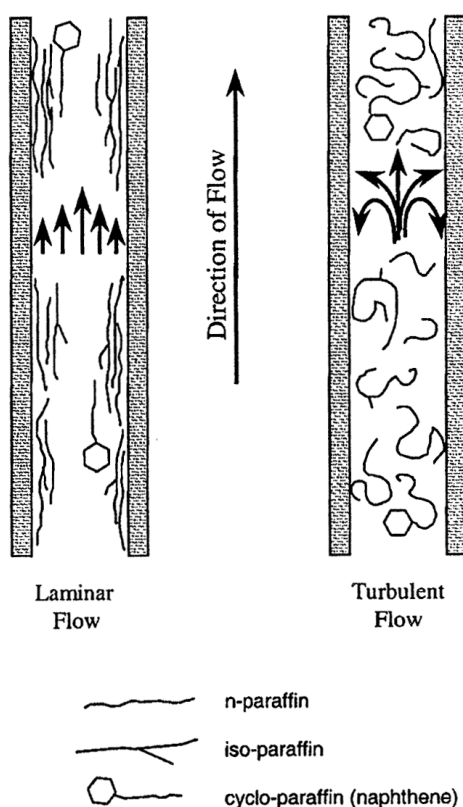


Fig. 3.16: Wax disposition within laminar and turbulent flow [11]

Low flow rates are more problematic, because the oil stays longer in the tubing and cools down faster so more paraffin wax precipitates and deposits. To reduce deposition a minimum flow rate of 0.17 m/s should be used.

Since the paraffin wax deposits on the pipe surface it is obvious, that the surface properties are very important and should be considered when trying to reduce the wax deposition. The paraffin wax is held in place by adsorption forces which depend on the free energy of the paraffin and the pipe surface. The wax is not held to the pipe surface by binding forces but because of the surface roughness. A rough material has a larger total surface than a smooth material and since the wax deposition is related to the total surface, on a rough material more wax deposits than on a smooth one [6].

### 3.3.2 Oil Composition

As mentioned at the beginning of chapter 3, n-paraffins are the constituents of macrocrystalline waxes which lead to paraffin problems in production and transportation. The microcrystalline waxes on the other hand compose most of the tank bottom sludges. The wax depositions formed during production and transportation consist to about 52 % of n-paraffins and to less than 5 % of asphaltenes and resins, the balance is crude oil, water and mechanical impurities.

Paraffin molecules normally contain more than 15 carbon atoms and have few branches. In some waxes, paraffin compounds up to  $C_{80}$  have been found. For oil-field operators paraffin compounds consisting of more than 20 carbon atoms count to potential troublemakers.

Even though n-paraffins and iso-paraffins are both flexible hydrocarbon molecules and tend to cluster together, the branched iso-paraffins normally form instable wax dispositions and delay the nucleation process on the contrary to n-paraffins. Aromatics are good solvents for paraffinic waxes and naphthenes which are stiff and bulky hinder or in some cases disrupt nucleation and growth processes.

While volatile light ends act as solvents and therefore restrain wax deposition. Impurities support nucleation and thus wax deposition, asphaltenes are a part of these impurities and resins on the other hand have no direct effect on wax precipitation [6] [11].

### 3.3.3 Pressure

Any dead oil set under pressure with a non-hydrocarbon gas leads to an increasing WAT or in other words the solubility of paraffin in oil decreases with increasing pressure. This means that the WAT is a linear function of pressure. The situation is different when a hydrocarbon gas or live oil is used, but previously it has to be noted, that light end hydrocarbons (like methane, ethane, etc.) act as solvents for paraffin as mentioned before. Additional to the fact that the dissolution of methane decreases the WAT it also reduces the relative amount of solid paraffin wax. Methane has its greatest effect on crude oils with high amounts of macrocrystalline waxes. At low pressures these light ends are not solved in the crude oil but in the gas phase and

hence as bubbles in the oil. With increasing pressure the gaseous light ends begin to dissolve in the crude oil and thus hinder the wax precipitation which yields a lower WAT. An example of such a WAT measurement of a live oil is given in Fig. 3.17, at first the WAT decreases because the hydrocarbon gas dissolves in the crude oil as described before. Above the bubble point at 285 bar the WAT increases linearly with the pressure since all gaseous light ends are solved in the crude oil just the pure pressure effect remains [17] [18] [19].

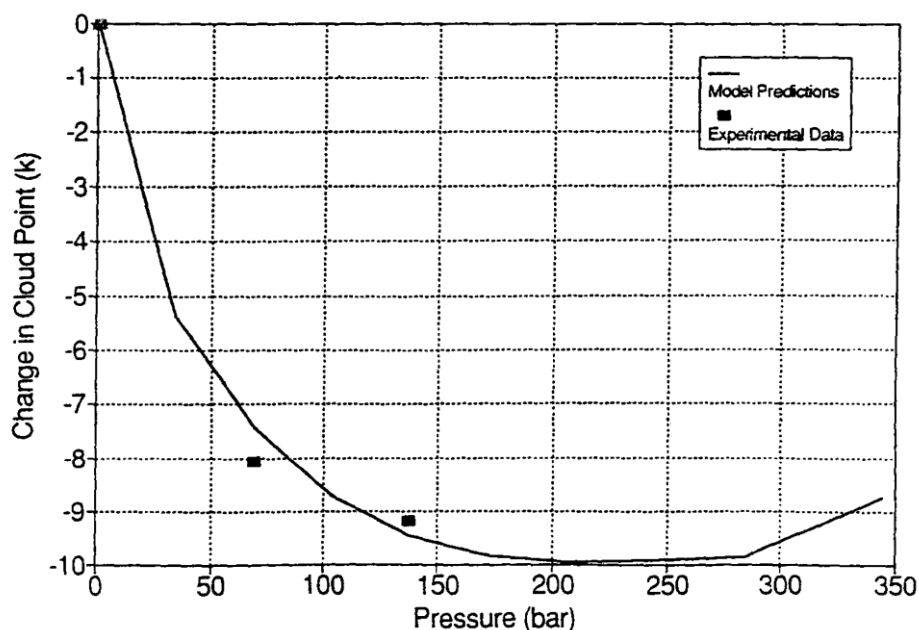


Fig. 3.17: Typical curve WAT vs. pressure [17]

Under reservoir conditions (heat and high pressure) the viscosity of crude oils is low because the heavy hydrocarbons are in solution by the light ones, but during production crude oils flow through production tubings and pipelines where the pressure falls and hence the temperature too due to the Joule-Thomson effect. This means that pressure loss leads to paraffin wax precipitation, because cooling is the main condition for wax crystallization [19].

### 3.3.4 Temperature Difference and Cooling Rate

The crystallization and hence the wax deposition is influenced by the temperature of the crude oil itself and by the temperature gradient between the bulk of solution and the cold pipe surface. The bigger this gradient becomes, the more wax deposits. The temperature difference between bulk and cold surface is considered less important than the one between WAT and cold surface. For wax deposition this surface temperature has to be lower than the temperature and the WAT of the crude oil. Once a wax layer has formed on the pipe surface, this layer acts as thermal insulation and thus reduces the temperature gradient which leads to less wax disposition than before. This wax disposition reduction leads to an asymptotic paraffin wax deposition behavior with the time. To observe this behavior a heat exchanger was used as

shown in Fig. 3.18. It consists of two unconnected circulation loops, one containing the cooling water and the other one contains the sample. Both are circulated through rectangular ducts which are separated by a deposition plate. The amount of deposited wax over a certain period of time is determined by weighing the deposition plate before and after the experiment and as can be seen in Fig. 3.19 the deposition curve is asymptotic which means as stated before that the deposition rate decreases until it reaches a constant value.

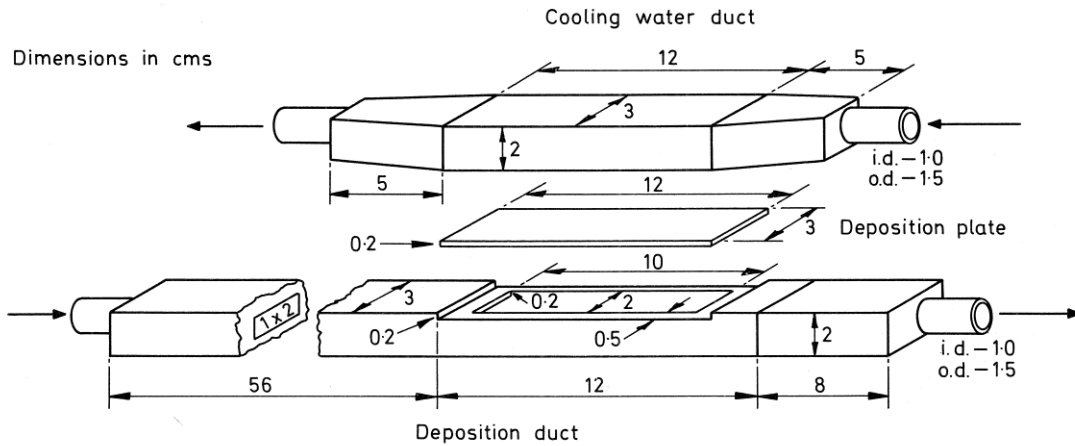


**Fig. 3.18:** Drawing of the heat exchanger to measure the amount of wax disposition in a flowing system [20]

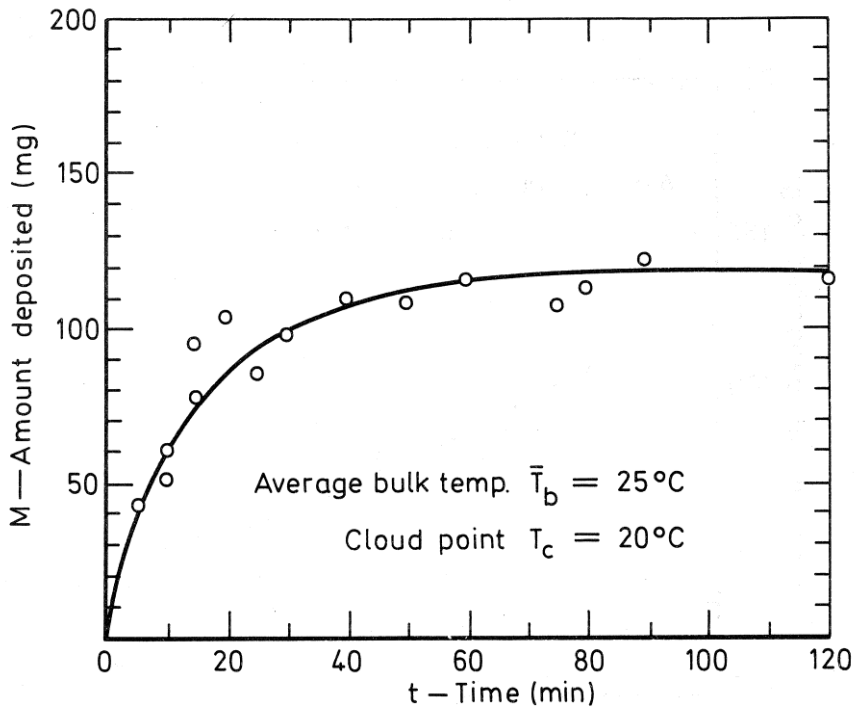


**Fig. 3.19:** Asymptotic behavior of the wax deposition over the time [20]

The size and number of wax crystals depend on the cooling rate and are very important for wax deposition. At low cooling rates the crystallization process is rather uniform, the crystal clusters are big and therefore not so many, and they have a relatively small surface and free energy. While high cooling rates lead to a large number of small crystals, and furthermore paraffins with low and high melting points crystallize simultaneously due to rapid cooling. For this reason the formed crystal structure is weak and porous with plenty of voids containing liquid oil [6] [20].



## 4 Pour Point of Crude Oils

The pour point is used as a reference for the solidification temperature of crude oils. With falling temperature the paraffin crystals in the crude oil grow which leads to a higher viscosity and consequently a crystal lattice forms if the oil is cooled down further. But even after having formed a crystal lattice the crude oil is able to flow as long as the pressure drop between start and end point is high enough, that's because of the shear thinning properties of crude oil. The crystal lattice starts to be a problem when the production or a pipeline has to be shut down and the flow in the pipe stops and the temperature is below a certain point (the pour point). In that case the crude oil in the whole pipe starts to solidify and the flow cannot be restarted because the pumps are not strong enough to create a pressure drop that exceeds the required yield stress of the crude oil to start flowing again. Therefore the pour point is defined as the lowest temperature at which the crude oil still flows freely under its own weight under specific test conditions as described in ASTM D 5853 [21], it is also referred to as lowest temperature of handling ability for certain applications. This test can be repeated with chemical additives in the crude oils to see if the pour point decreases to a level, that will allow to handle the crude oils without deposits [21] [22] [23].

### 4.1 Methods to determine the Pour Point

There are two ways to determine the pour point of crude oils, the first one is described in 4.1.1 and is the older and more popular method. It has the disadvantage that has to be performed manually and hence an operator has to be present all the time and it takes much longer than the newer automatic method described in 4.1.2.

#### 4.1.1 Manual (Tilt) Method – ASTM D 5853

The pour point test apparatus set up is shown in Fig. 4.1, it consists of:

1. Thermometers with ranges of -38 °C to +50 °C for the high cloud and pour thermometer, -80 °C to +20 °C for the low cloud and pour thermometer and +32 °C to +127 °C for the melting point thermometer
2. Cylindrical Test Jar of clear glass with a flat bottom
3. Jacket which is made of a cylindrical watertight metal with a flat bottom
4. Gasket which is a ring of leather, rubber or any other elastic material that fits snugly around and clings to the test jar but it shall also fit loosely inside the Jacket, so that the Test Jar does not touch the Jacket
5. Disk of cork or felt which fits loosely in the Jacket
6. Cork that fits in the Test Jar with a hole for the test thermometer in its center
7. Cooling bath or baths with a support to hold the Test Jar and a proper thermometer

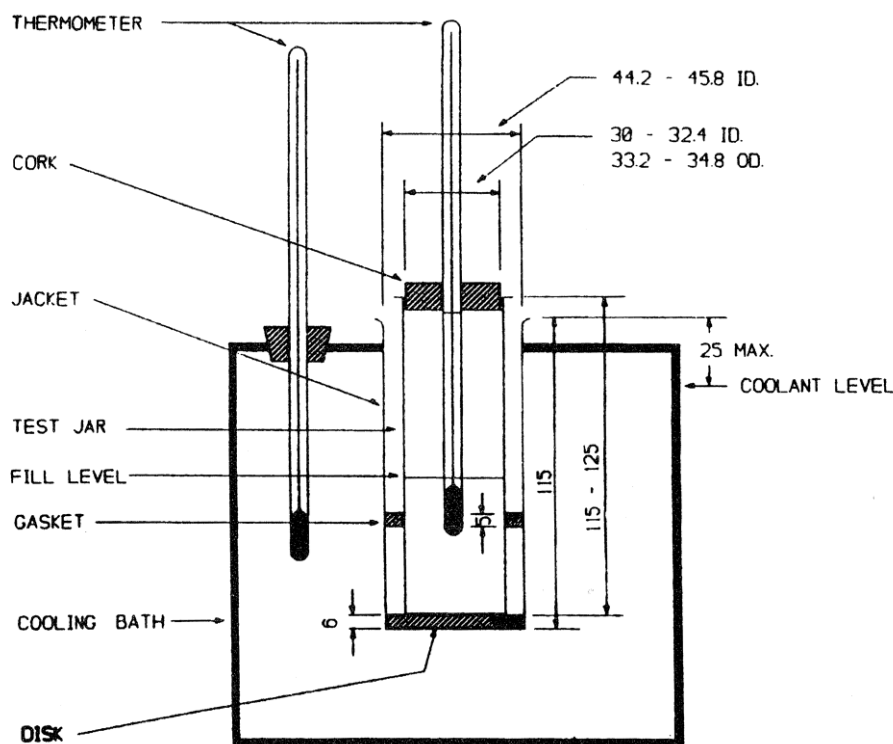


Fig. 4.1: Pour point test apparatus setup (all dimensions are stated in millimeters) [21]

Two different kinds of pour points can be measured, the first is the maximum (upper) pour point which can be obtained after a special treatment with the goal to enhance the gelation of wax crystals and the solidification of the tested crude oil. The second is the minimum (lower) pour point, for this one the pretreatment is designed to delay the wax crystal gelation and the solidification of the specimen. In the range of these two pour point temperatures a crude oil can be liquid as well as solid depending on its thermal history.

To determine the maximum pour point the test sample is poured in the Test Jar and if the expected pour point is higher than  $36\text{ }^{\circ}\text{C}$  the sample has to be heated  $9\text{ }^{\circ}\text{C}$  above the expected pour point. But if it is less than  $36\text{ }^{\circ}\text{C}$  the sample has to be heated to  $45\text{ }^{\circ}\text{C}$ . Then the Test Jar which contains the specimen is put in the Jacket which is in the cooling bath. The pour point is stated in positive or negative multiples of  $3\text{ }^{\circ}\text{C}$ , this means every time the test thermometer reads a multiple of  $3\text{ }^{\circ}\text{C}$  below the starting temperature the Test Jar is removed from the Jacket and tilted until a movement of the specimen in the Test Jar can be observed, if so the Test Jar is returned in the Jacket and cooled down further. This procedure is repeated till the sample does not flow away for 5 seconds when the test Jar is held in a horizontal position which is when the pour point is reached.

For the determination of the minimum pour point the sample is put in a pressure vessel (see Fig. 4.2) which is made of stainless steel and is able to withstand a pressure of 7 bar. The pressure vessel containing the sample is heated to  $105 \pm 2\text{ }^{\circ}\text{C}$  for at least 30 min in an oil bath (or any other suitable fluid). Then the container has to be homogenized by swirling it around gently afterwards the pressure vessel is left to cool down at room temperature, after precisely 20 min it is opened very carefully because

the specimen still has approximately 50 °C and therefore the vapor pressure can still be higher than 1 bar. Then the specimen is poured in the Test Jar which is closed instantly with the cork and the high cloud and pour thermometer, or the melting point thermometer if the expected pour point is above 36 °C, in its center. From here on the same procedure as before is performed.

The determination of the maximum pour point has a repeatability, which means a difference between successive test results measured by the same operator using the same apparatus under constant operating conditions with identical test samples, of 3.1 °C while the repeatability for the minimum pour point is 5.8 °C, these values are only exceeded in one of 20 cases. The reproducibility is the difference between two single and independent results obtained by different operators who are working in different laboratories on identical test samples and its value for the maximum pour point is 18 °C and for the minimum pour point the reproducibility is 22 °C, these two values also are only exceeded in one case out of 20 [21] [24].

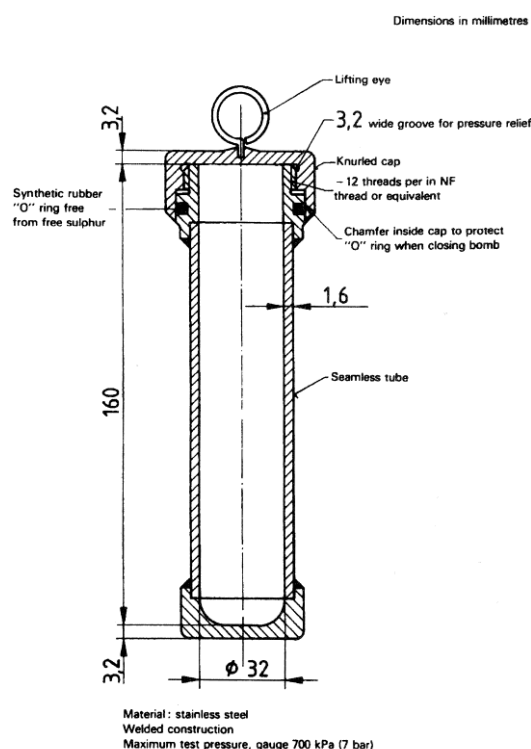


Fig. 4.2: Pressure vessel [21]

#### 4.1.2 Automatic (Rotational) Method – ASTM D 5985

Even if this test method is, in accordance with the ASTM D 5985 standard [25], not intended for crude oils, it yields good reproducible results and therefore is used for crude oils in the OMV labs.

The test apparatus mainly consists of an L-shaped pendulum with a temperature sensor at the end of the longer arm while the end of the shorter arm is mounted above a light barrier. The measuring unit is controlled by a microprocessor and capa-

ble of heating, cooling, rotating and recording the temperature of the sample. Once started the Pour Point Tester first heats and then cools the sample by keeping the temperature difference between heating/cooling block and temperature sensor in the sample constant. The cylindrical metal container in which the specimen is put rotates with 0.1 rpm as can be seen in Fig. 4.3. As the sample cools down its viscosity grows due to wax crystallization. As long as the measuring arm is not moved the sample still flows, but when the viscosity gets high enough that the shorter arm of the pendulum triggers the light barrier, this means that the sample does not flow anymore and the no flow point is reached. The pour point is the lowest temperature at which movement of the specimen is observed.

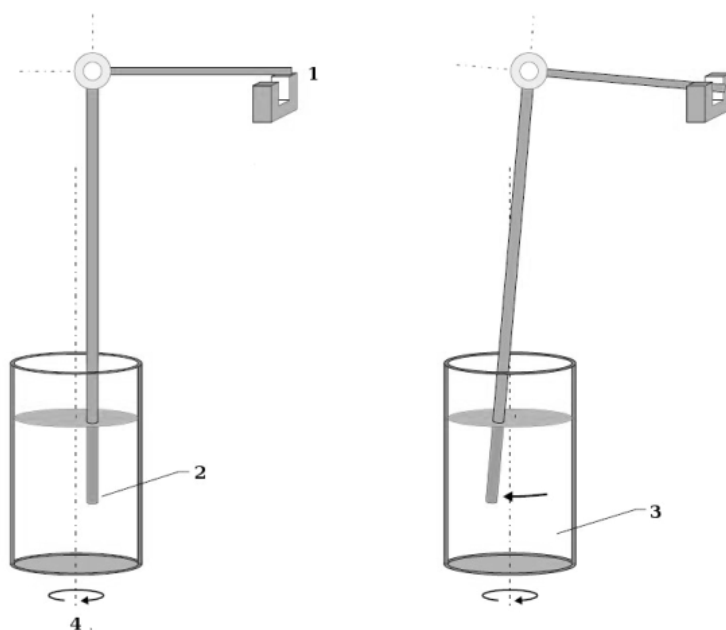


**Fig. 4.3:** *Pour Point Tester principle; 1 light barrier, 2 temperature sensor, 3 test specimen, 4 motor (ca. 0.1 rpm) [26]*

As written above in the description of the tilt method (4.1.1), and also when using the rotational method, the sample is heated to 9 °C above the expected pour point but at least to 45 °C. This temperature shall also be used if the expected pour point is not known. The temperature can be recorded with an accuracy of 0.1 °C. This method has a repeatability of 2.3 °C and a reproducibility of 8.7 °C, as before these values are only exceeded in one out of 20 cases [25] [26].

Compared to the tilt method the rotational method has two main advantages, the first one is that the temperature is measured directly in the specimen and can therefore give information about crystallization processes in the sample. The second advantage is that the container with the specimen has not to be tilted in contrast to the tilt method which mechanically disturbs the sample and hence influence the crystallization processes and reduce the reproducibility [26].

## 5 Thermal History of Crude Oils

In praxis the main problem related to the thermal history of crude oils is the shutdown of transportation pipelines because of emergencies like line damage, power failure or earthquakes and many others. As mentioned before crude oil is shear thinning, which means as soon as the flow stops, it becomes more viscous and the crude oil starts to cool down statically and hence the crystal growth and the precipitation of wax increases. So the temperature of the crude oil may drop below its pour point and a strong waxy crystal interlocking network forms in the oil. The strength of this waxy structure depends on nearly everything in the cooling process, like starting and end temperatures, cooling rate, the isothermal holding time at the end temperature of the cooling process before the restart of the pipeline and the temperature cycling. Once the pipeline is filled with crude oil that has developed a wax crystal interlocking network, the yielding of the crude oil which is required to restart the flow is achieved by application of a sufficient pressure. This yield stress required for a pipeline restart is highly dependent on the temperature of the crude oil and on the cooling rate. The lower the temperature is the higher is the yield stress and a low cooling rate leads to a high yield stress while a high cooling rate results in a low yield stress, since the wax structure is depending on the cooling rate as described in section 5.2.

The influence of thermal history or heat treatment on the flow properties of crude oils has been known for a long time. Earlier very often the pour point was used as a gauge for the pumpability of crude oils but during an investigation started in 1970 it was found out that the yield stress is a better measure for the pumpability [27].

But nevertheless the pour point is still a very important value to classify crude oils in the praxis and to decide how they should be treated for production and transportation.

### 5.1 Influence of Temperature on Wax Precipitation

Chang and Boger [27] used a CPM to investigate the amount, size and shape of the wax crystals of a crude oil that was heated to 65 °C before. It was cooled down statically with a cooling rate of 2 °C/min then at first the WAT was determined at 50 °C, afterwards images were taken at 45 °C, 28 °C, 24 °C and 20 °C which is shown in Fig. 5.1. In the first of the four pictures (Fig. 5.1 (a)) the temperature is with 45 °C just under the WAT and therefore the crystals are very few, small and widespread in the crude oil. At this temperature the wax crystals just have a very small rheological influence due to their small size. As the temperature is decreased further to 28 °C (Fig. 5.1 (b)), more wax crystals appear and the ones observed at a higher temperature increased in size, in addition very little agglomeration can be seen. Since no hint of a crystal lattice can be observed at this temperature, there is no yield point. Further cooling to 24 °C (Fig. 5.1 (c)) leads to even bigger crystals and a lattice which connects neighboring agglomerations starts to form but it is not very strong and therefore

the yielding behavior does not show any solid like characteristics. The last of the four images (Fig. 5.1 (d)) shows the wax crystals of the used sample at 20 °C which form a strong interlocking network that leads to a yielding behavior of a solid structure. It is interesting that the shape of the crystals is that of irregular spherulites and not plates or needles, they agglomerate and form various random chain structures which consequently build up the crystal lattice. Crude oils contain many different paraffins and other strong-polarity-large-molecule material, so they have rather malcrystalline masses than regular ones [27].

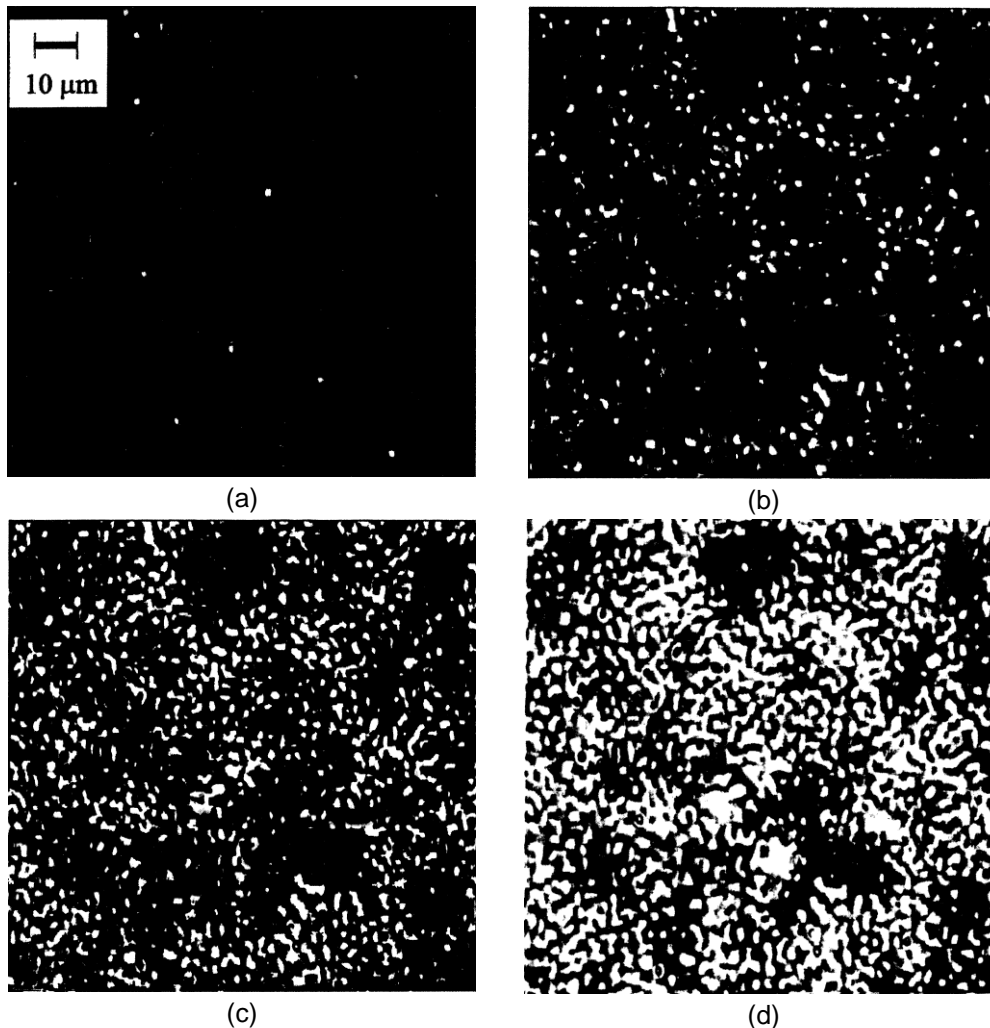


**Fig. 5.1:** Effect of temperature on wax precipitation determined by a CPM during a static cooling process of 2 °C/min. At 45 °C (a), 28 °C (b), 24 °C (c) and 20 °C (d) [27]

## 5.2 Influence of Cooling Rate on Wax Structure

Another factor influencing the size and the number of wax crystals is the cooling rate which is shown in Fig. 5.2. In this picture also the difference between the agglomerations of the used crude oil at different cooling rates can be seen. A high cooling rate like 2 °C/min (Fig. 5.2 (a)) results in smaller crystals and fewer agglomerations. The

lower cooling rate of 0.5 °C/min leads to bigger crystals and as displayed in Fig. 5.2 (c) to more agglomerations and furthermore a crystal lattice starts to form. This means that a slower cooling rate always leads to bigger wax crystals and more agglomeration. This size difference of the wax crystals due to the cooling rate is detectable by rheological measurements. Hence the cooling rate dependence of the yield stress can be explained through the influence of the cooling rate on the waxy structure. At higher temperatures where the crude oil sample is in a liquid or a weak gel state the previously discussed influence of the cooling rate on the wax structure cannot be detected by rheological means. Only at lower temperatures where the sample is in a solid or nearly solid state the effect becomes detectable by rheological measurements. It is still not clearly understood why the lower cooling rates result in higher viscosities and therefore in higher yield stresses [9] [27].

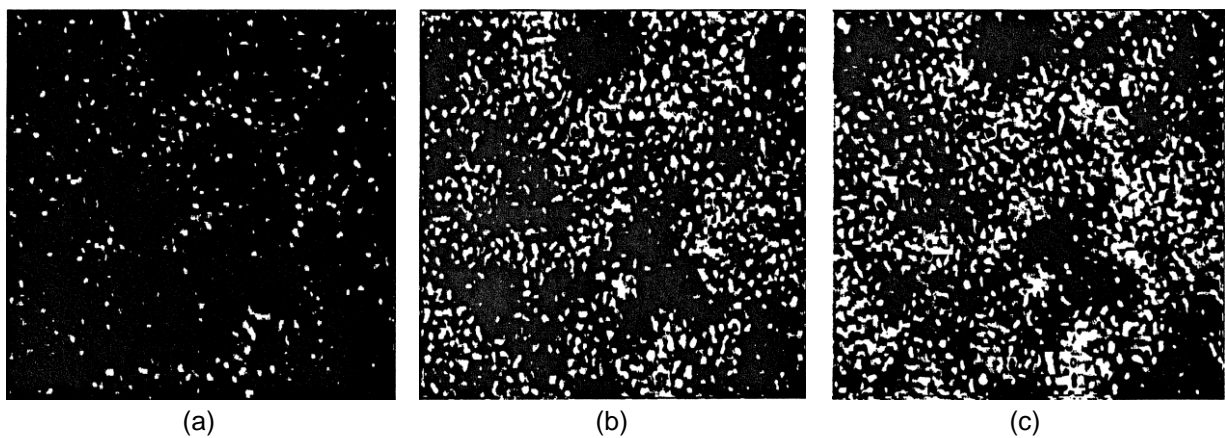


**Fig. 5.2:** Effect of cooling rate on wax precipitation. All three pictures were taken at the same temperature which was below the pour point, just the cooling rates were different: 2 °C/min (a), 1 °C/min (b) and 0.5 °C/min (c) [27]

## **6 Problems due to Wax Dissipation**

The precipitated wax from crude oils causes problems to every piece of equipment used in production and transportation of crude oil, such as pressure losses in the tubing and in pipelines or depositions on the string of a sucker rod pump. Which produce high costs because of the additional weight on the string. The needed energy for production increases and the string has to be replaced more often, in the worst case the depositions grow so big that the string can get stuck and even tear apart. Other problems are the deposits at the bottom of oil storage tanks, the high yield stresses which occur at pipeline restarts as described in Chapter 5 and the wax precipitation in the formation itself which decreases the flow down in the wellbore [5].

### **6.1 Formation Damages**

A crude oil reservoir mainly consists of porous rocks which are called formation or formation material and the whole crude oil is enclosed in these pores. The crude oil of the whole reservoir is connected through the pores in the formation material so it can flow towards the wellbore during the production process. If a crude oil in such a reservoir contains many heavy hydrocarbon molecules it is often called waxy crude or heavy oil. In colder regions of the formation such as the region near the wellbore, the heavy hydrocarbon molecules may start to crystallize and hence plug the pores in the formation. This leads to a pressure drop in the production process due to the higher viscosity of the crude oil because of the lower temperature and the smaller effective diameter of the pores, which is caused by the wax precipitations.

The main reasons for the cooling down of the formation near the wellbore which leads to formation damages are the pressure loss due to the production and to far bigger part maintenance jobs of the tubing like cold fluid injections or various gas floods which cool down the formation due to the expansion of the used gases.

Another reason for formation damages is the use of hot oiling jobs to remove the wax depositions in the tubing because the hot oil melts the wax on the tubing wall and this wax consists of the heaviest hydrocarbons from the produced crude oil which flow down to the wellbore where they can plug the pores of the formation material.

When nearly all pores in the formation close to the wellbore are plugged this results in a dramatic drop in production, to increase the production again high pressures are used to make artificial cracks in the formation material or fracturing fluids are injected to enlarge the pores or make new ones. But the big problem here is, that if the temperatures of these fluids are below the WAT of the crude oil, the fracturing fluid will cause further wax crystallization.

The detection of formation damages is very difficult, often a formation damage is mistaken for the exhaustion of a reservoir due to the dramatic drop in the production. To avoid such a mistake the composition of the crude oil is observed continuously because since the light ends move faster than the heavy molecules, they reach the



wellbore earlier if the formation there is not plugged. Consequently the part of heavy molecules in the produced crude oil increases over the lifespan of a well but if it decreases again, it is likely that wax deposits in the pores [4] [5].

## 6.2 Paraffin Deposition in Storage Tanks

The problem of the paraffin deposition in storage tanks is completely different to the one discussed in section 6.1, since the heaviest molecules have already precipitated in the pores of the formation or in the tubing and no flow occurs in a tank, gravity is a main reason for the accumulation of the tank bottom sludges which consist of clay, silt, scale, sand, rust, several percent of water and of course of paraffin wax. It has to be considered that these sludges reduce the tank volume, hence the outlet valves should be installed high enough above the bottom of the tank that not too much paraffin comes along with the stored crude oil.

Solvents can be used to make the bottom sludges pumpable again if they are not too hard, and then they can be mixed with crude oil again and sold along with the other produced oil. Instead of using solvents it is possible to heat the whole tank above the WAT that the paraffin separates from the water and the bottom sludges. But if these two methods are not sufficient, the sludges have to be excavated.

If different crude oils are stored in a tank they should not be mixed at different temperatures because this can lead to very high yield stresses [5].

## 6.3 Pressure Losses

One reason for high flow line pressures is the use of turbulent flow conditions to have less wax precipitation on the pipe walls. Two other causes are high viscosity of the crude oil and the wax depositions on the pipe walls (Fig. 6.1). When paraffin starts to crystallize the viscosity increases this leads to a decrease of the flow rate if pump performance is not raised. But if the viscosity gets too high and the pump performance cannot be raised any more, the flow rate decreases therefore the flow conditions become laminar which supports further wax crystallization and wax deposition on the pipe walls (as mentioned in section 3.3.1), hence the effective diameter of the tubing is reduced which results in an even higher viscosity and a higher pressure loss.



**Fig. 6.1:** *Reduced effective pipe diameter due to wax depositions [7]*

Such laminar flow conditions can be described by the law of Hagen-Poiseuille [28]

$$I = \frac{V}{t} = \frac{\pi R^4}{8\eta} \cdot \frac{p_1 - p_2}{L} = \frac{\pi R^4}{8\eta} \cdot \frac{\Delta p}{L} \quad (6.1)$$

$I$  = the current strength or flow rate of the fluid is the volume  $V$  which flows through the whole pipe cross section during the time  $t$

$R$  = radius of the pipe

$\eta$  = viscosity of the fluid

$\Delta p$  = pressure difference of the pressures  $p_1$  and  $p_2$

$L$  = length of the pipe

The linear pressure drop along the pipe is described in the equation (6.1) by the factor  $\Delta p/L$  and is graphically displayed in Fig. 6.2. It has to be noted that the flow rate  $I$  is proportional to  $R^4$  times of the pressure drop which indicates how severe the problem of a reduced effective pipe diameter due to wax deposition is.

The behavior of a turbulent flow is more complex than the behavior of the laminar flow. Nevertheless the radius and the pressure drop affect the flow rate in a similar way [4] [6] [28].

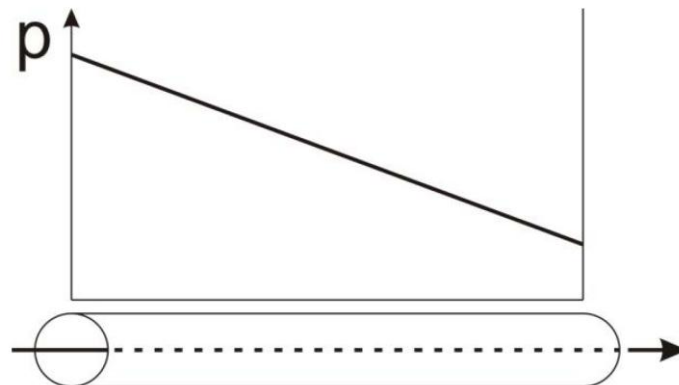


**Fig. 6.2:** Pressure loss in a pipe with a certain length for laminar flow conditions [4]

## 7 Methods of Wax Reduction/Removing

Over the years several methods to remove deposited wax or even to prevent paraffin wax from depositing have been developed. They range from complex chemical techniques that manipulate the crystallization processes itself, to simple mechanical removal of the wax from the pipe wall. But it should be mentioned that simple does not mean that it is easily done, for instance "pigs" which are used to remove the depositions in pipelines (see section 7.3.1) can be very complicated high tech machines.

### 7.1 Chemical Methods

#### 7.1.1 Pour Point Depressants

Pour point depressants (PPDs) are also known as paraffin inhibitors, crystal modifiers or viscosity modifiers.

Unlike other methods paraffin inhibitors do not prevent paraffin molecules from crystallizing but they influence the crystallization process. When the temperature of the crude oil becomes lower than the WAT and the crystal growth begins, the paraffin molecules arrange parallel and form mono- or multi-molecular layers (see section 3.2.2). Paraffin inhibitor molecules are branched polymers which have a structural affinity to paraffin molecules and small structural irregularities. The paraffin inhibitors have to be added to crude oils above the WAT because they play an active role in the crystallization process. Hence they have to be pumped downhole where the temperature of the crude oils is still above the WAT and there they dissolve. There are three possible ways how these polymers modify the wax crystals:

1. The paraffin inhibitor molecules drop out of solution just over the WAT and act as nuclei for the nucleation (see section 3.2.1).
2. The paraffin inhibitor molecules precipitate at the WAT together with the paraffin molecules and co-crystallize with them.
3. The paraffin inhibitor molecules drop out of solution just below the WAT and adsorb to the paraffin crystals.

This means that the paraffin inhibitor molecules prevent the formation of big paraffin crystals and wax agglomerations or in other words they decrease the cohesive forces between the paraffin crystals, they also decrease the cohesive forces between paraffin crystals and the pipe wall. A schematic sketch of this mechanism is displayed in Fig. 7.1 and Fig. 7.2.

Such paraffin inhibitor molecules are mostly polyethylenes, vinyl acetate copolymers and high molecular weight long chain polyacrylates [4] [5] [29] [30].

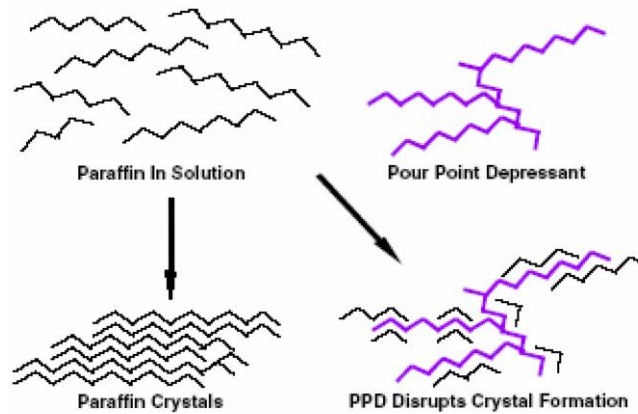


**Fig. 7.1:** Wax crystallization with and without paraffin inhibitors or PPDs; left: uninhibited paraffin crystallization, right: paraffin inhibitor molecule and paraffin crystallization with inhibitor [5]

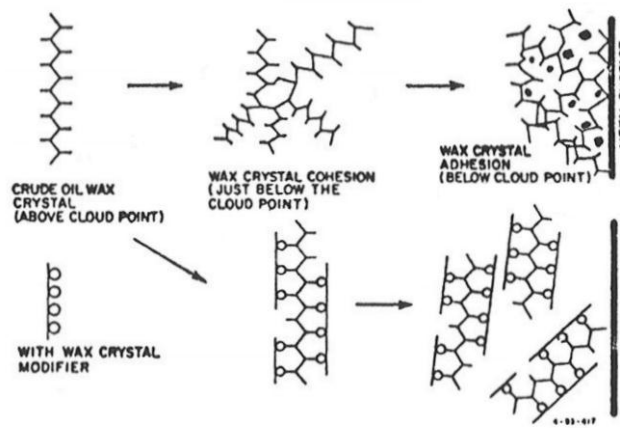


**Fig. 7.2:** Wax crystallization; top: uninhibited paraffin crystallization, bottom: inhibited paraffin crystallization [29]

### 7.1.2 Wax Dispersants

Dispersants decrease the surface tension of wax accumulations and hence break them in smaller pieces which can disperse in the crude oil. This is because one end of the dispersant molecules has a high affinity to paraffin while the other end of these molecules has a good solubility in hydrocarbons or water, depending on the type. The wax dispersants can adhere to the pipe wall and hinder paraffin crystals to do the same or in other words they make the pipe wall oleophobic. Using the same mechanism they build up a layer around wax crystal clusters which decreases the cohesion between such clusters and hence prevent the formation of accumulations and depositions. Besides wax dispersants are able to penetrate solid wax accumulations, the higher their ability to penetrate wax accumulations, to build up layers around wax crystal clusters and on the pipe wall and the higher their ability to transport paraffin crystals in the crude oil, the better the dispersants are.

They can be used as preventive measure to avoid paraffin depositions or to remove already existing deposits, to accomplish better results it is common to use dispersants together with paraffin inhibitors.

Often used dispersants are alkyl sulfonates, alkyl aryl sulfonate and fatty amine ethoxylates [4] [5].

### **7.1.3 Paraffin Solvents**

In earlier times it was quite common to dilute crude oils with other crude oils mainly, consisting of light end molecules, which act as natural solvents as mentioned in Chapter 3 [30].

But unfortunately such light end crude oils are not always available so other solvents have to be found. For instance benzene  $C_6H_6$ , chlorinated solvents and combinations of them have been used in the past, they have the big disadvantage that most of them are toxic. And many other solvents have a low flashpoint which makes their use very dangerous like carbon disulfide  $CS_2$  which is still in use. Currently toluene and xylenes are preferred but they are also toxic and pollute the environment. Therefore another option to replace the previously mentioned toxic paraffin solvents would be solvents based on limonene  $C_{10}H_{16}$  which is a terpene.

Additionally should be mentioned that the efficiency of all these solvents generally can be increased by heating them before they are mixed with crude oils [4].

## **7.2 Electromagnetic and Magnetic Methods**

Another idea to reduce the wax precipitation and deposition is the use of magnetic fields. The technique is also known as magnetic fluid conditioner. Polar molecules like asphaltenes are influenced by magnetic fields via the Lorentz forces. Since paraffin is non-polar the exact interaction between magnetic field and paraffin molecules is difficult to explain, but the magnetic field induces weak magnetic dipoles in the paraffin molecules which create a repulsion force between the paraffin molecules and hence hinder the agglomeration of the paraffin molecules so that less depositions can form on the pipe walls. The more polar molecules are in the crude oils, the higher is the impact of this method but unfortunately the mechanism is still not entirely understood. Labor tests with synthetic paraffin showed a time dependent viscosity reduction of samples which did undergo a magnetic treatment. Using a scanning electron microscope (SEM) it is possible to observe the change of the crystal form, as can be seen in Fig. 7.3. An interesting fact is that even though a change in the viscosity and the crystal form was observed, no change in the WAT or pour point due to a magnetic treatment could be measured.

Nevertheless a few successful field applications have been installed and tested. The main advantage of this method is it being much cheaper than continuously adding inhibitors to the crude oils [31].

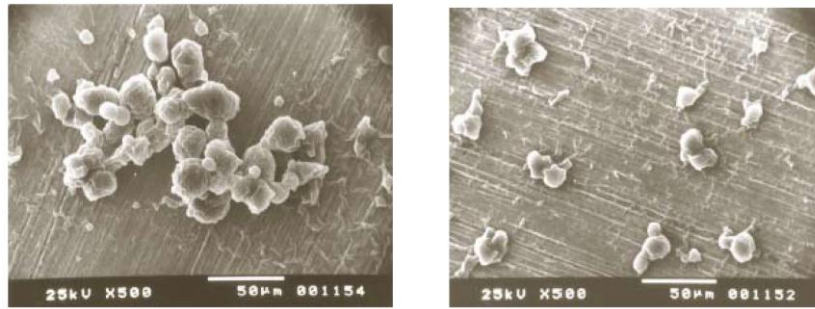


Fig. 7.3: Paraffin crystals before (left) and after (right) magnetic treatment [5]

## 7.3 Mechanical Methods

### 7.3.1 Pigging

The so called "pigs" are devices which are sent through pipelines for cleaning, sealing or simply to inspect them. In general pigs are solid insoluble plugs that are pushed through the pipeline by the flow of the transported crude oil. Their purpose is to remove the soft deposits on the pipe walls with brushes or blades attached to them. The faster a pig runs through a line the higher is the cleaning impact but only a thin layer of the deposits is removed. The scraped off deposits are pushed in front of the pig through the line, if the part of the pipeline which is pigged is too long or the scraped off material is too much, it can plug the line and the pig gets stuck. In this case chemicals have to be used to clean the plug away, when even that is not possible anymore the line has to be abandoned.

To avoid such a scenario the part of a pipeline which is pigged should not be too long and the pig should have the right diameter. In the case of a thick layer of deposits many pigs with increasing diameter should be used that the layer of removed material is thin enough that this material cannot block the line in the chosen length.

If the deposits are very hard, simple pigs may not be sufficient to remove them hence more complex methods have to be used, e.g. with high pressure water jets. Such a system is very effective but cannot be used for longer pipelines because of the limited length of the supplying hoses with the attached cleaning head. When facing a thick layer of deposits even with this method several runs might be required to clean the whole layer away without blockade of the line.

Another technique is the hydraulically activated power pig as pictured in Fig. 7.4, this technology uses the transported fluid to clean the depositions away. Thanks to the brake system the pig can go up to 60 times slower than the fluid velocity and since the whole transported fluid can bypass the device through the jets. This means the slower the pig goes the stronger the jets become. Another advantage of the HAPP is that it only needs one cleaning run and does not get stuck because the removed deposits are immediately flushed away so that no plug can form in front of the pig.

Whatever pigging method is used pipelines should be cleaned this way at regular intervals to avoid pressure loss and other problems which can result in plugged lines [5] [32].

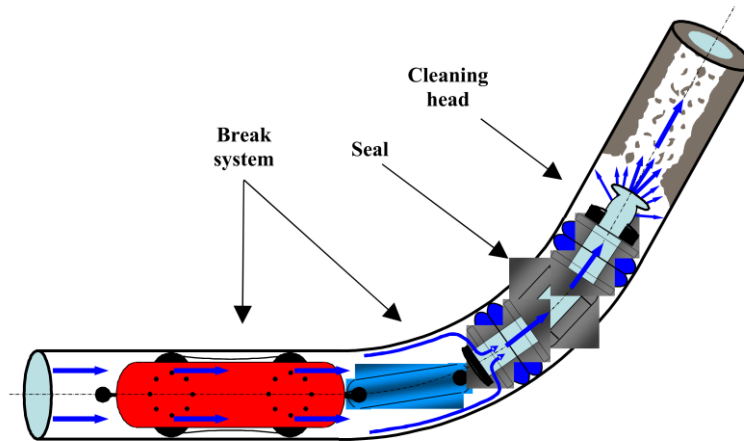


**Fig. 7.4:** *Hydraulically activated power pig HAPP (uses high pressure fluid jets to remove dispositions) [32]*

### 7.3.2 Scraping

Unfortunately it is not possible to use the previously described pigs in the tubing of a well, because both ends of a pigged pipe have to be accessible, to insert and retrieve the pig. Hence other ways to remove the depositions mechanically have to be considered and similarly to pigging here are many different variants of scrapers available. One of the easiest methods is mostly applied when a sucker rod pump is used to bring the crude oil from the reservoir to the surface because the scraping devices can be mounted on the sucker rods (see Fig. 7.5). Since the sucker rod moves up and down in the tubing, the blades of the scraping devices scrap off all kind of depositions like wax, salt, scale and dirt from the pipe walls. The advantages of this technique are that no additional drive is needed, it does not require as much resources and energy as other methods like e.g. hot oiling (see section 7.5.1), the scraping is independent to temperature and to the depth of the pump. To enhance the performance of the scrapers a sucker rod rotator can be installed, this device rotates the sucker rod and hence the scrapers on it by a fraction of one revolution each upstroke.

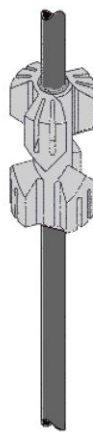


**Fig. 7.5:** *Scrapers mounted on a sucker rod [5]*

But problems can occur when scraped off particles fall down and plug the tubing or the perforations at the bottom of the wellbore, though these things can also happen when thermal methods are used to remove wax depositions [5] [33].

## **7.4 Microbial Methods**

Crude oils consist of hydrocarbons and are consequently organic substances, therefore microbes which can digest long-chained hydrocarbons can be used to break the long hydrocarbon molecules in shorter ones which do not form wax depositions. This leads also to less wax depositions on the pipe walls and a lower viscosity of the crude oil during production and transportation. But the use of these microbes is limited, they cannot withstand temperatures higher than 120 °C, the problem here is that the ambient temperature of reservoirs can be much higher. Also the microbes do not survive in sour ambiances, which is bad if the crude oil contains hydrogen sulfide (H<sub>2</sub>S). The microorganisms need water to propagate and live and therefore they cannot move very fast away from the wellbore if the water cut is too low, in that case they are produced back up to the surface along with the crude oil. Hence the microbes have to be injected with a certain amount of water in reservoirs with too low water cut [5] [30].

## **7.5 Thermal Methods**

It is obvious to use heat to melt and hence remove troublesome wax depositions in the tubing and downhole in the wellbore, but the big challenge is to get the heat to the place where it is needed. Some of the different approaches that can be used for this purpose are described below.

### **7.5.1 Hot Oiling**

The method of hot oiling is very simple, some of the earlier produced oil is stored in tanks for hot oil treatments of the well. This oil is heated above the ambience temperature of the reservoir and then it is poured down the annulus which is the space between the tubing and the casing where it heats the tubing and the wax depositions on the tubing walls. The melted wax and the tank oil used for the treatment are produced to the surface along with the crude oil from the reservoir. This process is sketched in Fig. 7.6. To enhance the dissolving process of the melted paraffin wax in the crude oil paraffin dispersants can be added. Since a lot of energy is needed to heat the big amounts of oil which are used for a hot oiling job, this method is quite expensive. Hot oiling jobs should not be done when large quantities of wax depositions are present in the tubing, because heated parts of the depositions may fall down and plug the tubing completely.

Of course it possible to use hot water or hot steam instead of crude oil to melt away the disposed wax. Water has a higher heat capacity than oil and does not contain paraffin molecules which can crystallize and plug the pores of the formation but on



the other hand if it is not filtered other impurities can plug the pores of the formation and water can cause corrosion. If hot water is used instead of hot oil the treatment is called hot watering. Hot steam is often utilized to melt wax which plugs the pores in the formation material near the wellbore. Naturally like hot water, hot steam can cause corrosion.

To decide if hot oil or hot water should be used for a wax deposition removal maintenance job, the heat capacity, the potential for formation damage and chemical properties should be taken into account [4] [5].

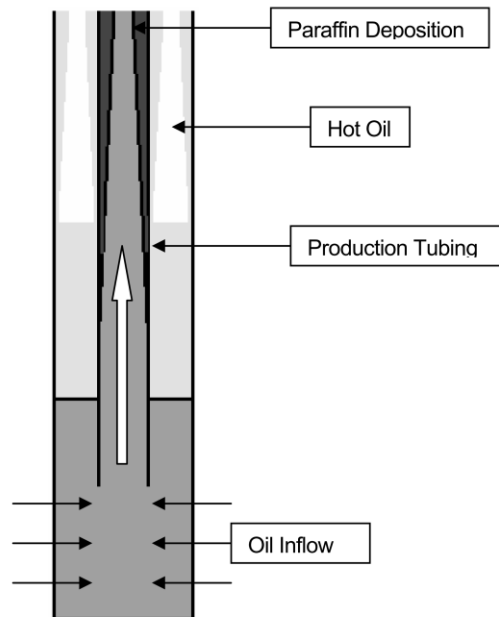


Fig. 7.6: Hot oiling [5]

### 7.5.2 Downhole Heater

A downhole heater is mostly an electrical resistance heater which is lowered to the bottom of the wellbore or attached to the side of the tubing (Fig. 7.7). The purpose of such a device is to heat the crude oil before it enters the wellbore and the tubing. Additionally this method ensures that the pores near the wellbore are not plugged with precipitated wax.

To prevent the crude oil from coking it should not be heated too high, to achieve that an automatic downhole heater can be installed, the principle of such a device is that the heating power is dependent on the downhole temperature. The resistance of the heater increases with the temperature hence the heating will be lower, so a temperature value can be preset that the crude oil cannot be overheated.

This method cannot avoid the wax precipitation on the tubing walls and like most methods used to reduce the wax problem during production and transportation it is very expensive due to the high power consumption of the device [5].

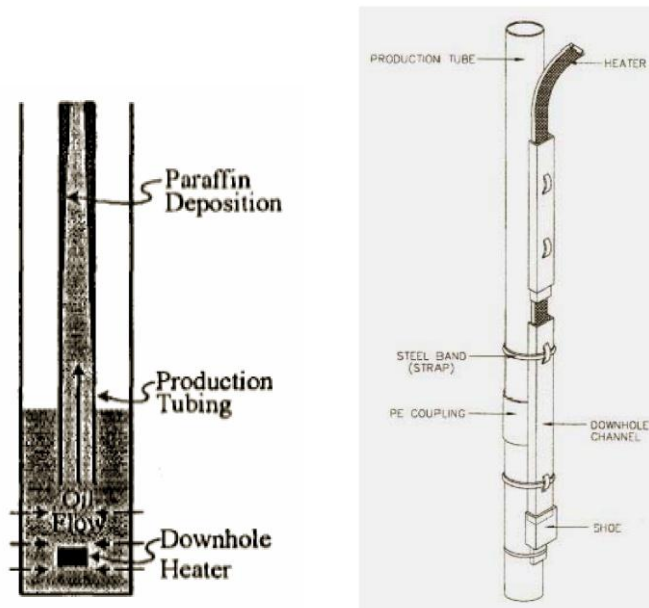


Fig. 7.7: Downhole heater [5]

### 7.5.3 Thermal Insulation

To prevent the paraffin in the crude oils from precipitating and disposing on the tubing walls, thermal insulation can be used. One approach is to use vacuum jacketed tubing pipes, these pipes are double-walled and the annulus between the two walls is evacuated. Such a design has two main advantages, the first is that the tubing can be very thin and hence the casing diameter can be kept as small as possible. The second advantage of such tubing pipes is their excellent thermal insulation. The heat loss of the crude oil on the way up to the surface during production is much less as when not insulated tubing pipes are used [5].

Another approach to the problem of the heat loss in the tubing during production is to insulate the annulus between tubing and casing because the most heat is lost due to heat convections in the annulus. The insulation fluids should not only be selected because of their thermal conductivity. Even though fluids like crude oil or diesel have a thermal conductivity of about 2.5 % of that from water they can transfer as much heat as water under the same temperature gradient. The viscosity of the insulation fluid has to be increased to lower the heat losses due to thermal conductivity. Hence gelled fluids can be used to insulate the annulus between tubing and casing to reduce the paraffin wax deposition on the inner tubing walls [34].

In general thermal insulation is more economic than chemical methods, because the insulation is an investment that has to be made just once while chemical additives have to be added continuously.

## 7.6 Thermochemical Methods

To remove downhole wax depositions thermochemical methods which are exothermal reactions can be used to produce the required heat to melt the wax depositions

exactly where it is needed. Of course it is also possible to use hot steam to melt away the depositions, but a lot of heat energy is wasted in the cooling process on the way down to the bottom of the wellbore. Consequently a lot of energy can be saved if the heat is created downhole by a chemical reaction.

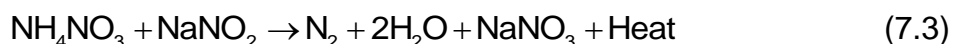
One example for such an exothermic reaction is the neutralization of acetic acid with sodium hydroxide which produces sodium acetate, water and of course heat, the reaction equation reads as follows:



But unfortunately this reaction cannot be delayed and often causes additional corrosion. There are many other and many better controllable reactions which can be used for this purpose but the two most commonly used are the reaction between ammonium chloride and sodium nitrite:



And the reaction between ammonium nitrate and sodium nitrite:



The reactions described in the reaction equations (7.2) and (7.3) are controlled by the pH-value of the solution in which the two starting components are dissolved. The higher the pH-value the slower is the reaction and the other way round. Normally the interval of this pH-value is between 5 and 8. Thermochemical methods using acids should not be used in calciferous formations because unwanted chemical reactions are possible in such formations.

It should also be considered, that this method is not economical for small and low producing wells due to the fact, that it is more expensive than hot oiling jobs [4] [5].

## 7.7 Ultrasonic Waves

Another method to reduce the wax problem in the tubing during production is the use of ultrasonic waves. The apparatus utilized to reduce the paraffin wax consists of one or more ultrasonic wave generators attached to the outer surface of the tubing. The frequency ranges of these ultrasonic wave generators are from 10 kHz to 500 kHz. Three frequencies have been found which have an impact on the paraffin wax:

1. The first frequency is the characteristic frequency of the production tubing, this frequency sets the production tubing vibrating and thus prevents the paraffin molecules from adding to the surface.
2. The second frequency breaks the wax and the wax depositions up into smaller particles because it breaks the bonds which hold the paraffin molecules together.

3. The third frequency breaks the paraffin molecules themselves into smaller pieces and the so formed shorter paraffin molecules do not precipitate and hence cannot cause problems in the form of wax depositions.

The ultrasonic wave generators can broadcast at one or all three of these frequencies, whatever frequency has no or not the desired effect therefore has not to be used [35].

## 8 Rheology Fundamentals

Rheology is the science of the deformation and the flow of substances. It is interdisciplinary and hence as well a branch of physics and physical chemistry as of mechanics. Rheological investigations range from the flow behavior of ideal viscous substances to the deformation of ideal elastic solids. All real substances have both a viscous and an elastic part, therefore their behavior is called viscoelastic and it is somewhere between the two extremes described before [36].

### 8.1 Viscosity

#### 8.1.1 Two Plates Model

To describe viscosity two parallel plates with a fluid between them are used (see Fig. 8.1 (a)). The lower plate is fixed and does not move thus it has the velocity  $v = 0$ . The upper plate has the (shear) area  $A$  and is moved through the (shear) force  $F$  with the velocity  $v_{max}$ . In the gap between the two plates with the height  $h$ , the fluid is sheared. It is assumed that the fluid sticks to the plates and does not glide and that the flow conditions are laminar, which means that the flow appears in layers (see Fig. 8.1 (b)). The layers are infinitesimal thin ( $dh$ ) and the velocity of each layer is higher by an infinitesimal element  $dv$  than the velocity of the layer below.

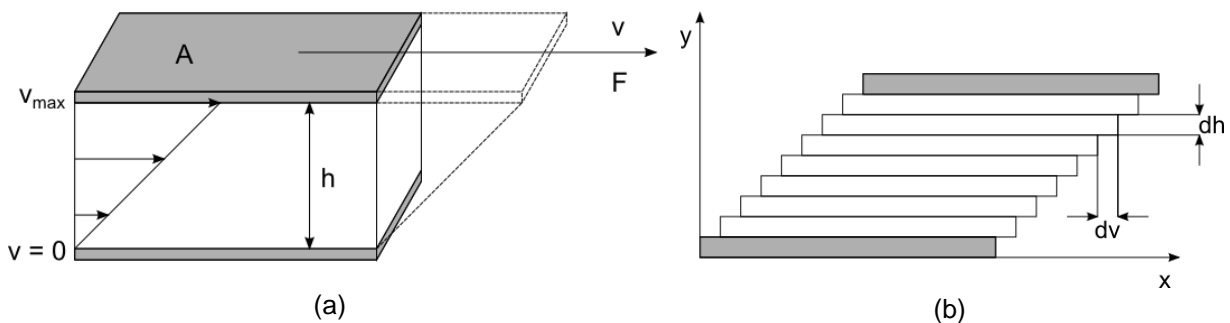


Fig. 8.1: Two plates model, two plates with the sample between them

The shear stress  $\tau$  of the fluid has the unit [Pa] (Pascal) which is also the unit of the pressure.

$$\tau = \frac{F}{A} \quad (8.1)$$

The velocity gradient from the upper plate to the lower plate is called shear rate, it has the unit [1/s] and is described in the following equation:

$$\dot{\gamma} = \frac{dv}{dh} \quad (8.2)$$

Using the assumptions made at the beginning of this section it can be said that the velocity decreases linearly from the upper to the lower plate and if the thickness of the single layers  $dh$  is assumed as constant, consequently  $dv$  and hence the shear rate is constant too.

$$\dot{\gamma} = \frac{dv}{dh} = \frac{v_{\max}}{h} = \text{const} \quad (8.3)$$

The flow resistance due to the friction forces between the molecules of a flowing fluid is called viscosity. All substances with more or less distinct flow ability are referred to as fluids, which are generally liquids and gases.

For an ideal viscous fluid and constant temperature the shear viscosity<sup>3</sup> can be written as:

$$\eta = \frac{\tau}{\dot{\gamma}} \quad (8.4)$$

The viscosity  $\eta$  has the unit [Pas] (Pascal second) but for low viscous substances it is common to use [mPas]. The correlation (8.3) and (8.4) can be used for diverse measuring systems but it has to be kept in mind that this relation is only valid under the mentioned assumptions.

If the density  $\rho$  is taken into account this leads to the kinematic viscosity:

$$\nu = \frac{\eta}{\rho} \quad (8.5)$$

This value is of interest when capillary viscometers, falling sphere viscometers or viscosity cups are used for measurements [36].

### 8.1.2 Newtonian Fluids

Ideal viscous (Newtonian) fluids can be described with the equation (8.4), the viscosity of such liquids is not dependent on the shear rate while the shear stress has a linear relation with the shear rate which can be seen in Fig. 8.2. Therefore ideal viscous fluids are often measured with viscosity cups, capillary viscometers or falling sphere viscometers. But the results obtained with these measuring systems cannot really describe the complex behavior of non-Newtonian fluids.

The biggest factor influencing the viscosity of an ideal viscous fluid is the temperature. The viscosity of nearly every fluid increases with decreasing temperature that is because the molecules are slower when they are cooled down. In crude oils the main factors which are responsible for the higher viscosity at lower temperatures are fric-

<sup>3</sup> The shear viscosity  $\eta$  is often just called viscosity

tion forces between the crystals that form when the crude oil is cooled under the WAT.

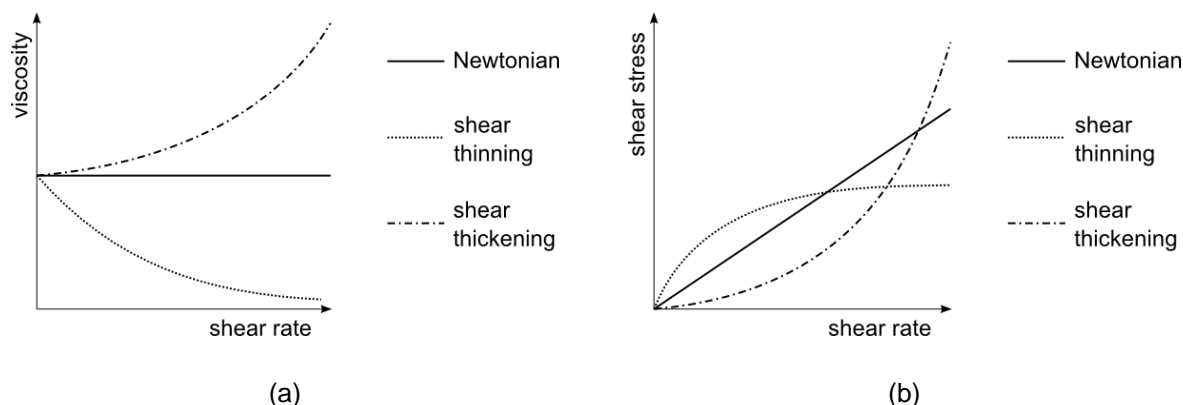


Fig. 8.2: (a) *viscosity over shear rate*; (b) *shear stress over shear rate*

### 8.1.3 Non-Newtonian Fluids

As mentioned in the previous section the viscosity of Newtonian fluids is temperature dependent but if the viscosity of a substance is also influenced by other factors like shear rate and shearing duration, it is called non-Newtonian.

#### 8.1.3.1 Shear-Thinning (Pseudoplastic) Behavior

When the viscosity decreases with increasing shear rate, this behavior is called shear thinning. When looking at equation (8.4) and Fig. 8.2 it can be seen that the shear stress is a function of the shear rate  $\tau(\dot{\gamma})$  which is non-linear if  $\eta$  is not constant. Some examples of shear thinning substances are lacquer, shampoo, blood, wallpaper paste and crude oil. One reason for this behavior is that the long-chained and unbranched molecules are entangled to themselves and form spherical structures. When they are sheared they justify in shear and shear gradient direction whereby they disentangle to some extent which lowers the flow resistance. In low concentrated polymer solutions almost entire disentanglement is possible. Other substances with shear thinning behavior are dispersions like e.g. suspensions or emulsions. In suspensions particle agglomerations degrade to their primary particles due to high shear stress and the dispersion fluid can flow again. In emulsions, if at rest, the dispersed droplets have a spherical shape because they tend to minimal surface energy, when sheared the droplets are deformed to ellipsoids in shear direction so that they have a smaller cross section and hence a lower flow resistance.

#### 8.1.3.2 Shear-Thickening (Dilatant) Behavior

Here the viscosity increases with increasing shear rate, consequently  $\tau(\dot{\gamma})$  is a non-linear function of  $\dot{\gamma}$  (Fig. 8.2). In most technical applications shear thickening behavior is not wanted because it always means, that problems occur in the flow process. In comparison with shear thinning, shear thickening behavior appears rarely in industrial applications and is mostly unwanted apart from e.g. dental filling. This effect can

be explained through the entanglement of polymers which are branched and hence inflexible, because of high shear rates the molecules constrain themselves so that they cannot slide from each other. But there are also suspensions with shear thickening behavior which can be explained with the structure of the dispersed particles. When at rest for instance cube-shaped or rod-shaped particles need less space as when they rotate because of shearing of the fluid, so there is less free space between the particles and consequently the flow resistance increases.

### 8.1.3.3 Time Dependent Behavior with constant Shear Rate

The decrease of the viscosity of a substance while sheared with a constant shear rate and the re-increase of the viscosity during the subsequent recovery (relaxation) is called thixotropy. If a substance does not recover even a long time after the shear stress is stopped, the inner structure of the substance is irreversibly changed or destroyed and it is called non-thixotropic.

The increase of the viscosity of a substance while sheared with a constant shear rate and its following decrease in the recovery phase on the other hand is the rheopectic behavior.

Both thixotropic and rheopectic behavior can be seen in Fig. 8.3 [36].

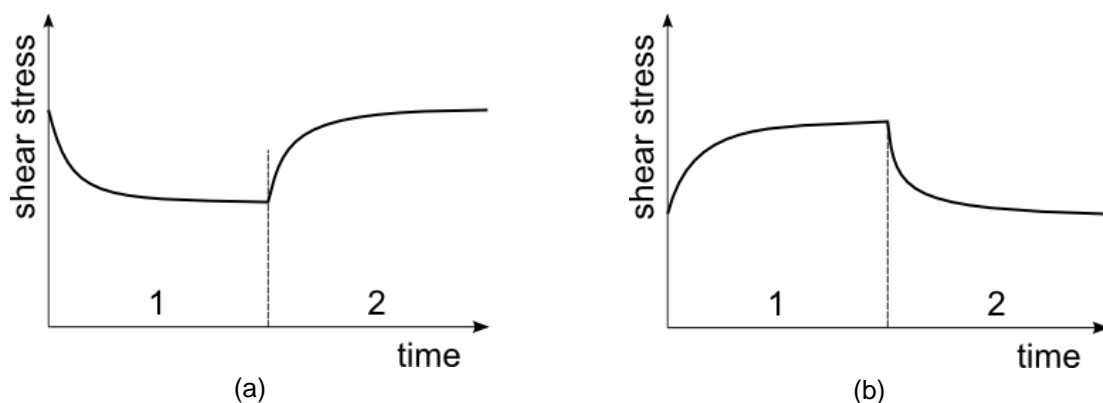


**Fig. 8.3:** Viscosity over time: (a) thixotropic behavior 1) region of constant shear, rate 2) recovery; (b) rheopectic behavior 1) region of constant shear rate, 2) recovery

## 8.2 Rheological Models

Most substances can be classified somewhere between ideal viscous fluids and ideal elastic solids, that means real substances have a viscoelastic behavior which is a mixture of viscous and elastic behavior. These three models are described below.

### 8.2.1 Ideal Viscous Behavior

This model is used to describe Newtonian fluids like water and crude oil at a sufficient high temperature. When such a substance is stressed, it deforms which can be observed as flow. Such a deformation is irreversible, which means that the substance stays deformed even after removing the stress. The reason for this is that the defor-



mation energy dissipates as heat energy due to the friction between the stressed molecules, this process is called shear heating.

Ideal viscous behavior can be described by a simple damper as pictured in Fig. 8.4 (a). As long as the piston is pushed it moves because the fluid bypasses the piston through the annulus between piston and cylinder. When the force stops the piston stands still and does not move anymore because the whole deformation energy is converted into frictional heat and is therefore lost for the fluid. Newton described this behavior with the following equation:

$$F = C_N \cdot v = C_N \cdot \dot{x} \quad (8.6)$$

$F$  = the force affecting the piston

$C_N$  = the damper constant

$\dot{x}$  = the velocity  $v$  of the piston or rather the time differential of the distance  $x$  covered by the piston

Equation (8.6) looks like  $\tau = \eta \cdot \dot{\gamma}$  the transformed equation (8.4) if the shear stress  $\tau$  corresponds to the force  $F$ , the viscosity  $\eta$  to  $C_N$  and the shear rate  $\dot{\gamma}$  to  $v$  [36].



Fig. 8.4: (a) Newtonian model (damper), (b) Hookean model (spring)

### 8.2.2 Ideal Elastic Behavior

To describe the elastic behavior of a substance, its deformation  $\gamma$  in the shear gap between the two plates (see Fig. 8.5) has to be defined:

$$\gamma = \frac{s}{h} = \tan \varphi \quad (8.7)$$

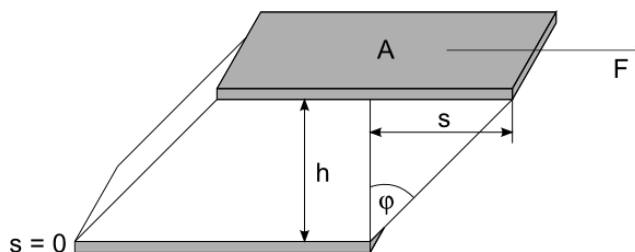


Fig. 8.5: Two plates model for ideal elastic behavior

The deformation  $\gamma$  is also the time differential of the shear rate which is therefore also called deformation velocity.

$$\dot{\gamma} = \frac{d\gamma}{dt} = \dot{\gamma} \quad (8.8)$$

For ideal elastic solids the relation between shear stress  $\tau$  and deformation  $\gamma$  is a material constant if it is measured in the reversible elastic deformation range or the linear-elastic range. This material constant is called shear modulus and is defined as follows:

$$G = \frac{\tau}{\gamma} \quad (8.9)$$

The behavior can be described by the Hookean law  $\tau = G \cdot \gamma$  which is the transformed equation (8.9). Examples for so called Hookean solids are e.g. stones and steel. The applied deformation energy is completely stored in ideal elastic solids during the deformation and when the material is relieved the whole stored energy is used to reverse the deformation, this means the deformation of ideal elastic solids is completely reversible when it is in the linear elastic range. If the deformation is not in this range, the material fractures brittle without any sign of a creep behavior.

A simple model to describe Hookean solids is a Hookean spring (Fig. 8.4 (b)), because when pulled with a certain force the spring deforms and when released it goes back to its original position.

$$F = C_H \cdot s \quad (8.10)$$

$F$  = the force affecting the spring

$C_H$  = the spring constant

$s$  = the spring travel

If this equation is compared to the Hookean law the force  $F$  corresponds to the shear stress  $\tau$ ,  $C_H$  to the shear modulus  $G$  and  $s$  to the deformation  $\gamma$  [36].

### 8.2.3 Viscoelastic Behavior

The most real substances are viscoelastic (VE), this means they show simultaneously viscous and elastic behavior. Such substances display a timely delayed response to applied load as well as to relieved load. It has to be differentiated between VE-fluids and VE-solids.

#### 8.2.3.1 VE-Fluids – Maxwell Model

This behavior can be described by a serial connection of a damper and a spring as shown in Fig. 8.6 (a). Under load at first the spring is suddenly deformed elastic, till it

reaches a constant displacement proportional to the force, not until then the piston of the damper starts to move and does not stop as long as the constant force is applied. As soon as the force stops, the spring goes back to its original state suddenly but the damper piston stays where it is, which means that the deformation process is irreversible because it does not go back to its original state after load relieving. That is why the substance basically behaves like a fluid (Maxwellian liquid).

With the assumptions that the shear stress of the viscous component and of the elastic component are the same  $\tau = \tau_v = \tau_e$  and that the total deformation is a sum of the viscous and the elastic deformation  $\gamma = \gamma_v + \gamma_e$ , using equation (8.8) the Maxwell differential equation reads as follows:

$$\dot{\gamma} = \dot{\gamma}_v + \dot{\gamma}_e = \frac{\tau_v}{\eta} + \frac{\dot{\tau}_e}{G} = \frac{\tau}{\eta} + \frac{\dot{\tau}}{G} \quad (8.11)$$

The second term can be explained by performing a time differentiation of equation (8.9) because if  $G$  is constant this yields  $G = \dot{\tau}/\dot{\gamma}$ .

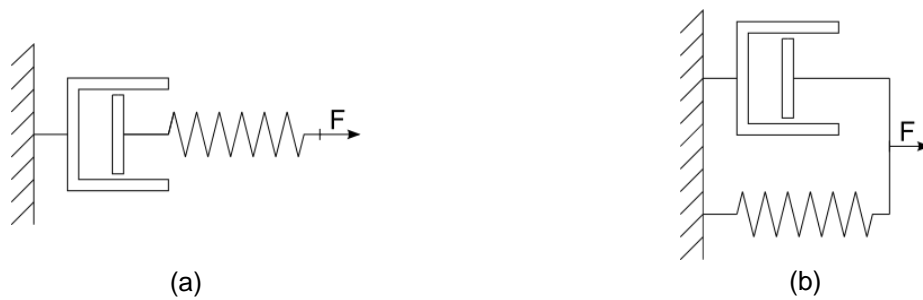


Fig. 8.6: (a) Maxwell model, (b) Kelvin/Voigt model

### 8.2.3.2 VE-Solids – Kelvin/Voigt Model

To describe this behavior a parallel connection of damper and spring is used (see Fig. 8.6 (b)). As long as loaded with a constant force both components deform, the damper and the spring can only be deformed simultaneously and in the same way, thus the spring cannot deform suddenly because it is slowed by the damper. After load relieving both, the spring and because of the connection the damper, go back to their original state. The temporally delayed but it is completely reversible, due to this behavior such substances are called VE-solids or Kelvin/Voigt-solids.

On the contrary to VE-fluids it is assumed that the shear stress of VE-solids consists of a viscous and an elastic part  $\tau = \tau_v + \tau_e$ , while the deformation as Fig. 8.6 (b) suggests is the same for both components  $\gamma = \gamma_v = \gamma_e$  or with the use of equation (8.8)  $\dot{\gamma} = \dot{\gamma}_v = \dot{\gamma}_e$ . This leads to the Kelvin/Voigt differential equation:

$$\tau = \tau_v + \tau_e = \eta \cdot \dot{\gamma}_v + G \cdot \gamma_e = \eta \cdot \dot{\gamma} + G \cdot \gamma \quad (8.12)$$

To describe real substances often a more or less complex combination of these two models has to be used [36].

## 8.3 Rheometers

The big advantage of rheometers over simple viscometers like capillary viscometers or falling sphere viscometers (a good overview of such viscometers is given by Mezger [36]) is that it is possible to preset the shear stress as well as the shear rate and apart from that also the temperature can be controlled and measured.

### 8.3.1 Rheometer Measurement Systems

Normally the measuring system (plate, cone or cylinder) is rotating or oscillating and the lower part of the rheometer (plate or hollow cylinder) is fixed<sup>4</sup>, rarely is it the other way round. To measure Newtonian fluids or VE-fluids rotational tests are used and to measure Hookean solids or VE-solids oscillation tests are performed.

#### 8.3.1.1 Plate-Plate System

The plate-plate measuring has a very simple geometry as can be seen in Fig. 8.8 (a). The gap between the two plates which is filled with the sample, the height  $h$  of the gap is adjustable, in most cases 1 mm is used, bigger values of  $h$  are necessary if suspensions with large solid particles are measured. The height of the gap  $h$  should be 5 or better 10 times bigger than the maximum particle size in the sample, so that they do not disturb the flow during the measurement but  $h$  should be kept as small as possible to avoid inhomogeneous shear behavior.

A disadvantage of this measuring system when performing rotational tests is that  $\gamma$  and hence  $\dot{\gamma}$  (see equation (8.8)) are not constant over the whole radius, because the velocity of a circle is the angular velocity or angular frequency  $\omega$  multiplied by the radius of the circle  $v = \omega \cdot r$ , that means  $v$  increases with increasing  $r$ . When performing oscillation tests the problems of the not constant shear rate over the whole radius and a big height of the gap are not so critical if small deformation amplitudes within the LVE range (see 8.3.3.2) are used.

#### 8.3.1.2 Cone-Plate System

This system uses a rotating cone instead of a plate as pictured in Fig. 8.8 (b), the angle  $\phi$  of the cone shall not be bigger than  $1^\circ$ . The main advantage of this measuring system is that the shear rate in the gap is constant and not dependent on the radius as showed in the following equation:

$$\dot{\gamma}(r) = \frac{v(r)}{h} = \frac{\omega \cdot r}{y} = \frac{\omega \cdot \chi}{\chi \cdot \tan \phi} = \frac{\omega}{\tan \phi} \quad (8.13)$$

Fig. 8.7 should help to explain equation (8.13).

<sup>4</sup> That kind of rheometer was used for this thesis.

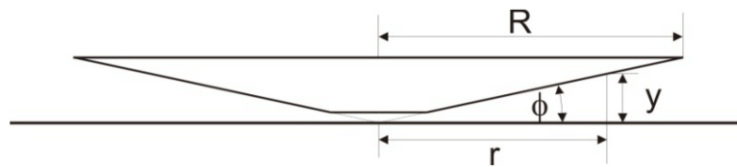


Fig. 8.7: Sketch of the cone plate measuring system [4]

To achieve constant shear rate over the whole radius, the cone point would have to touch the lower plate which would result in friction between the plate and the cone, to avoid such a scenario the cone point of such measuring systems is cut off. The gap height between the lower plate and the cut off cone point is much smaller than of the plate-plate system. Since the gap cannot be varied, because then the shear rate would not be constant any more, suspensions with particles that are bigger than a fifth or better a tenth of this gap should be measured with the plate-plate system.

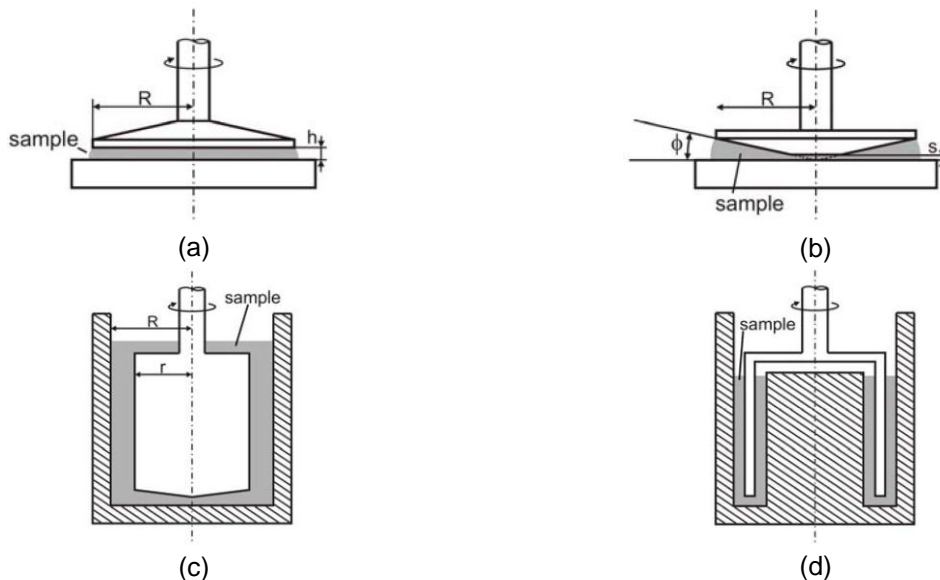


Fig. 8.8: Measuring systems: (a) plate-plate, (b) cone-plate, (c) cylinder, (d) double gap [4]

### 8.3.1.3 Cylindrical System

The cylindrical measuring system consists of a cup that contains the sample and is commonly fixed while the concentric measuring cylinder which is lowered in the cup rotates (see Fig. 8.8 (c)). Due to its geometry the cylindrical system has the big advantage that low viscous samples cannot flow out of the measuring gap when heated or sheared. But on the other hand, the needed sample quantity is relatively big and the cleaning process is time-consuming.

### 8.3.1.4 Double Gap System

For very low viscous samples a double gap system can be used, which has twice the shearing surface and hence nearly twice the torque of a cylindrical system. As shown in Fig. 8.8 (d) a cylinder is mounted in the middle of the cylindrical cup, the annulus between the cup wall and the cylinder wall contains the sample. The hollow cylinder

which can rotate or oscillate is lowered in this annulus and has contact to the sample on its outer and inner wall [36].

### 8.3.2 Rotational Tests

Since the torque of the measuring system depends on the angular frequency  $\omega$  and the viscosity of the sample  $\eta$  can be determined if  $\omega$  is known. The shear rate is related to the angular frequency as shown in equation (8.13) and the shear stress is related to the torque. According to equation (8.4) a certain shear stress is needed for a constant shear rate. The rheometer can either measure the angular frequency or the torque which leads to two different measuring modes:

1. CSR (controlled shear rate), using this mode the shear rate is preset and is held constant during the test while the shear stress is measured
2. CSS (controlled shear stress), here it is the other way round, and the shear stress is preset and stays constant during the whole test while the shear rate is measured.

For industrial applications like production and transportation in oil industry it is of great value to be able to control the shear rate of measuring systems to simulate actual occurring shear rates in tubings and pipelines.

### 8.3.3 Oscillation Tests

The way of measuring data acquisition is the same as for rotational tests the main difference is that the measuring system does not rotate in one direction but changes the rotation direction periodically so that the deformation  $\gamma(t)$  is normally a sine function. Again the two measuring modes are possible:

1. CSD (controlled shear deformation), this is the equivalent to the CSR of the rotational tests. The sine functions of the angle  $\varphi(t) = \varphi_A \cdot \sin(\omega t)$  or rather the deformation  $\gamma(t) = \gamma_A \cdot \sin(\omega t)$  are preset and the results are sine functions with a phase displacement of the angle  $\delta$ , which are the torque  $M(t) = M_A \cdot \sin(\omega t + \delta)$  or rather of the shear stress  $\tau(t) = \tau_A \cdot \sin(\omega t + \delta)$ .
2. CSS (controlled shear stress),  $\tau(t)$  or rather  $M(t)$  is preset and the amplitudes  $\gamma_A$  or rather  $\varphi_A$  and  $\delta$  of  $\dot{\gamma}(t)$  or rather  $\varphi(t)$  are measured.

The most common measurements performed with oscillation tests are amplitude sweeps (constant frequency and increasing amplitude) and frequency sweeps (constant amplitude and increasing frequency). In combination with those two temperature sweeps are possible too.

#### 8.3.3.1 Terminology

Again the two plates model can be used to describe the behavior of the measured substances (see Fig. 8.5), only this time the force alternates the algebraic sign periodically.

At first the complex shear modulus has to be defined:

$$G^* = G' + iG'' \quad (8.14)$$

$G'$  is the so called storage modulus which represents the stored deformation energy in the sample and consequently the elastic behavior.  $G''$  on the other hand is the loss modulus and stands for the dissipated or lost energy in the sample, it represents the viscous behavior of the sample. As can be seen in Fig. 8.9 (a) the length of  $G^*$  can be calculated with the Pythagorean Theorem:

$$|G^*| = \sqrt{(G')^2 + (G'')^2} \quad (8.15)$$

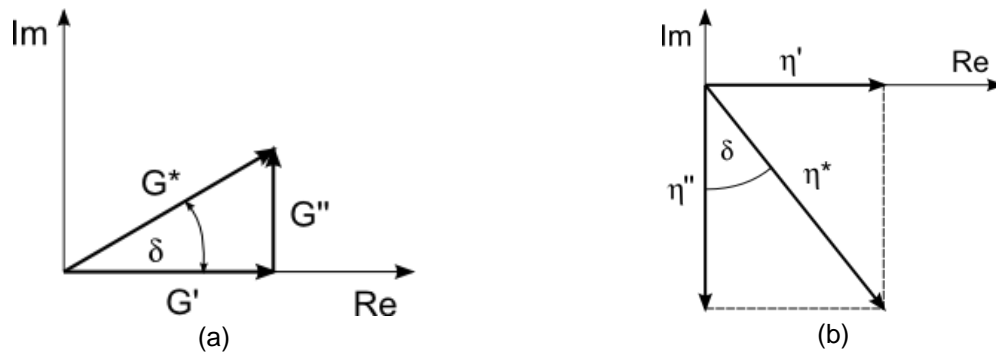


**Fig. 8.9:** (a) complex shear modulus, (b) complex viscosity

And the so called loss factor or damping factor is defined as follows:

$$\tan \delta = \frac{G''}{G'} \quad (8.16)$$

To describe viscous substances also the complex viscosity (Fig. 8.9 (b)) can be used and its length and loss factor are calculated analog to the complex shear modulus:

$$\begin{aligned} \eta^* &= \eta' - i\eta'' \\ |\eta^*| &= \sqrt{(\eta')^2 + (\eta'')^2} \\ \tan \delta &= \frac{\eta'}{\eta''} \end{aligned} \quad (8.17)$$

Of course it is possible to convert the values of the complex shear modulus to values of the complex viscosity:

$$\begin{aligned} G^* &= i\omega \cdot \eta^* \\ G'' &= \omega \cdot \eta' \\ G' &= \omega \cdot \eta'' \\ |G^*| &= \omega \cdot |\eta^*| \end{aligned} \quad (8.18)$$

If the upper plate of the two plates model is oscillating the deformation and hence the shear rate are time dependent sine functions:

$$\begin{aligned}\gamma(t) &= \gamma_A \cdot \sin(\omega t) \\ \dot{\gamma}(t) &= \gamma_A \cdot \omega \cdot \cos(\omega t)\end{aligned}\tag{8.19}$$

It should be mentioned that  $\gamma_A$  is the amplitude of the deformation and  $\omega = 2\pi \cdot f$  is the angular frequency with  $f$  being the frequency.

To explain the results measured by the rheometer written at the beginning of section 8.3.3 the ideal elastic behavior and the ideal viscous behavior have to be described using the previously discussed complex values.

The equation (8.9) of the ideal elastic behavior can now be written as follows:

$$\tau_e(t) = G^* \cdot \gamma(t) = G' \cdot \gamma_A \cdot \sin(\omega t)\tag{8.20}$$

$G''$  is zero because an ideal elastic solid has no loss modulus.

Equation (8.4) which represents the ideal viscous behavior reads as follows:

$$\tau_v(t) = \eta^* \cdot \dot{\gamma}(t) = \eta'' \cdot \gamma_A \cdot \omega \cdot \cos(\omega t) = G'' \cdot \gamma_A \cdot \cos(\omega t)\tag{8.21}$$

The  $\eta''$  or rather  $G''$  is zero because an ideal viscous substance has no storage modulus. The last step in equation (8.21) was performed by the use of (8.18).

If (8.20) and (8.21) are set into (8.12) and the phase displacement between  $\gamma(t)$  and  $\tau(t)$  is  $\pi/2$  for ideal viscous substances, this yields for the VE-behavior

$$\begin{aligned}\tau(t) &= \tau_e(t) + \tau_v(t) = G' \cdot \gamma_A \cdot \sin(\omega t) + G'' \cdot \gamma_A \cdot \cos(\omega t) \\ &= G' \cdot \gamma_A \cdot \sin(\omega t) + G'' \cdot \gamma_A \cdot \sin\left(\omega t + \frac{\pi}{2}\right) \\ &= \sqrt{\gamma_A^2 (G'^2 + G''^2)} \cdot \sin\left(\omega t + \arctan\left(\frac{G''}{G'}\right)\right) \\ &= \tau_A \cdot \sin(\omega t + \delta)\end{aligned}\tag{8.22}$$

with  $\tau_A = \gamma_A \cdot |G^*|$  and  $\tan \delta = G''/G'$ . Equation (8.22) is what is measured if the  $\gamma(t)$  is preset. But when  $\tau(t)$  is preset by the user the rheometer measures the time dependent shear rate which can be calculated analog  $\gamma(t) = \gamma_A \cdot \sin(\omega t + \delta)$ .

The loss factor  $\tan \delta$  can be used to differentiate between VE-fluids and VE-solids because since the phase displacement angle varies between  $0 \leq \delta \leq \pi/2$  for VE deformation behavior the loss factor is between  $0 \leq \tan \delta \leq \infty$ . So VE-substance can be classified as follows:



1. liquid state (sol-state):  $\tan \delta > 1$  because  $G'' > G'$
2. solid state (gel-state):  $\tan \delta < 1$  because  $G' > G''$
3. sol-/gel-crossover:  $\tan \delta = 1$  because  $G' = G''$

### 8.3.3.2 Linear Viscoelastic (LVE) Range

When using very small amplitudes logarithms of  $G'(\gamma)$  and  $G''(\gamma)$  each show a plateau value if plotted against the  $\lg \gamma$  as pictured in Fig. 8.10. This means the substance shows either the behavior of a fluid  $\tau_A/\dot{\gamma}_A = \text{const}$  if  $G'' > G'$ , the behavior of a solid  $\tau_A/\dot{\gamma}_A = \text{const}$  if  $G' > G''$  or the behavior of a gel if  $G' = G''$ . But if the deformation amplitude is so big that it is not in the LVE range of the sample anymore, the rheological fundamental laws do not count anymore, such a behavior is called non-linear. Non-linear behavior can only be calculated by approximation with complicated calculations. To avoid that, an amplitude sweep always should be done before the actual test [36].

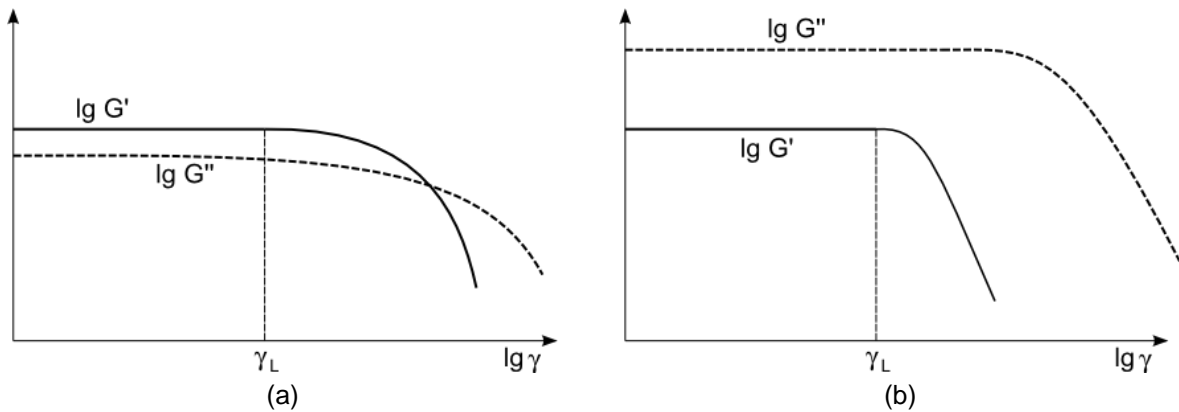


**Fig. 8.10:** LVE range: (a) sample with VE-solid behavior, (b) sample with VE-fluid behavior

# **II**

# **Experimental**

# **Part**

## 9 Thermal History Experiments

As mentioned in the theoretical part of this thesis the temperature and of course the holding time at a certain temperature of a crude oil are important factors that influence the behavior and consequently the Pour Point (PP) of such a crude oil. Therefore among other things test series with different heat pretreatment of 4 different crude oils were performed.

For reasons of clarity the following abbreviations are used for the tested crude oil samples in this and the next chapters:

Abbreviation	CHE-Number	Full denotation	Origin
BeS5old	20102025	Bernhardsthal Süd 5	Austria
BeS5	20105147	Bernhardsthal Süd 5	Austria
Sp23	20105148	Spannberg 23	Austria
Folesti 2600	20100011	Folesti Well 2600	Romania
Pecica 652	20100013	Pecica Well 652	Romania
Pecica 654	20100014	Pecica Well 654	Romania
Păcureti 90	20100015	Păcureti Well 90	Romania

**Tab. 9.1:** Full description of the crude oils used in this thesis. CHE-Number is the OMV internal numeration.

### 9.1 Pour Point Measurements

The PP is still of great value for field applications in oil industry, especially for pipelines in regions where the temperature can drop below 0 °C. Often crude oils are preheated in storage tanks before they are transported to the refinery via pipeline, hence it would be beneficial to know how different heat pretreatment influences the PP and the crystallization processes to have a maximum impact to minimal costs.

#### 9.1.1 Experimental Setup/ The Pour Point Tester (PPT)

In the OMV lab a PPT as described in section 4.1.2 is used to determine the PP of crude oils. The device used for this thesis is a Pour Point Tester 45150 from PSL Systemtechnik (Fig. 9.1 and Fig. 9.2), it heats and cools the sample via a Peltier element but the cooling process is supported by a water cooler to reach temperatures far below 0 °C. The measuring cup is filled to the mark at its inside with 35 ml of the sample. The data is recorded by a computer with the software WinPPT from PSL Systemtechnik. The PPT measures the temperature every second and the computer program records the time and the temperature which is plotted in the main window as can be seen in Fig. 9.3.

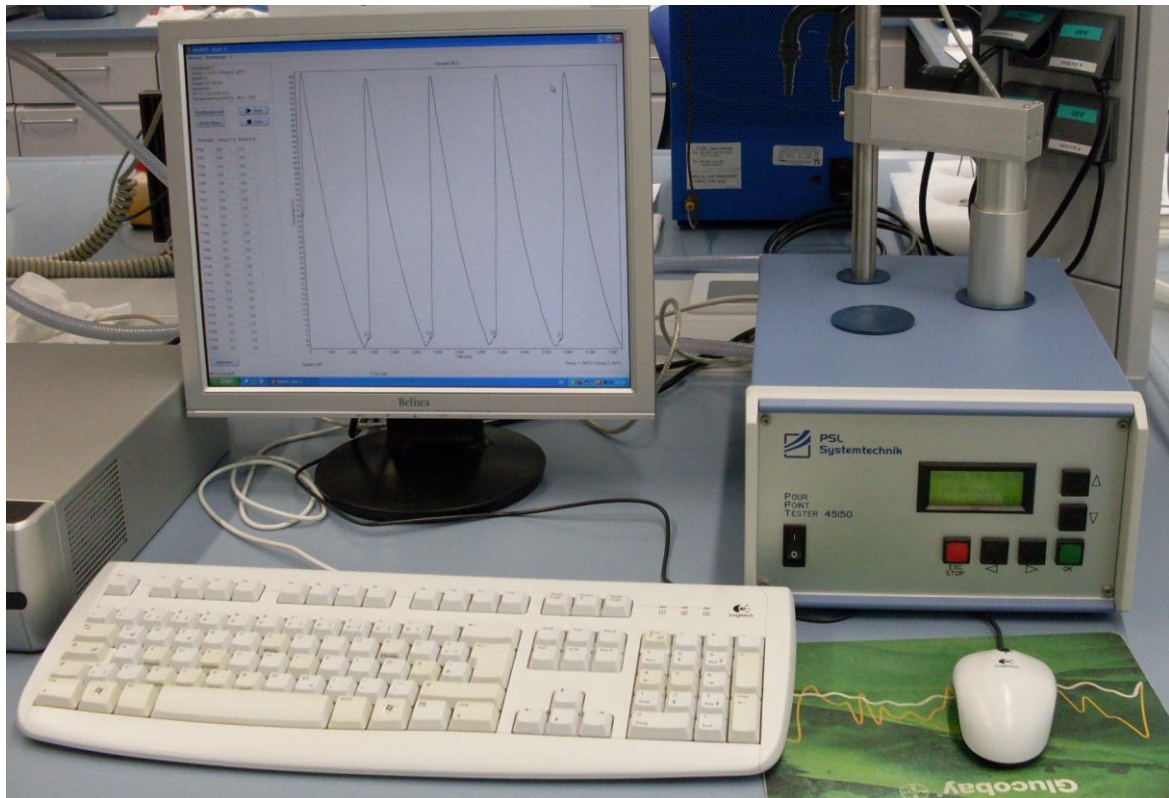


**Fig. 9.1:** PPT Setup

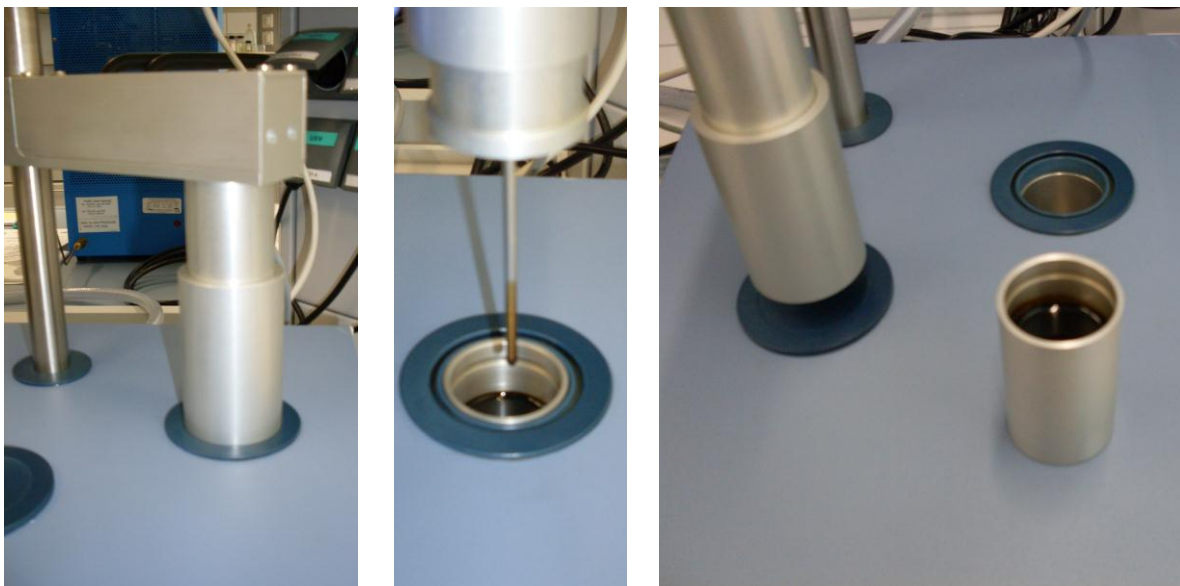


**Fig. 9.2:** PPT: measuring arm and measuring cup with sample

The temperature range of the PPT is between  $-45\text{ }^{\circ}\text{C}$  and  $150\text{ }^{\circ}\text{C}$ , the starting temperature for one PP measurement or for more PP cycles can be preset within this range but it should be  $9\text{ }^{\circ}\text{C}$  above the expected PP or at least  $45\text{ }^{\circ}\text{C}$  as mentioned before in section 4.1.2. With the WinPPT program up to 9 PP cycles in a row can be performed, which means the sample is put in the measuring cup and then the PP is measured 9 times without a sample replacement.

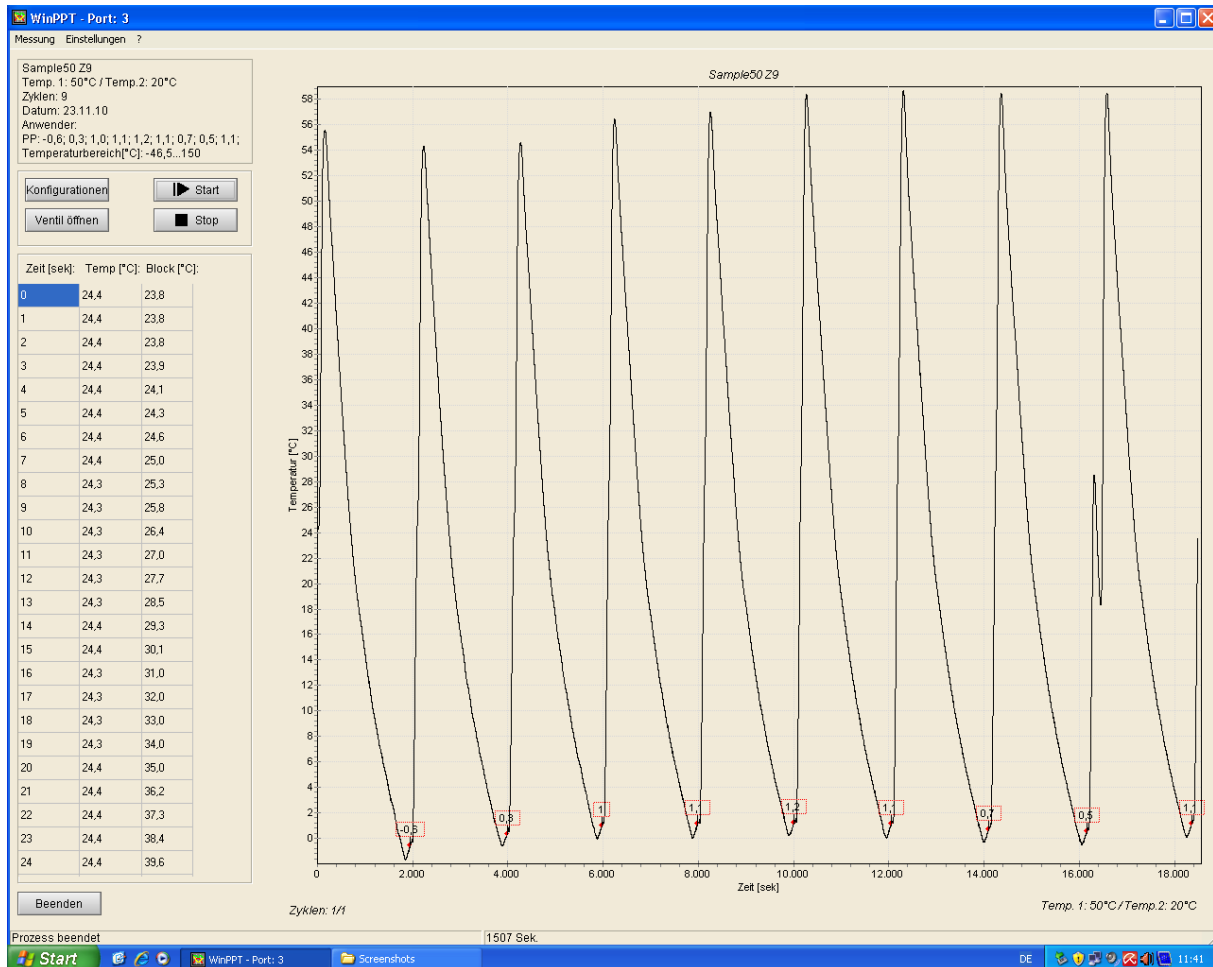


Fig. 9.3: WinPPT: measured curve of CHE20105147 Bernhardsthal Süd 5

The repeatability of the PPT measurements is 2.3 °C as stated in the ASTM Standard D 5985 [25]. Which means that the discrepancies, between the lowest and the highest PP values of several measuring cycles or single measurements (of up to 2.3 °C), are in the range of the measuring inaccuracy of the PPT. This means a PP measured with the same PPT in the same lab using the same sample has an error of up to  $\pm 1.7$  °C. Depending on the crude oil this value can be lower, but in the worst case it should only be exceeded in one out of 20 cases.

But to actually get this repeatability it is very important to always use the same pre-treatment like e.g. the temperature. Another thing that should not be disregarded, is the homogenization of the test sample especially when using a sample that has not been moved for a while and hence paraffin crystals may have accumulated at the bottom of the container. This is achieved by shaking the sample container before pouring the sample in the measuring cup or dividing it into smaller containers e.g. for heating. But heating the container to pour the crude oil out, should be avoided if it is not really necessary because this can change the crystal structure and hence the PP of the sample (as described in the following sections). The smaller vessels used for heating should also be shaken before a measurement unless it is wanted that e.g. water separates from the crude oil at the bottom and is not poured in the measuring cup with the rest.

### 9.1.2 Different Heat Pretreatment/PPT Starting Temperatures

Normally the PPT starting temperature, used in the OMV labs to measure the PP of crude oils, is 50 °C. The first measurements for this thesis were performed with this value to find appropriate samples for the planned test series, which means that the PP should not be below -5 °C because then the measurements would take too long and in some cases the PP is so low (below -35 °C) that the PPT is not even able to measure it, because the water temperature of the supporting cooling system is above 8 °C.

During these measurements it was found out that the PP of the sample BeS5old was lower, when tested after more than 24 h at room temperature, than when tested after being heated about 24 h to 55 °C. Since the WAT of this sample is about 30 °C (the WAT was determined by rheological means as described in section 3.1.6) and it is recommended to heat a sample at least 15 °C over the WAT for about 12 h, the fact that the PP measured after this pretreatment is higher than the PP without pretreatment suggests that the true WAT of this sample is even above 55 °C and that this temperature is ideal for the formation of paraffin crystals (this will be discussed later in section 9.2). Another recommendation found in most literature is that the sample can alternatively be heated to 80 °C for about 2 h, considering this leads to the expected behavior, that the PP is lower than without heat treatment.

This means with three different preheat temperatures one gets three different PP values as showed in Fig. 9.4. In this figure two other very interesting effects can be seen, the first is that a sample which is preheated to 80 °C and measured directly afterwards, has the same PP as a sample that is preheated to 80 °C and then stored at 55 °C for several hours before being tested (showed by the two lowest curves in Fig. 9.4). This means a crude oil sample with erased thermal history, which is achieved by heating it to 80 °C for a certain time (it turned out that 20 min are sufficient for BeS5old) can be stored at a far lower temperature, that has to be over the measured WAT of the sample, without a change in the PP value.

The second information that can be read out of Fig. 9.4 indicates the difference from the first of the 5 or more cycles to the following ones that appears when a preheated sample is measured directly after the heating process without letting it cool down to room temperature first. This phenomenon can be explained with the help of the crystallization (section 3.2). Directly after heating the paraffin is completely melted and dissolved in the sample or if the heating temperature is not so high the crystals are small. With decreasing temperature the crystals start to grow, agglomerate and form lattices till the PP is reached, then the sample is heated to 50 °C. But this temperature is below the true WAT (for the used sample) and the duration time at this temperature is very short (approximately 2 min), so the crystals in the specimen are more and bigger than before the first PP measurement. Since they act as nuclei for paraffin crystals during the next cooling process the crystal lattice and hence the PP is reached earlier. Depending on the preheat temperature and the crude oil the PPs after the first cycle can be constant, which means in the range of the repeatability of the PPT. They can also increase with every cycle.

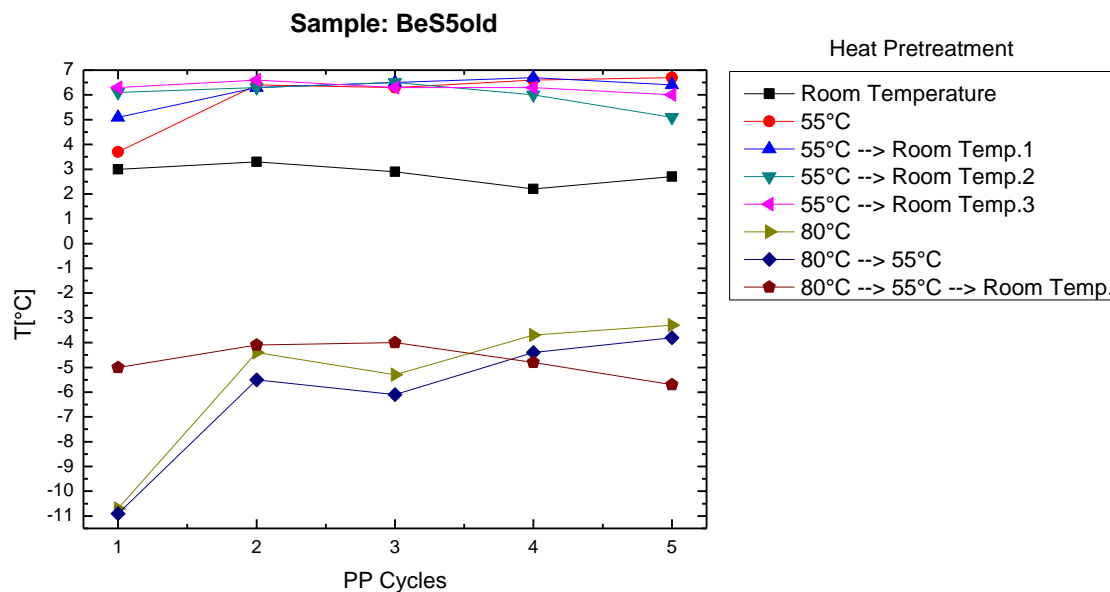


**Fig. 9.4:** *BeS5old: three different preheat temperatures*

Furthermore it has been tested if the same results can be achieved by different PPT start temperatures instead of preheating a sample in an oven or a water bath to 80°C. The first tested start temperature was 105 °C, because this temperature shall be used to determine the lower PP with the tilt method as mentioned in section 4.1.1. But since there is no pressure vessel available for the PPT and there still are small amounts of water in the crude oil samples, this water starts to boil particularly at the walls and the bottom of the measuring cup. That is because the Peltier element temperature is always kept 8 °C higher than the sensor temperature in the specimen during a heating process, thus the walls and the bottom of the measuring cup have a temperature of about 113 °C when the crude oil sample near the sensor reaches 105 °C. The problems with the boiling water are, that the steam bubbles drag along small amounts of the crude oil sample which soil the whole measuring arm (Fig. 9.2), hence the sample amount is not constant anymore and due to the high temperature some of the light end hydrocarbons vaporize which makes the PP higher again.

To avoid such problems the PPT start temperature for the following test was set to 70 °C. One sample container of BeS5old was heated to 55 °C for more than 24 h and another was left at room temperature. The curves of the two measurements are plotted in Fig. 9.5 and for comparison the measuring curve of the same sample with the same pretreatment but different PPT start temperature are plotted below in Fig. 9.6.

The test results show that for this crude oil 2 min at 70 °C in the PPT are sufficient to melt away all crystals and have therefore the same effect as 20 min in an oven heated to 80 °C. But the measuring cup of the PPT cannot be sealed air tight, thus some of the light end hydrocarbons vaporize and the results are not entirely comparable to the test results of samples preheated in an oven or a water bath. Among others the dissipation of the light ends is one reason why for the thermal history experiments in

the next section (9.1.3) a water bath and the PPT start temperature of 50 °C were used.

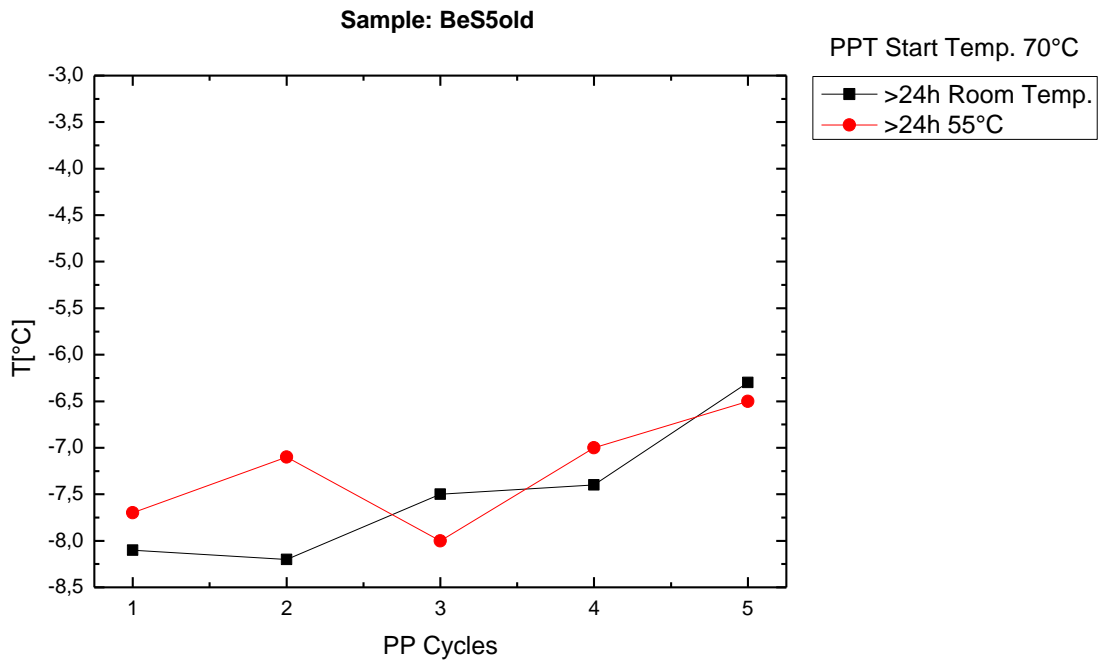


**Fig. 9.5:** Four points of BeS5old with two different heat pretreatments and 70 °C PPT start temp.

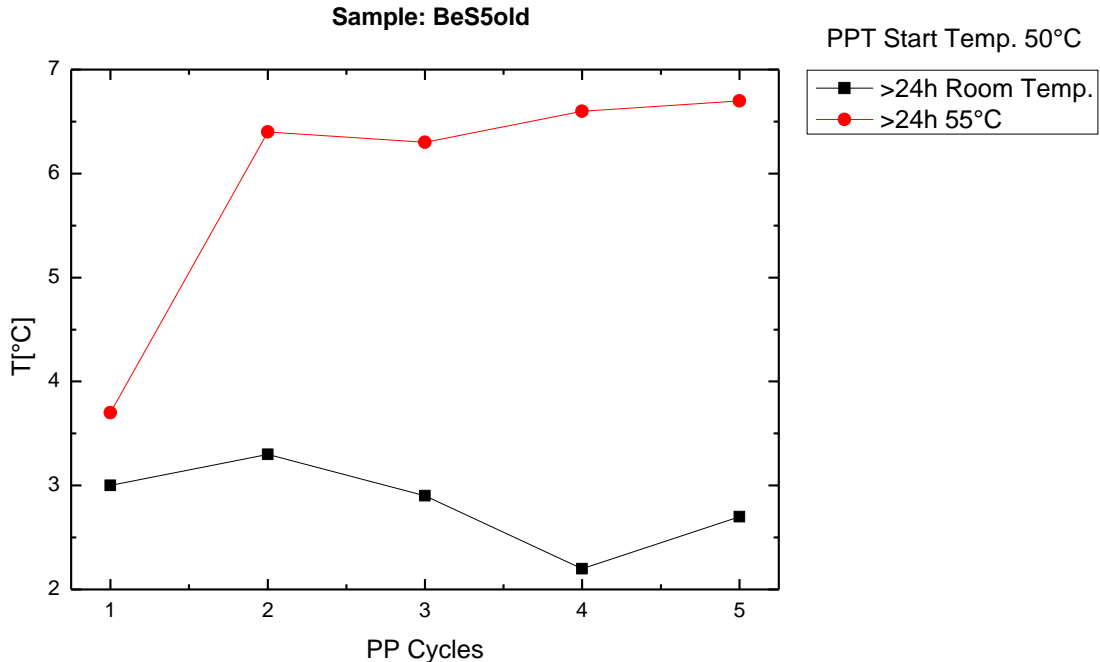


**Fig. 9.6:** Four points of BeS5old with two different heat pretreatments and 50 °C PPT start temp.

Nevertheless other PPT start temperatures and their influence on the PP were tested for BeS5old. These measurements provide results (plotted in Fig. 9.7) that are somewhat different from the ones obtained from the pretreated samples which are pictured in Fig. 9.4. For instance a PPT start temperature of 30 °C, shows similar re-



sults as when preheated to 55 °C and measured with a PPT start temperature of 50 °C.

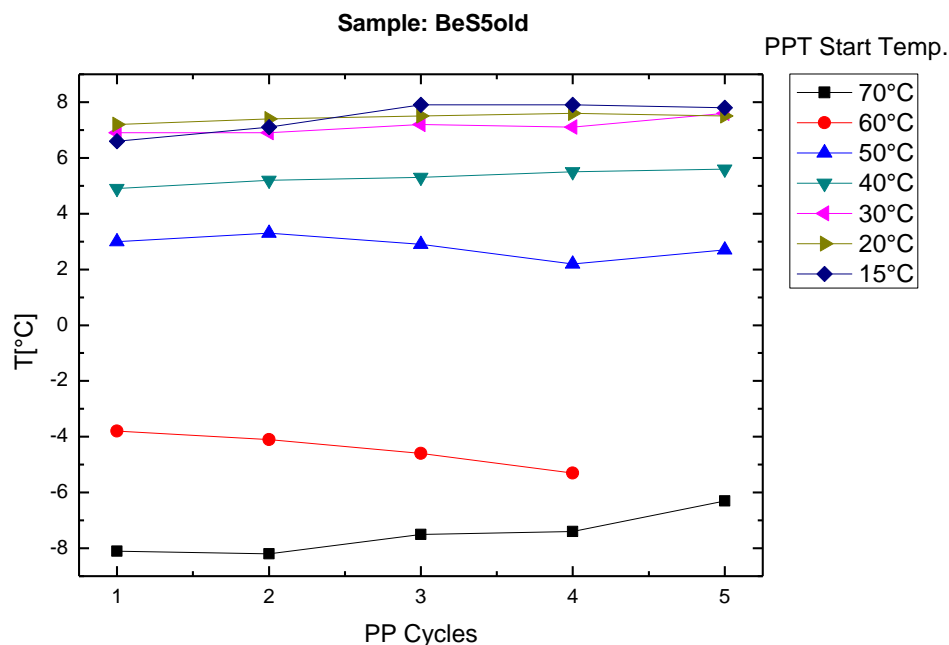


Fig. 9.7: BeS5old untreated tested with different PPT start temperatures

Looking at Fig. 9.7 another restriction of the PPT can be seen, it is not possible to use a start temperature lower than 30 °C, even when selecting a temperature lower than room temperature the PPT heats to 30 °C, which is another reason why the following thermal history measurements were performed with a start temperature of 50 °C.

### 9.1.3 Thermal History Measurements of 4 Crude Oils

For further investigation of the influence of the thermal history of crude oils on their PPs, more than one oil and more than three preheat temperatures are needed. Therefore four different crude oils were measured at 13 different temperatures, ranging from 25 °C to 85 °C. Two oils were taken from Austria BeS5 and Sp23 and the other two from Romania Pecica 652 and Folesti 2600. Small containers, that can be sealed air tight, were filled with 35 ml each for every crude oil sample and every preheat temperature. Six additional sample containers per crude oil were prepared, two of them to measure the density and weight before and after the heat treatment to see if the seal was actually air tight and the other four to determine how long it takes at room temperature until the PP of each sample equals the original value again after the preheating. For the heat treatment itself the sample containers were put in a water bath, but since the water bath has a limited space only two crude oils could be treated at a time. Therefore two experiment runs with a duration time of 2 weeks each had to be performed. The water bath temperature started at 25 °C and was increased by 5 °C after both samples were measured, until a water bath temperature of

85 °C was reached. Each temperature step was kept for at least 12 h before the first of the two samples was tested.

It was decided to let the samples cool down to room temperature before testing them with the PPT, to avoid the lower PP at the first cycle which was described in the previous section. During production of crude oil its temperature also decreases on the way up to the surface. Unfortunately the room temperature and hence the cooling rate was not always the same.

The PPT start temperature was 50 °C and 9 PP cycles were performed which was due to the fact that the PPT does not heat to the same temperature every time even with the same preset as can be seen in Fig. 9.3 and Fig. 9.8 by looking at the varying peak heights. And since the PP values depend very strongly on the PPT start temperature (see Fig. 9.7), it is more reasonable to use the average value and the error of as much values as possible. But the WinPPT software can measure at most 9 PPs in a row, therefore this is the number of cycles used for the measurements as described in this section.

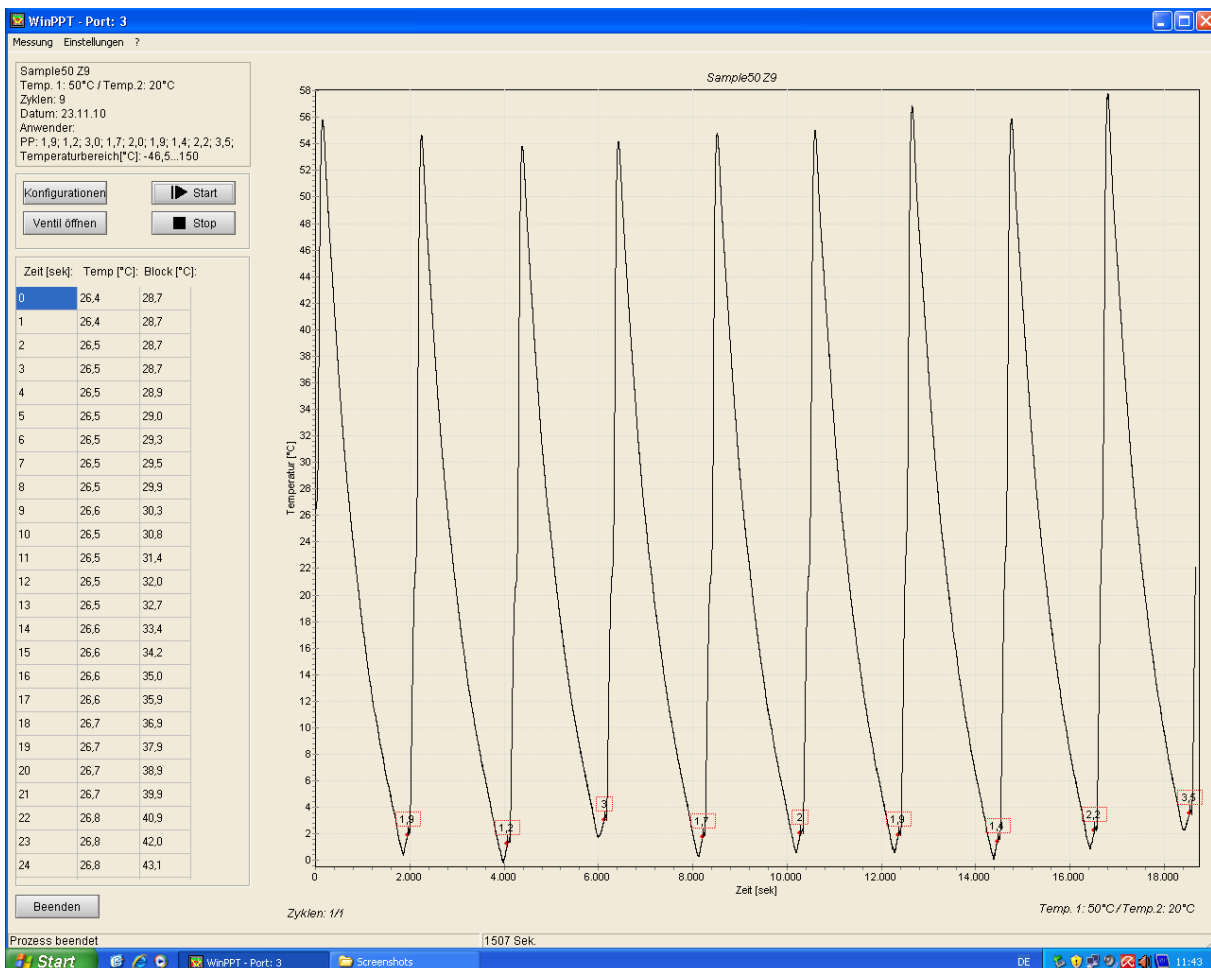


Fig. 9.8: Measuring curve of Sp23 with 9 PP cycles

The average value  $\bar{x}$  of  $n$  statistically allocated measuring values  $x_i$  can be calculated with the following formula:

$$\bar{x} = \frac{1}{n} \sum_{i=0}^n x_i \quad (9.1)$$

Two other very useful formulas are the error or standard deviation of the average value

$$\sigma_m = \sqrt{\frac{\sum (\bar{x} - x_i)^2}{n(n-1)}} \quad (9.2)$$

and the error of a single measuring value

$$\sigma = \sqrt{\frac{\sum (\bar{x} - x_i)^2}{n-1}} \quad (9.3)$$

The 9 PP cycles were determined for all 4 crude oils mentioned at the beginning of this section and additionally the average value, its error and the error of the single measuring value were calculated for each of the 13 temperatures as shown in Tab. 9.2 for the sample BeS5. The tables of the other three samples can be seen in the appendix A1.

Pre heat T [°C]	PP cycles									$\bar{x}$	$\sigma_m$	$\sigma$
	1	2	3	4	5	6	7	8	9			
	PP [°C]									[°C]		
25	-0.6	0.3	1.0	1.1	1.2	1.1	0.7	0.5	1.1	0.71	0.19	0.58
30	0.0	0.4	0.4	0.5	1.4	1.6	2.0	1.8	1.9	1.11	0.26	0.78
35	1.9	3.4	1.5	2.5	1.8	1.7	1.7	3.4	2.4	2.26	0.24	0.73
40	1.3	1.3	1.6	1.7	1.1	1.2	1.4	1.9	1.8	1.48	0.09	0.28
45	4.1	2.9	3.7	3.3	3.7	3.4	3.3	3.7	3.9	3.56	0.12	0.36
50	4.5	3.9	3.3	3.5	2.6	3.4	3.5	4.1	3.8	3.62	0.18	0.54
55	0.8	1.9	2.6	2.5	3.0	2.8	3.1	3.4	3.5	2.62	0.28	0.84
60	-3.9	-1.9	0.0	1.1	1.6	2.5	3.0	2.7	2.8	0.88	0.80	2.40
65	-7.7	-5.6	-4.1	-3.7	-3.4	-2.5	-2.0	-2.2	-1.8	-3.67	0.65	1.94
70	-9.6	-5.5	-6.9	-4.5	-4.8	-5.5	-3.9	-3.7	-4.0	-5.38	0.63	1.88
75	-9.2	-7.9	-8.3	-6.3	-6.8	-6.9	-6.1	-6.6	-6.0	-7.12	0.37	1.10
80	-7.4	-4.8	-5.3	-3.6	-2.6	-2.8	-2.5	-3.7	-2.0	-3.86	0.57	1.72
85	-6.6	-5.5	-5.4	-3.2	-2.9	-2.4	-2.0	-1.3	-1.4	-3.41	0.65	1.95

**Tab. 9.2:** 9 PP cycles, average value and error for BeS5 at 13 different temperatures

The data from this table is plotted below in Fig. 9.9, Fig. 9.10 and Fig. 9.11. The diagrams showing just the first of the measured cycles were made to compare the results of these tests with common literature and other measurements performed using the tilt method. Since the graphics containing all PP cycles of each preheat temperature are pretty unclear, the ones for the other three samples are also shown in appendix A1 along with the graphics showing only the first PP of the 9 cycles. In this

section only the plots of the average values of all PP cycles for each pretreatment temperature are shown.

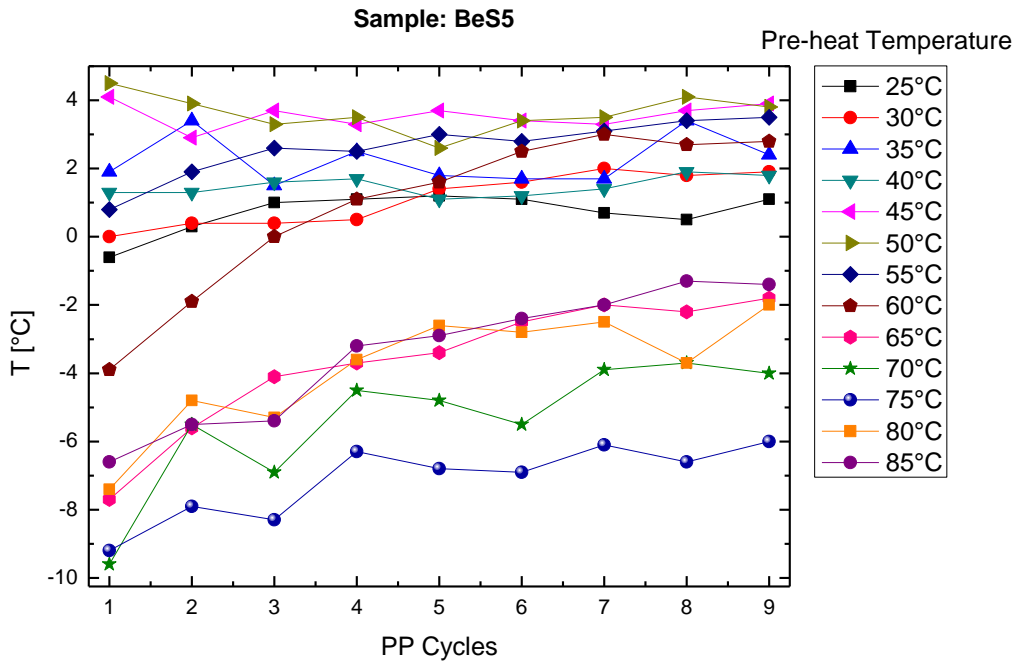


Fig. 9.9: 9 PP cycles at 13 different preheating temperatures of the sample BeS5

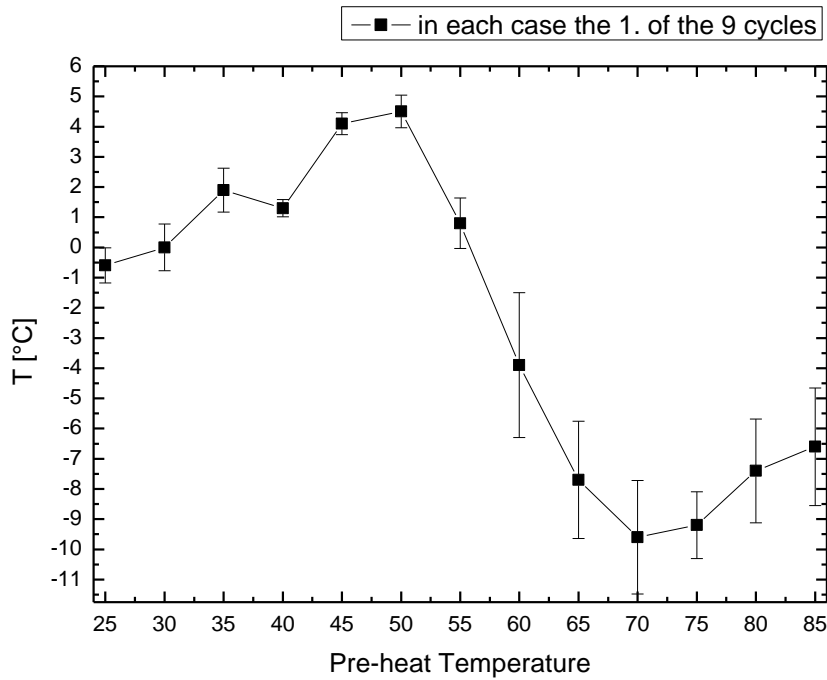


Fig. 9.10: BeS5: the first value of the 9 cycles for each pretreatment temperature with the error of the single measuring values

Watching Fig. 9.9 or the three similar figures of the other samples in the appendix A1, it can be seen that at higher preheat temperatures it is possible that the PP increases with each measuring cycle. This phenomenon is already described in section 9.1.2. This "wandering" of the PP means that the sample temperature was above or at the WAT at the time the measurement was started, which can be a consequence of the varying room temperature and the fact that the temperature was not measured before the sample containers were opened and the sample poured in the measuring cup of the PPT.

The results plotted in Fig. 9.11-Fig. 9.14 show that the PP increases at first with increasing preheat temperature but for the sample Folesti 2600 where the PP remains the same till 65 °C. Then for all samples except for Sp23 the PP drops below the value it had at 25 °C preheat temperature. BeS5 has a PP maximum around 50 °C and Pecica 652 around 55 °C preheat temperature. BeS5 and Folesti 2600 have a minimum at 75 °C and Pecica 652 has the minimum at 70 °C preheat temperature. If a crude oil in a container that is sealed air tight is left at room temperature after it has reached its minimum PP due to heat pretreatment, it can take from hours (e.g. BeS5) to several days or weeks (e.g. Folesti 2600) until the PP of the crude oil reaches the value it had originally at room temperature.

For unknown reasons the sample Sp23 is the only one that has its PP minimum when it is not preheated at all. At first it was supposed that only this or all 4 samples loose some of their light end hydrocarbons during the two weeks of heating, because the seals cannot withstand the pressure building in the containers. But this assumption was proven wrong with measurements of the density  $\rho$  of the samples and of the weight  $m$  of the sealed vessels containing the crude oils before and after the two-week heating process, because no significant change in density or weight of any sample could be observed as shown in Tab. 9.3.

crude oils		before heating		after heating	
		$\rho$ [g/cm <sup>3</sup> ]	$m$ [g]	$\rho$ [g/cm <sup>3</sup> ]	$m$ [g]
BeS5	vessel 1	0.8155	76.7167	0.8270	74.9758
	vessel 2		77.5280		76.9067
Sp23	vessel 1	0.8497	79.0369	0.8499	78.9872
	vessel 2		79.0506		78.9978
Folesti 2600	vessel 1	0.8404	79.6792	0.8425	79.4566
	vessel 2		78.6151		78.2247
Pecica 652	vessel 1	0.8263	79.6094	0.8284	79.5772
	vessel 2		77.8422		77.7260

**Tab. 9.3:** Density and weight of the 4 samples before and after the heat pretreatment

In fact Sp23 has the lowest deviation of the 4 crude oils, which totally excludes a density or weight change due to the loss of light end hydrocarbons during the heating process as reason for the behavior this sample shows in Fig. 9.12. Maybe this behav-

ior is caused by a chemical additive like an inhibitor which could not be confirmed or investigated any further.

The only experiment similar to the thermal history experiment described in this section, that could be found in literature was performed by Zettlitzer [30], who made also PP measurements with different preheat temperatures. He used inhibited crude oil which may be the reason why the PP maximum in his plot (see Fig. 9.15) is at 40 °C and not around 50 °C. But apart from that, it confirms the results of the samples BeS5, Folesti 2600 and Pecica 652.

In general it can be said that even though every crude oil behaves slightly different, crude oils should not be heated to temperatures between 45 °C and 65 °C e.g. in storage tanks, because the resulting PP can be far greater than without heating. It is more reasonable to heat a crude oil for a short time to 70 °C or 75 °C, than to heat it to 50 °C for several hours. Before heating a crude oil to 50 °C it is far better in most cases not to heat at all, which can save plenty of money. Of course a crude oil should be tested in the lab before doing any heating process with bigger amounts, because there can exist exceptions as demonstrated with sample Sp23.

This result is quite stunning, since the OMV heats most storage tanks to 50 °C to get a lower PP and to have less wax precipitation problems, which can be exactly the wrong thing to do if the crude oil was not tested adequately.

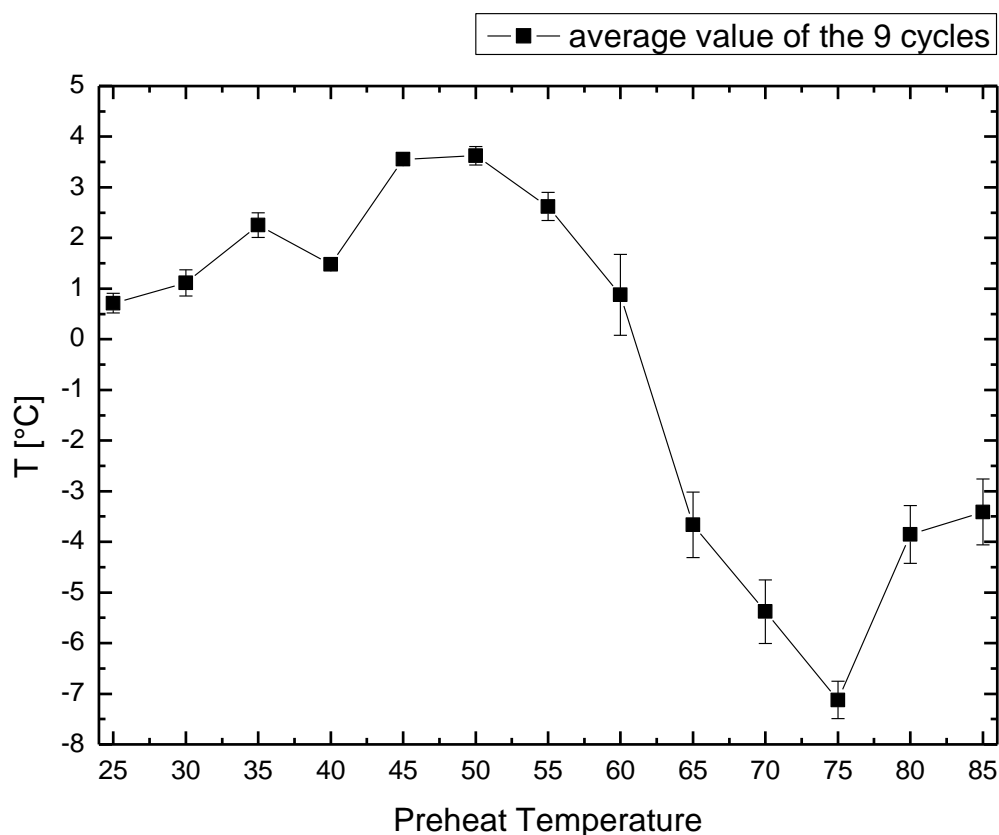


Fig. 9.11: BeS5: average value and error of the PP cycles for 13 different Preheat Temperatures

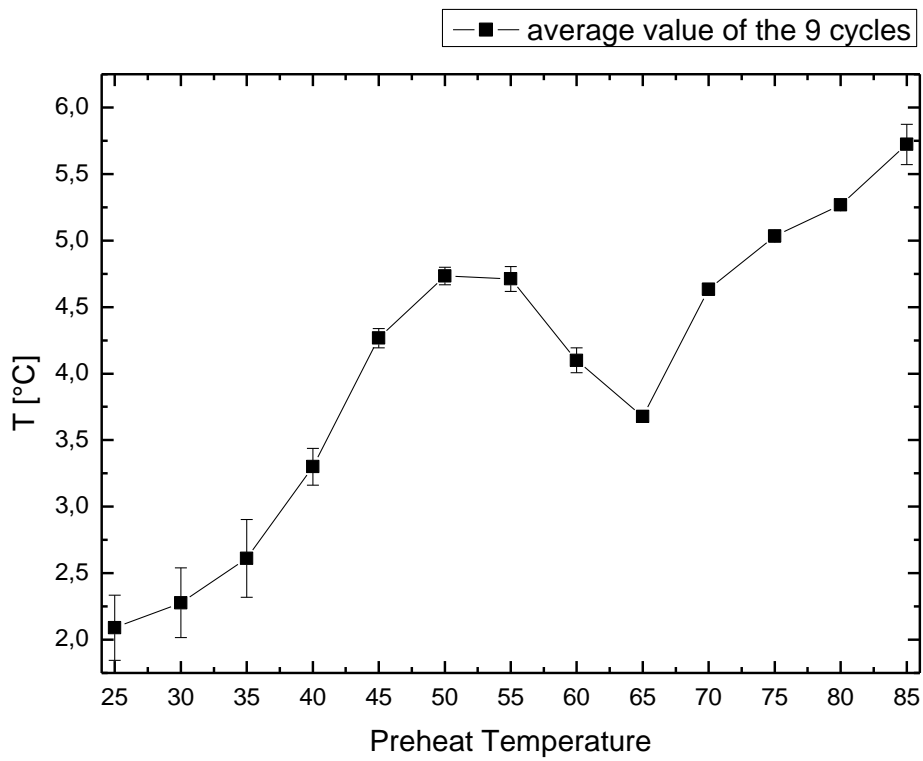


Fig. 9.12: Sp23: average value and error of the PP cycles for 13 different Preheat Temperatures

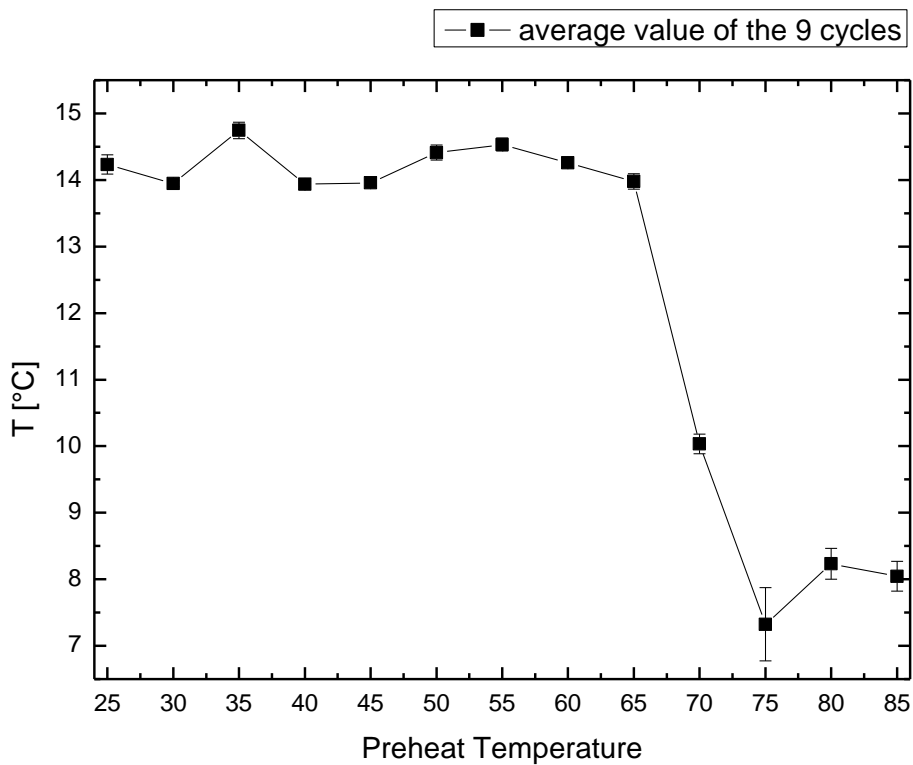


Fig. 9.13: Folesti 2600: average value and error of the PP cycles for 13 different Preheat Temperatures

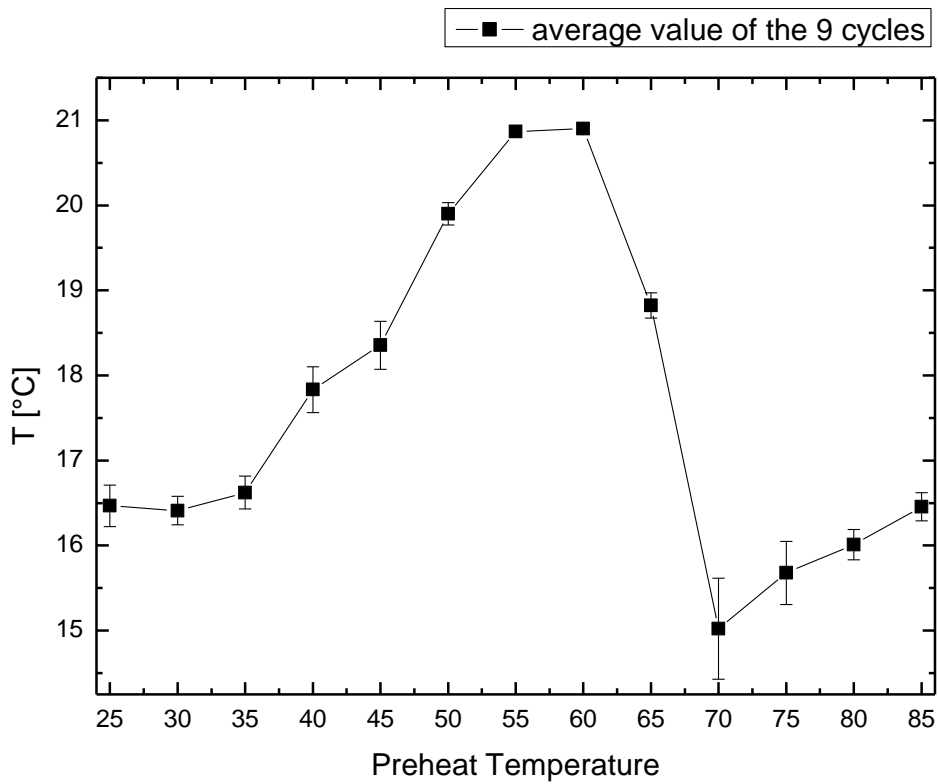


Fig. 9.14: *Pecica 652*: average value and error of the PP cycles for 13 different Preheat Temperatures

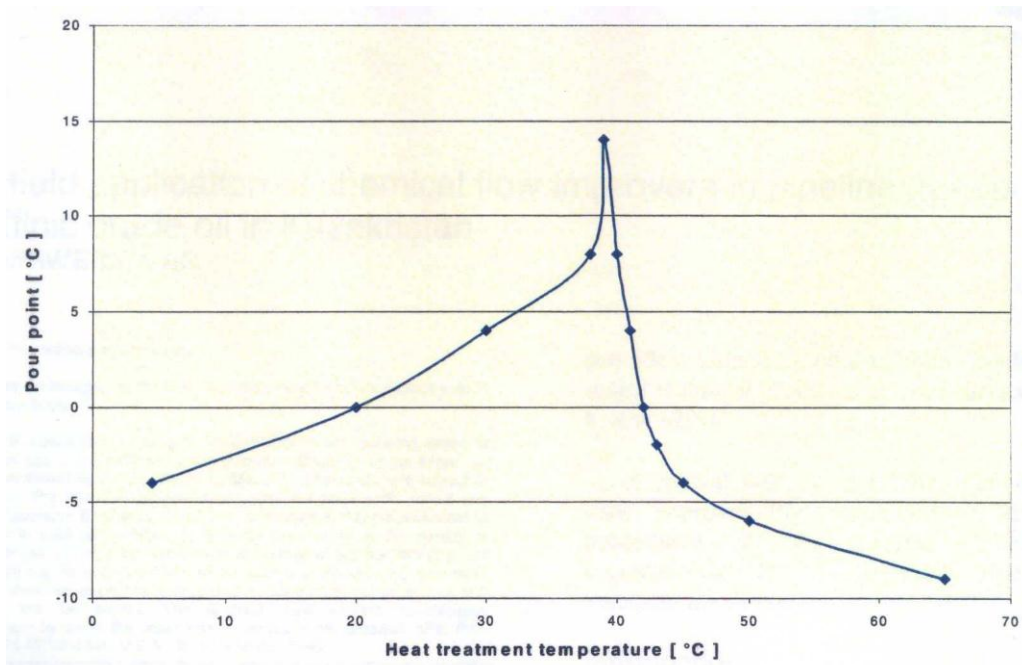


Fig. 9.15: PP of inhibited Akshabulak crude oil over Preheat Temperature [30]



## 9.2 Microscopical Measurements

To gain a better understanding of the crystallization processes that lead to the PP and how they are influenced by the pretreatment temperature, microscopical measurements using a transmission microscope and a scanning electron microscope were performed.

### 9.2.1 Transmission Microscope (TM)/CPM

The TM has a polarized light source and if wanted a polarization filter can be used to see if the observed sample rotates the plane of polarization as paraffin crystals do. This means the TM in the OMV lab which was used for this thesis is in fact a CPM as described in section 3.1.1 with only one difference: no heating/cooling stage was available, which is a big disadvantage, because it was not possible to control the temperature of the sample observed under the TM, which limited the measuring possibilities.

#### 9.2.1.1 Sample Preparation

For the TM measurements just a few drops of the sample were put on a microscope glass slide and then covered with a cover glass. For thermal pretreatment the whole slide with oil and cover glass was put in an oven for half an hour, afterwards it was transported to the microscope. But unfortunately the TM was one floor lower and the way took about 1 min 30 sec. Due to the small amount of crude oil and the small size of a microscope slide it takes approximately 5 min until a slide with crude oil is cooled down to room temperature. Therefore the samples had to be carried in a glass container with a cover which was preheated to the same temperature as the samples. But in spite of this procedure the temperatures of the samples were down to approximately 40 °C when preheated to 55°C or down to 60 °C when preheated to 80 °C at the time of application.

To observe the crystal structure of the samples below and at the PP the slides were cooled after the preheating. At first they were taken out of the oven and then left to cool down to room temperature, afterwards the slides were put in a refrigerator at 9 °C and then in an icebox with -35 °C. The samples were transported to the microscope in a cooled glass container with cover, at the time of application the samples had temperatures between -10 °C and -5 °C.

#### 9.2.1.2 Measurement Results

The first measurements were made with Pecica 652 because it has the highest PP and the most paraffin wax of the 4 crude oils. Pecica 652 was observed with no heat pretreatment, with 55 °C and 85 °C preheat temperature. The photographed microscope pictures show cool down/heat up processes or samples not undergoing any temperature changes. It clearly can be seen that depending on the preheat temperature the crystal structure looks different. When not preheated the crystals look like

needles or little rods (see Fig. 9.16). After preheating to 55 °C there are clearly more crystals and they have the form of little spheres (dots) and bent rods, which seem to consist of the spheres (see Fig. 9.17). In contrast to measurements described in common literature, the microscopical measurements described in this thesis were performed without a polarization filter, except to check if all structures in the image are paraffin crystals as can be seen in Fig. 9.17 (c) and (d).

The crystallization process in Fig. 9.18 confirms that the crystals are completely melted when the oil is heated to 85 °C. The crystals look like spheres, they are bigger than the ones in Fig. 9.17, but there are fewer crystals in the crude oil than when preheated to 55 °C, which is in compliance with the results in section 9.1.3. Using a higher magnification it can be seen that the spheres are in fact little hook-shaped crystals that form voids which can entrap liquid crude oil as shown in Fig. 9.19.

This means both the crystal structure as well as the amount of paraffin crystals are influenced by the preheat treatment. The changes of these two factors are responsible for the PP behavior which was measured in section 9.1.3.

To verify the above discussed measurements, samples of the other three crude oils (BeS5, Sp23 and Folesti 2600) were observed under the microscope. But since these three crude oils have much less paraffin wax than Pecica 652, they have fewer and smaller crystals, therefore it is hardly possible to see these crystals on the microscope photographs. Consequently concerning these three crude oils, only pictures of samples that were cooled after the preheating, are shown in this thesis. Because the crystals are bigger, if the temperatures of the crude oils are close to, or under their PPs. For comparison samples of Pecica 652 were prepared with the same procedure and then viewed under the microscope. The photographs of BeS5 are displayed in Fig. 9.20 to show that the crystal structure of the samples Pecica 652 and BeS5 are similar for the same pretreatment.

When preheated to 55 °C the crystals of the crude oil Folesti 2600 have the same shape as when not pretreated at all which fits to the PP curve in Fig. 9.13, but after preheating to 85 °C no crystals can be found with the TM even if the sample was cooled before it was applied to the microscope.

It is very interesting that the crude oil Sp23 has the same crystal structure without pretreatment as when heated to 85 °C even though the crystal structure is different when the crude oil is preheated to 55 °C. But since it is not known why the crystal structure of a sample without heat pretreatment is the same as the one of a sample that was preheated to 85 °C even though the PP is higher at this preheat temperature, this phenomenon was not investigated any further in this work. The photographs of these measurements as well as the photographs of the cooled Pecica 652 and Folesti 2600 samples can be seen in the appendix A2.

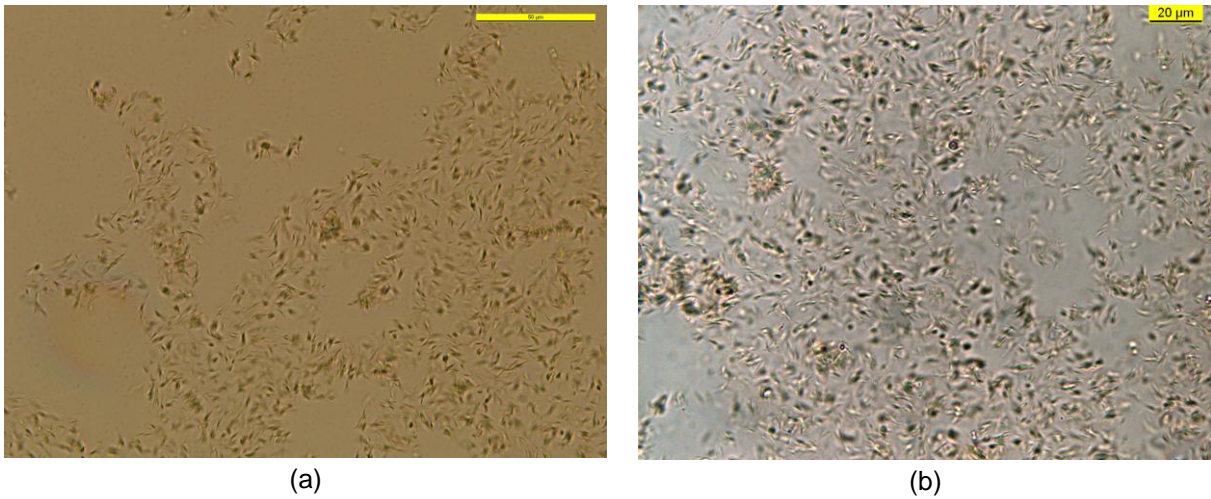


**Fig. 9.16:** *Pecica 652 without thermal pretreatment, needle- and rod-shaped crystals: (a) the yellow bar scales 50  $\mu\text{m}$ ; (b) higher magnification, the yellow bar scales 20  $\mu\text{m}$*

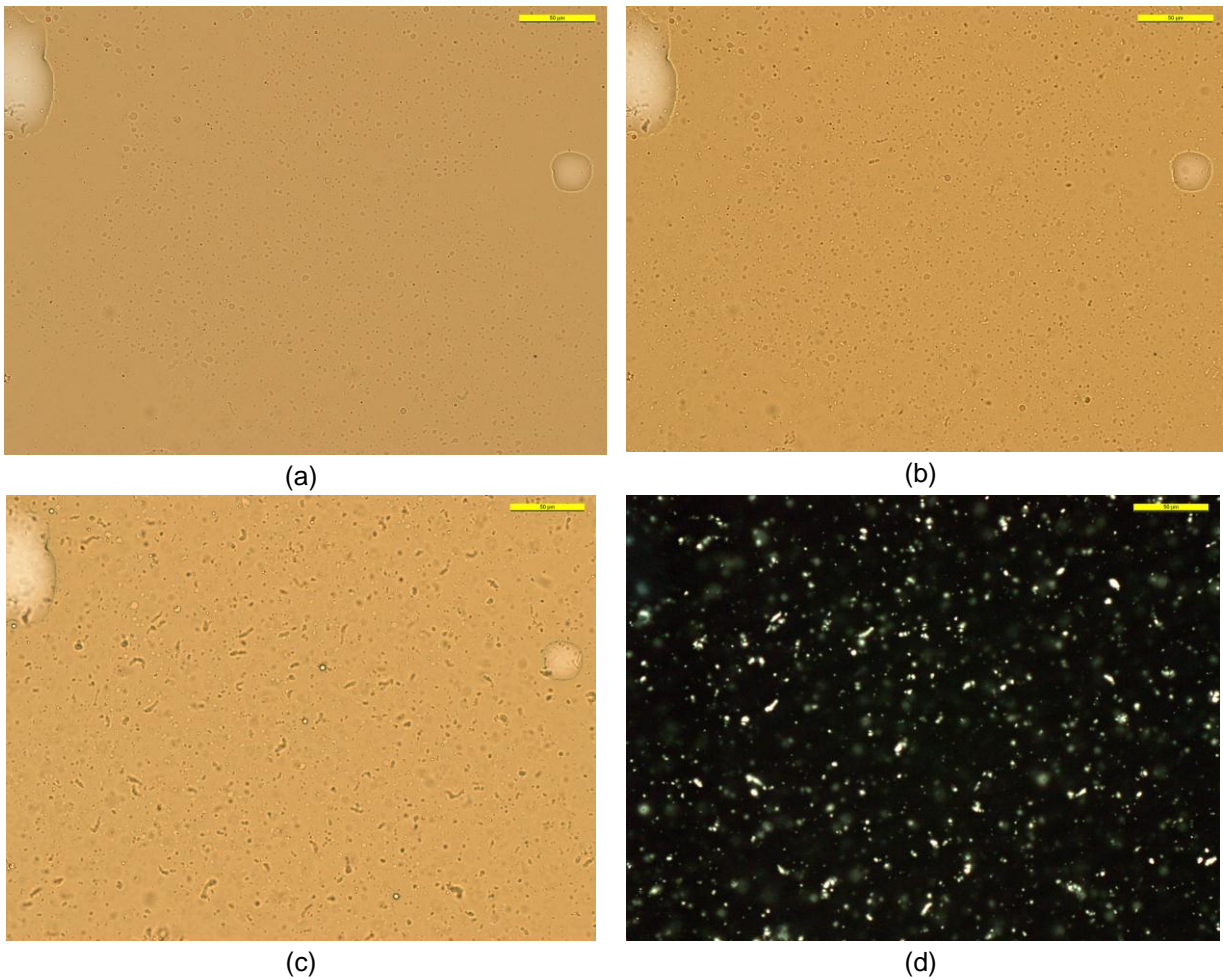


**Fig. 9.17:** *Cool down process of Pecica 652 preheated to 55  $^{\circ}\text{C}$ , the yellow bar scales 50  $\mu\text{m}$  in all 4 pictures, the dots and the bent rods are paraffin crystals: (a) photograph taken directly after application, small dots are visible; (b) 1 min 23 sec after application, the crystals are bigger and some have agglomerated to rods; (c) 3 min 29 sec after application, the crystals have grown a lot and many rod shaped agglomerations have formed, afterwards not much change could be observed even after one hour; (d) this picture was taken 1 min after (c) using a polarization filter*



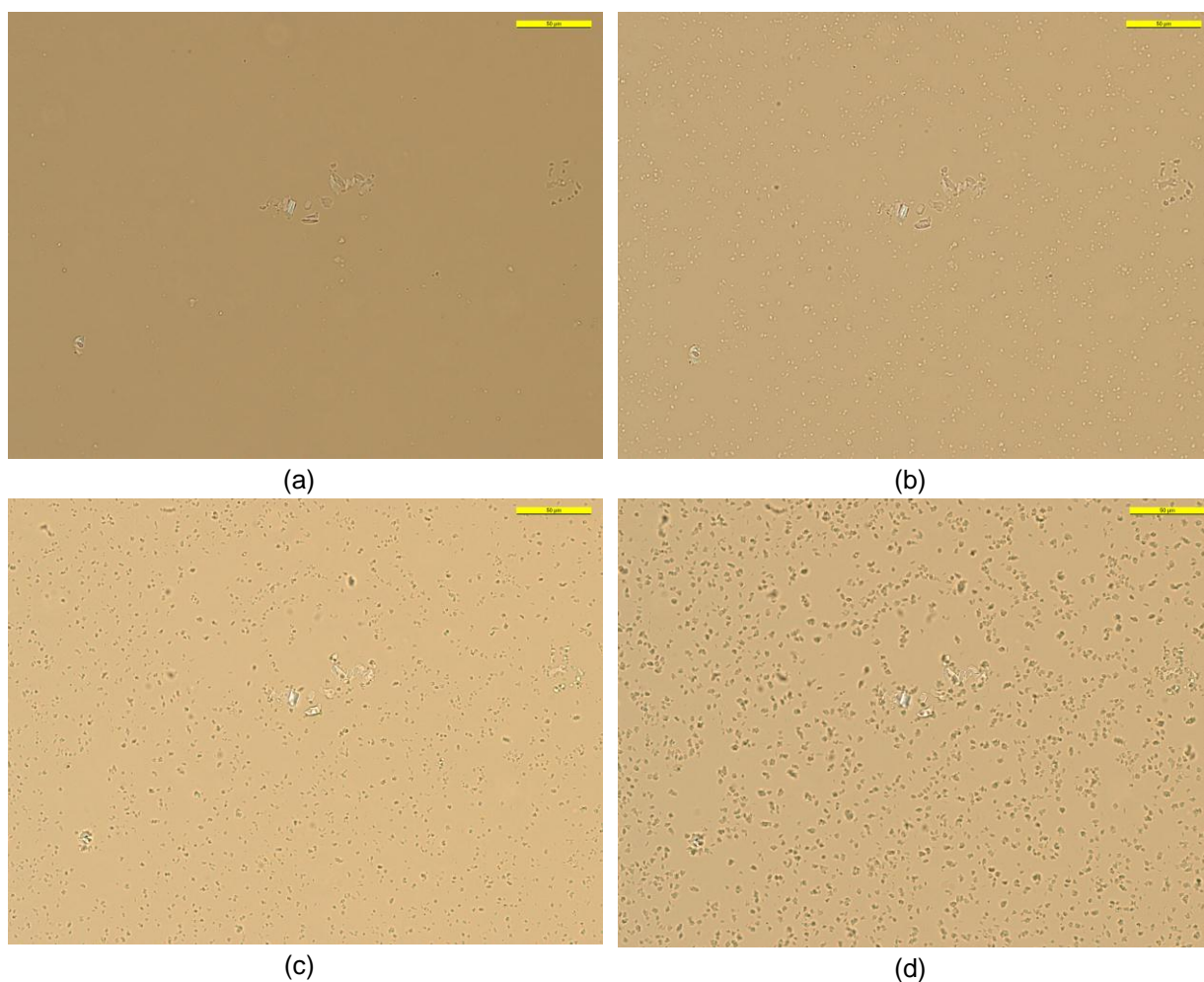


**Fig. 9.18:** Cool down process of Pecica 652 preheated to 85 °C, the yellow bar in the 4 pictures scale 50 µm each: (a) directly after application, very few crystals are visible; (b) 1 min 48 sec after application, more crystals (small white dots) but still the same size as in (a); (c) 2 min 18 sec after application, the crystals have grown but not many new ones have formed; (d) several min after application, the crystals have grown bigger but no agglomerations have formed

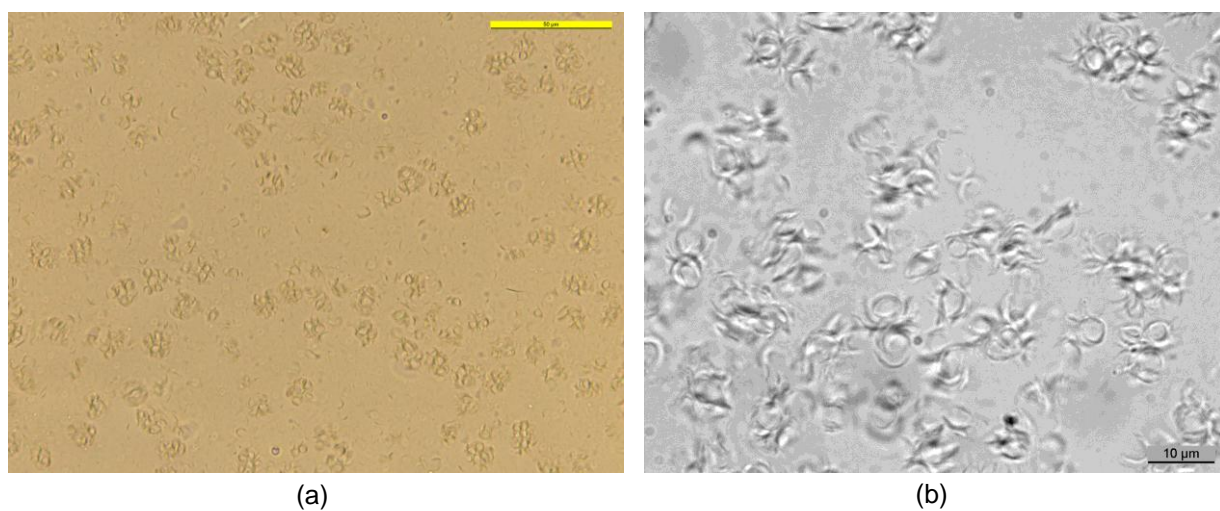


**Fig. 9.19:** Pecica 652 preheated to 85 °C, the sample had room temperature for several minutes before it was observed: (a) higher magnification (yellow bar scales 50 µm), (b) even higher magnification (grey bar scales 10 µm); the spherical crystals from Fig. 9.18 are in fact little hook-shaped crystals which entrap liquid crude oil

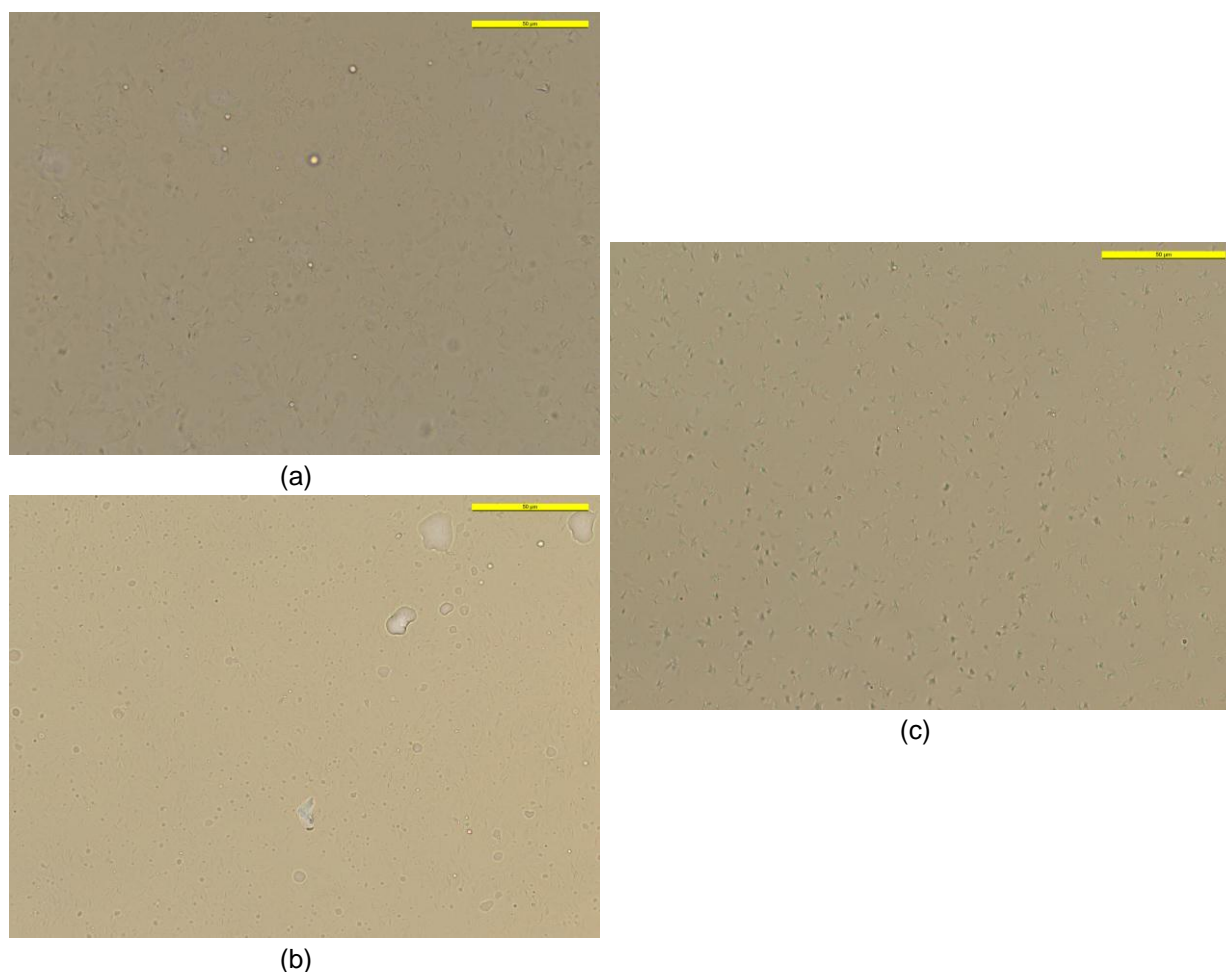


**Fig. 9.20:** *BeS5* cooled before viewed under the microscope, the yellow bar scales 50  $\mu\text{m}$  in all three photographs: (a) without pretreatment, needle-shaped crystals; (b) preheated to 55  $^{\circ}\text{C}$ , dots and needles or rods; (c) preheated to 85  $^{\circ}\text{C}$ ; hook-shaped crystals like in Fig. 9.19 (a) and (b)

Altogether it can be said that the TM measurements confirm the results from section 9.1.3. They also confirm the suggestion from section 9.1.2, that the true WAT of the sample *BeS5old* is higher than 55  $^{\circ}\text{C}$  and that a temperature around 55  $^{\circ}\text{C}$  is ideal for the formation of paraffin crystals for the used sample. In Fig. 9.17 - Fig. 9.20 it can be seen that the amount of crystals at 55  $^{\circ}\text{C}$  is more than at the other two preheat temperatures. When the results from the PP measurements in the previous section are also taken into account, this proves that the preheat temperature range, which leads to maximum PP values for most crude oils, supports paraffin crystal formation. This may be because crude oils being held in that range have a high enough temperature for the paraffin molecules to move around far enough to form many crystals and that the formed crystals can agglomerate to the described rods. But in this range the temperature also is not too high, so that the formed crystals and agglomerations are stable and do not decompose due to the increased movability of the crystals and molecules.

## **9.2.2 Scanning Electron Microscope (SEM)**

As the microscope pictures in section 9.2.1 show, it was not possible to focus on all crystals in the display window, which is mostly because they have different dimensions in along the z-axis (the axis normal to the image plane). And unfortunately the crystals could not be scaled any larger without losing sharpness.

Therefore it was decided to observe a sample using an SEM but due to the lack of time only one crude oil could be tested. Of course Pecica 652 was chosen for these measurements, because the crystal structure of this sample could be determined most precisely compared to the other three crude oils due to their size and their quantity.

### **9.2.2.1 Sample Preparation**

The sample preparation for the SEM was much more difficult than for the TM, mainly because of the reason that liquid oil must not enter the vacuum chamber of the SEM. If liquid oil comes inside the vacuum chamber it can vaporize and condense on the walls of the chamber, where it continuously vaporizes and hence prevents the achievement of the needed vacuum for the operation of the SEM. Consequently it was absolutely necessary to clean the paraffin crystals before putting them into the vacuum chamber.

For the not pretreated crude oil a microscope slide was put in a beaker glass, and then the crude oil was poured in the beaker glass, which was then left at room temperature for one day without an air tight cover. Afterwards the crude oil was poured away and the microscope slide being still at the bottom of the beaker glass was washed with benzine until only the white paraffin crystals remained on the slide. Subsequently the slide was fixed on a specimen holder, and then was gold-evaporation-deposited before it was put in the vacuum chamber of the SEM. The sample which was preheated to 55 °C was prepared similarly with the only difference, that the beaker glass containing the microscope slide and the crude oil was put in an oven with a temperature of 55 °C before letting it cool down to room temperature. The following procedure was the same as for the sample without heat pretreatment. Unfortunately this preparation method did not work for a preheat temperature of 85 °C, because too many oil inclusions for SEM measurements formed on the slide. Therefore the crude oil was first preheated to 85 °C and the poured in the beaker glass containing the microscope slide and afterwards left at room temperature for one day. The remaining preparation was the same as used for the other two samples.

### **9.2.2.2 Measurement Results**

Due to the completely different preparation method compared to the samples observed under the TM, paraffin wax accumulations form on the slides (see Fig. 9.21), which consist of the needle-shaped crystals that can also be seen on the TM photographs in the previous section.

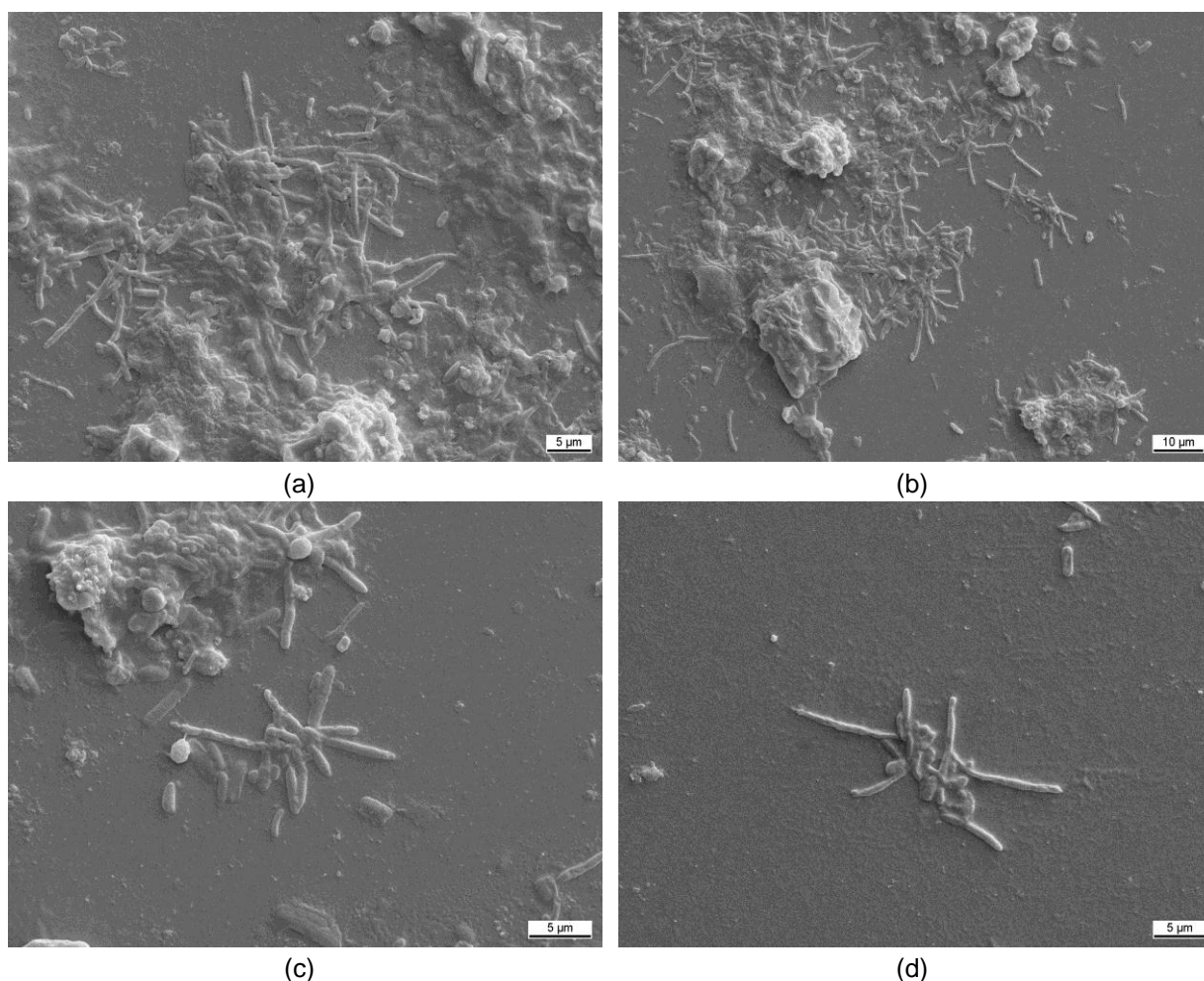


**Fig. 9.21:** *Pecica 652 without heat pretreatment: (a) paraffin crystal accumulations consisting mainly of needle-shaped crystals, (b) paraffin crystal accumulations and NaCl crystals covered with paraffin crystals, (c) and (d) needle-shaped crystals with different lengths*

Also the SEM pictures like the ones in Fig. 9.21 and in the appendix A3, show the heterogeneous nucleation on NaCl crystals. But this crystallization process can be seen much better in the pictures taken from the sample which was preheated to 55 °C (Fig. 9.22), because the conditions for the crystal formation were ideal and hence much more nuclei were built in this sample. These results indicate that the SEM tests are in accordance with the PP and the TM measurements described in the two previous sections.

The big accumulations in the pictures Fig. 9.22 (a) and (b), which are in fact structures with many voids that contain liquid crude oil, are a good representation for paraffin precipitations on pipe walls that form during production and transportation.

In Fig. 9.23 it can be seen that much less crystal material is available on the slide, this might be not only because of the preheat temperature of 85 °C, but also due to the different preparation method which has caused that the crystals did not form directly on the glass slide at the bottom of the beaker glass. Or maybe because the crystals formed in the crude oil after being preheated over the true WAT could have lower adhesive forces to the glass and therefore were mostly washed away by the benzene in the cleaning process.



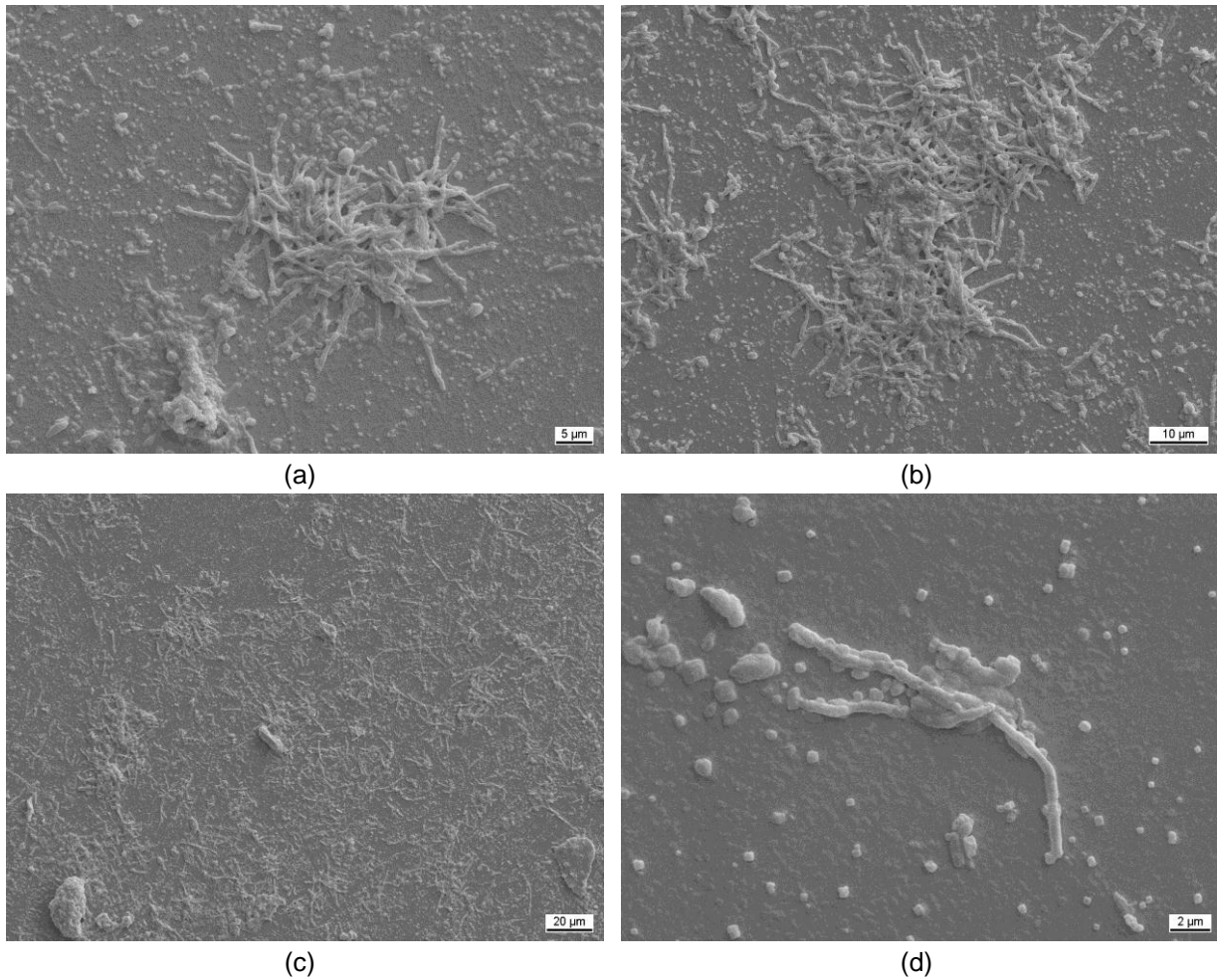


**Fig. 9.22:** *Pecica 652* preheated to 55 °C: (a) and (b) big paraffin crystal accumulations, (c) much more crystal material than in Fig. 9.21 an Fig. 9.23, (d) many paraffin covered NaCl crystals, which show the heterogeneous nucleation



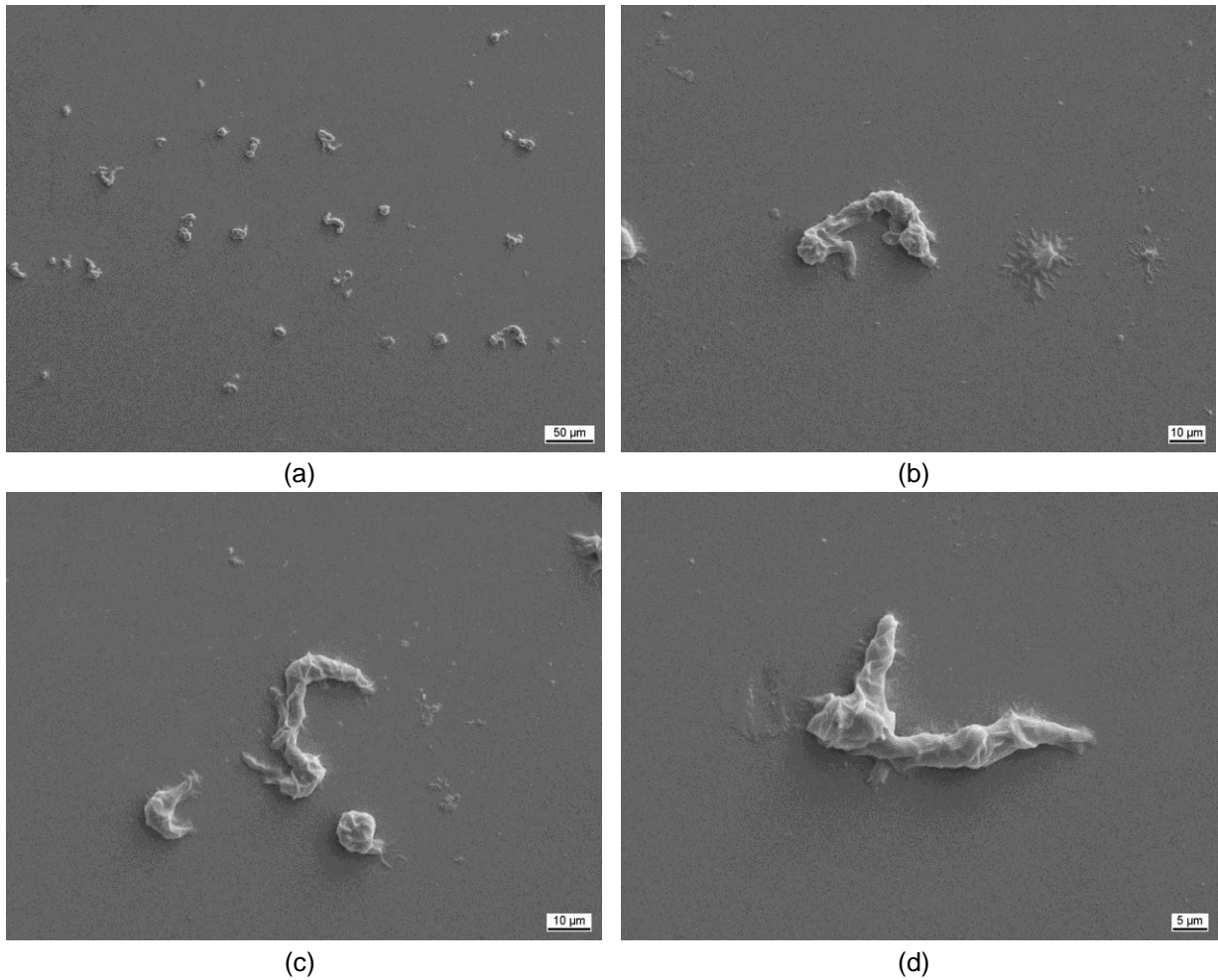


**Fig. 9.23:** *Pecica 652 preheated to 85 °C: (a) not very much crystal material compared to Fig. 9.21, (b)-(d) big structures consisting of a mixture of short needle- and small hook-shaped crystals*

### 9.2.3 Comparison between TM and SEM Pictures

Even though the preparation methods of the SEM samples were completely different compared to the method used for the TM samples, in the pictures of both measurements, structures of the similar shape and size can be found. In the following pictures (Fig. 9.24 - Fig. 9.26) it was tried to point out these similar crystals and crystal structures.

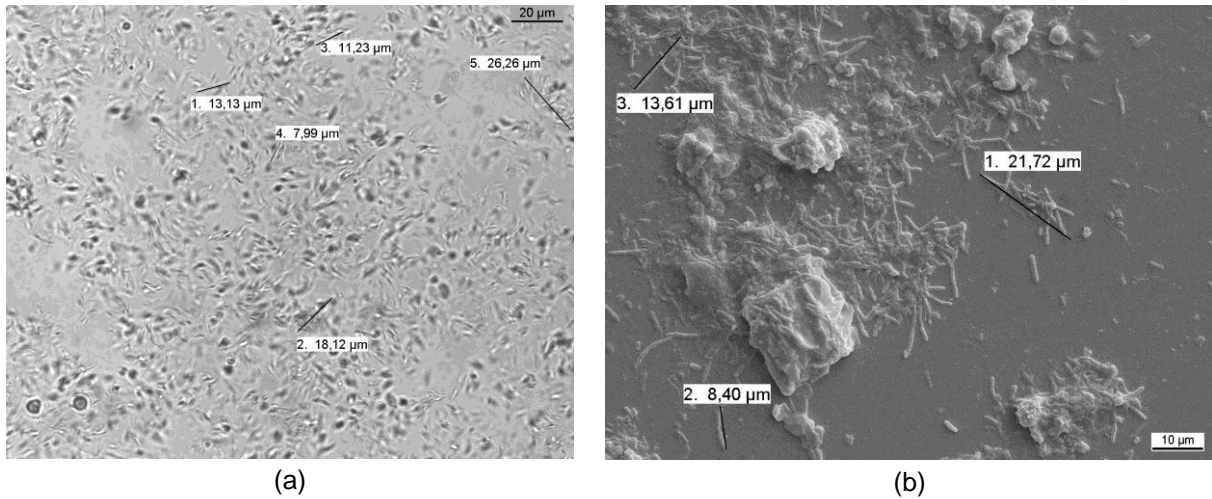


**Fig. 9.24:** *Pecica 652 without thermal pretreatment: comparison between TM and SEM pictures; (a) TM photograph, (b) SEM photograph*

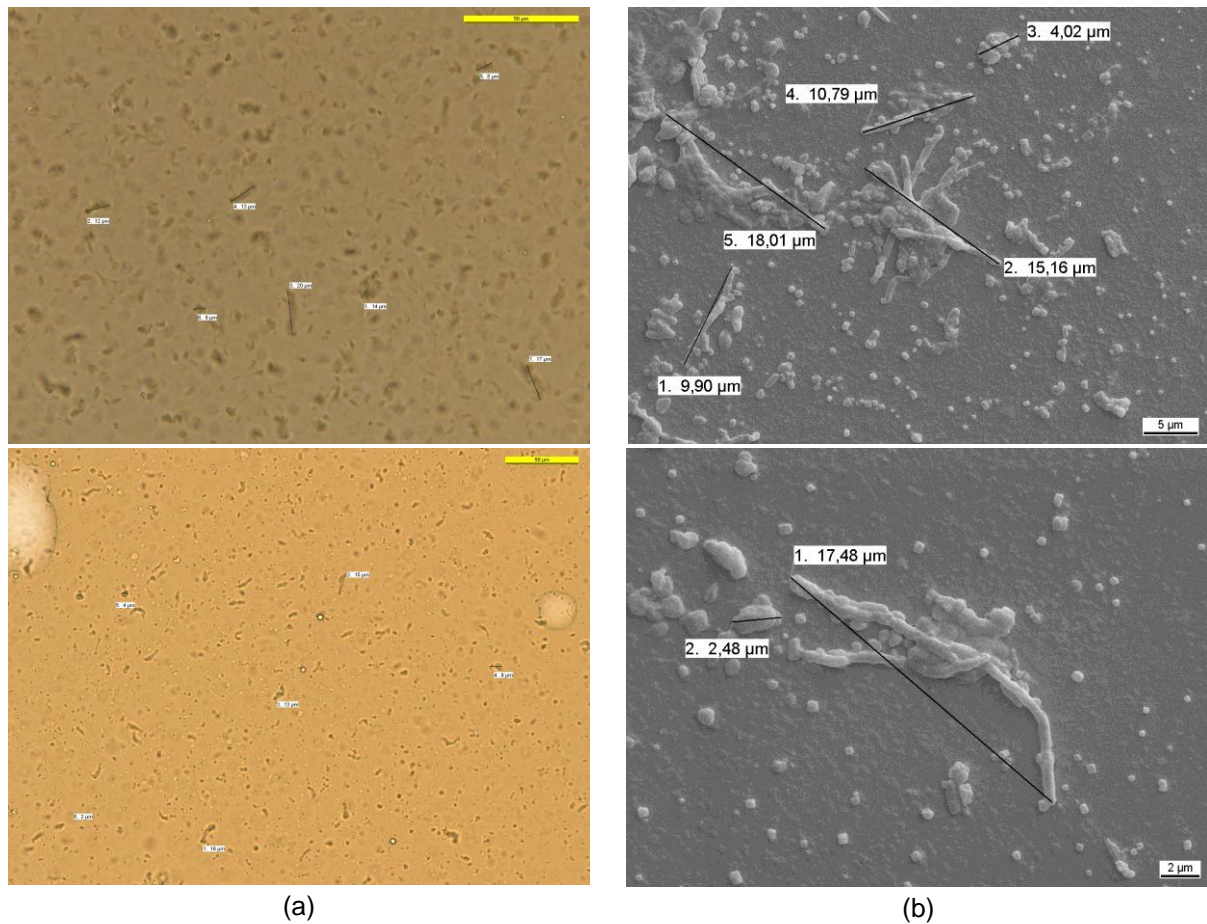


**Fig. 9.25:** *Pecica 652 preheated to 55 °C: comparison between TM and SEM pictures; (a) TM photographs, (b) SEM photographs*

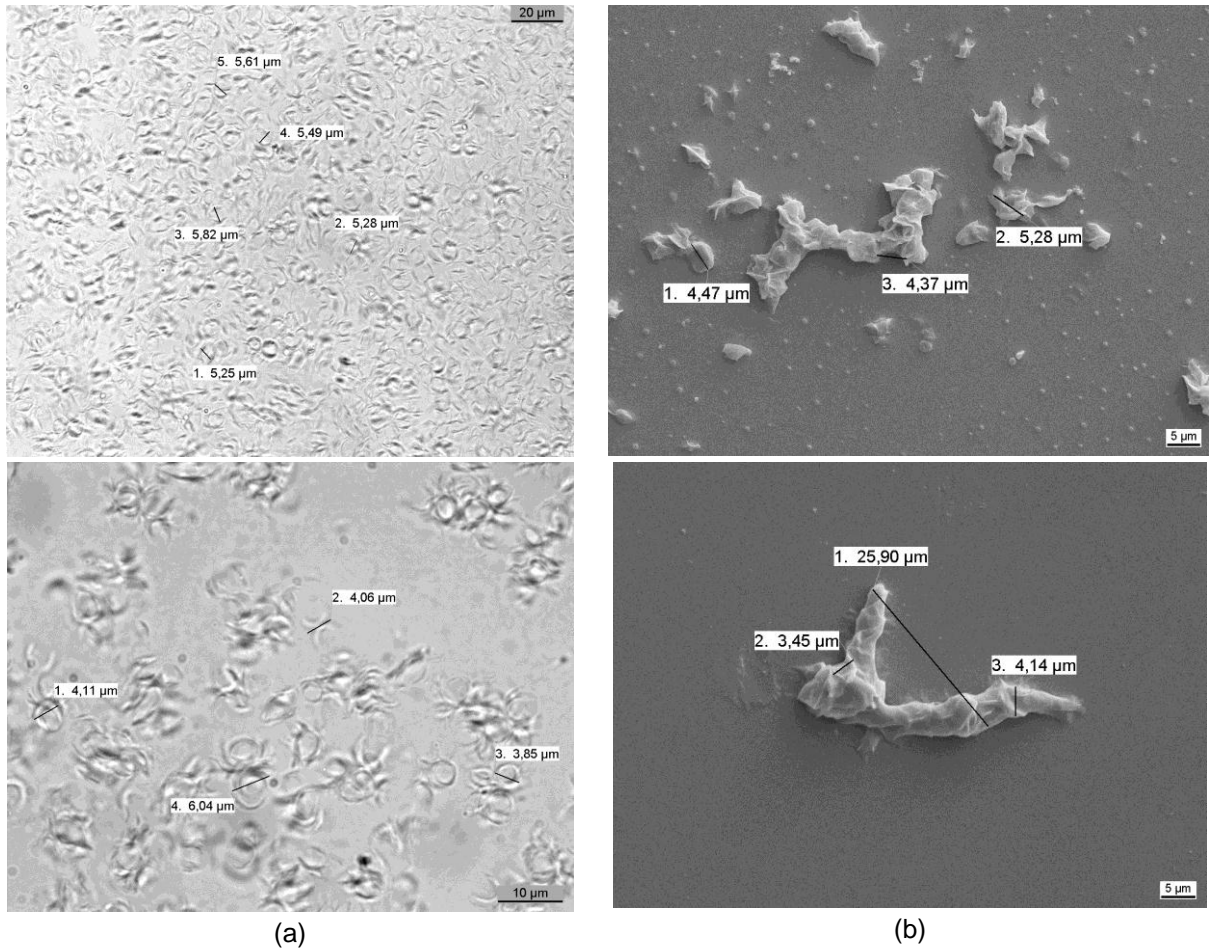


**Fig. 9.26:** *Pecica 652 preheated to 85 °C: comparison between TM and SEM pictures; (a) TM photographs, (b) SEM photographs*

## 10 Influence of Cooling Rates on the PP

As mentioned in the theoretical part (section 5.2) the cooling rate also has an influence on the PP. Unfortunately it was not possible to set a cooling rate for the PPT and the cooling rate the device uses is not constant but dependent on the characteristics of the sample, which means if the properties of the sample change, e.g. because of the formation of a crystal lattice, the cooling rate changes too. That is because the PPT controls the cooling by keeping a constant temperature gradient of 8 °C between the temperature measured by the sensor in the sample and the Peltier element. Therefore other devices have to be used which can control the temperature, the cooling rate and can determine the PP. One device that can achieve that is a rheometer but unfortunately up to now no method to determine the PP with a rheometer is known. That means to see how the cooling rate influences the PP at first a method to measure the PP with a rheometer had to be developed.

### 10.1 Experimental Setup

A Physica MCR 301 rheometer (see Fig. 10.1) which was built by Anton Paar was used in the OMV lab for the measurements described in this Chapter. The Peltier element that is sitting in the fixed bottom plate can be set to temperatures between -30 °C and 200 °C when using a plate-plate or cone-plate measuring system. To achieve a better temperature control and homogeneous conditions with these two systems, a hood that covers the sample and that has another Peltier element attached to itself is used. Furthermore an evaporation blocker from Anton Paar was attached to the hood to prevent the volatile light end hydrocarbons in the samples from vaporizing during the measurements.

#### 10.1.1 Selection of the Measuring Method/System

To measure the PP of crude oils with a rheometer a very low shear rate of 0.056/s has to be used, the reason for this will be explained in section 10.2.1. When performing rotational tests to measure the viscosity and using such a low shear rate the sample is not in the Newtonian range anymore. At the PP crude oils have a VE behavior and hence the viscosity is no longer sufficient to describe their characteristics, thus the complex shear modulus or the complex viscosity which are determined by oscillation tests should be used.

Since there are many crystals in the crude oils at the PP, they should be tested with a plate-plate system (PP50) as mentioned in section 8.3.1. Due to the small amplitudes which should be used to stay in the LVE range of the samples, the biggest disadvantage of the plate-plate system, namely the shear rate not being constant over the whole radius, can be disregarded according to Mezger [36]. That is why this system was used for the following tests with a gap of 1 mm.





Fig. 10.1: Rheometer with plate-plate measuring system and Peltier hood

## 10.2 Oscillation Tests

One attempt to determine the PP with oscillation tests was made by Lopes da Silva and Coutinho [37]. They assumed that the gel point ( $G' = G''$ , see section 8.3.3), was equivalent to the PP and came to the conclusion that this assumption was incorrect. In this work a different approach was made, the goal was to find a value for the absolute value of the complex shear modulus or the complex viscosity that is the same for all tested samples, at the PP of course. To achieve this, the samples were tested with the PPT at first to get their PPs, which were used to determine the proper parameters for the oscillation tests and to find the desired value of  $|G^*|$  or  $|\eta^*|$ .

### 10.2.1 Selection of the Proper Parameters

To get the same behavior of a sample when measured with the PPT as when measured with the rheometer, the shear rate of the crude oils has to be the same during the measurement. To calculate the shear rate, the measuring cup wall and the rod with the sensor at the end are approximated as the two plates model (see section 8.1.1) which is pictured in Fig. 10.2, with the distance  $h$  between the measuring cup wall and the rod being the gap of the two plates model. Hence the shear rate can be calculated with equation (8.3).

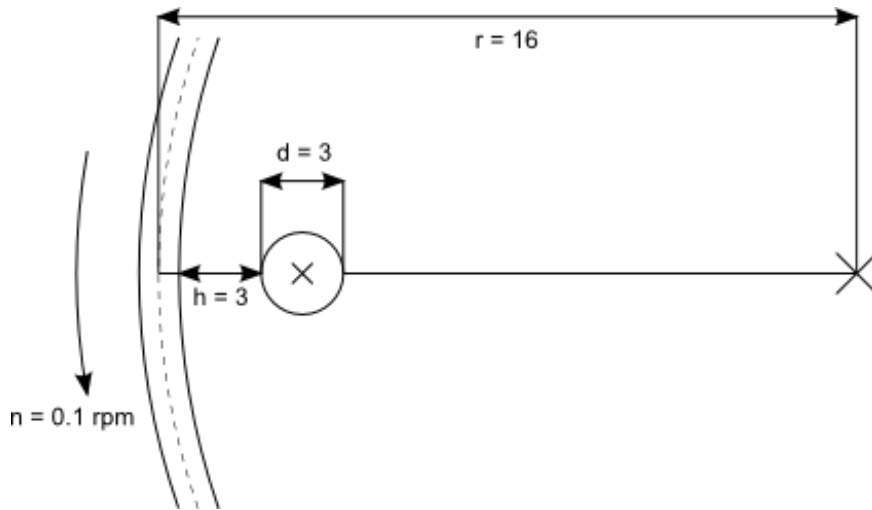


**Fig. 10.2:** Sketch of the PPT measuring cup with the sensor to determine the PP (small circle); length unit [mm]

$$\dot{\gamma} = \frac{v}{h} = \frac{\omega \cdot r}{h} = \frac{2\pi n \cdot r}{h} \quad (10.1)$$

In this case  $\omega$  is the angular velocity,  $n = 0.1$  rpm,  $r = 16$  mm is the radius of the measuring cup and  $h = 3$  mm, all this yields:

$$\dot{\gamma} = \frac{2\pi \cdot 0.1/\text{min} \cdot 0.016\text{m}}{0.003\text{m}} = \frac{2\pi \cdot 0.0017/\text{s} \cdot 0.016\text{m}}{0.003\text{m}} = 0.056/\text{s} \quad (10.2)$$

For the oscillation tests two other parameters have to be set, the first is the amplitude  $\gamma_A$  and the second is the angular frequency  $\omega$ . The amplitude  $\gamma_A = 0.05\%$  for the first tests was taken from literature [37], hence the angular frequency can be calculated to  $\omega = 112$  rad/s, because when looking at equation (8.19) it can be seen that:

$$\dot{\gamma}_A = \gamma_A \cdot \omega \quad (10.3)$$

Another important factor is the cooling rate which was estimated to be  $1$  °C/min by the duration of the PPT measurements. The start temperature of the measurements was of course  $50$  °C to get the same results as with the PPT.

### 10.2.2 Pour Point Measurements

With the parameters from the previous section, 6 crude oils were measured with the rheometer. The samples were applied at room temperature and then heated to  $50$  °C, as soon as this temperature was reached the measurement was started. During the measurement the temperature was kept at  $50$  °C for 1 min, then the samples were cooled down at least  $5$  °C below their PPs, which were determined with the PPT earlier, for the whole measurement and for all 6 samples the same parameters  $\gamma_A = 0.05\%$  and  $\omega = 112$  rad/s were used. A list of the PPs of the 6 crude oils (with-

out heat pretreatment) is shown in Tab. 10.1. The PPs of Sp23 and BeS5 had been measured again because their last PP measurement was performed 3 months earlier, with the result, that the average value of several PPs of Sp23 was 1.5 °C and of BeS5 2.8 °C higher than before the 3 months. But the samples of these two crude oils which were used for the rheometer measurements could have slightly higher PPs because the two containers were left half full for over 3 months before the PP measurements with the rheometer were performed.

	Sp23	BeS5	Pecica 654	Folesti 2600	Pecica 652	Păcureti 90
PP [°C]	3.6	3.5	13.8	14.2	16.5	20.8

Tab. 10.1: PPs of the 6 crude oils which were measured with the rheometer

However, the oscillations tests of the 6 samples with  $\gamma_A = 0.05\%$ ,  $\omega = 112$  rad/s and a cooling rate of 1 °C/min have already yielded some very good results. With the PP values from Tab. 10.1 it is possible to define that the temperatures of the measured samples at  $|\eta^*| := 150$  Pa·s are their PPs, which can be read out of Fig. 10.3 and the PPs are listed in Tab. 10.2.

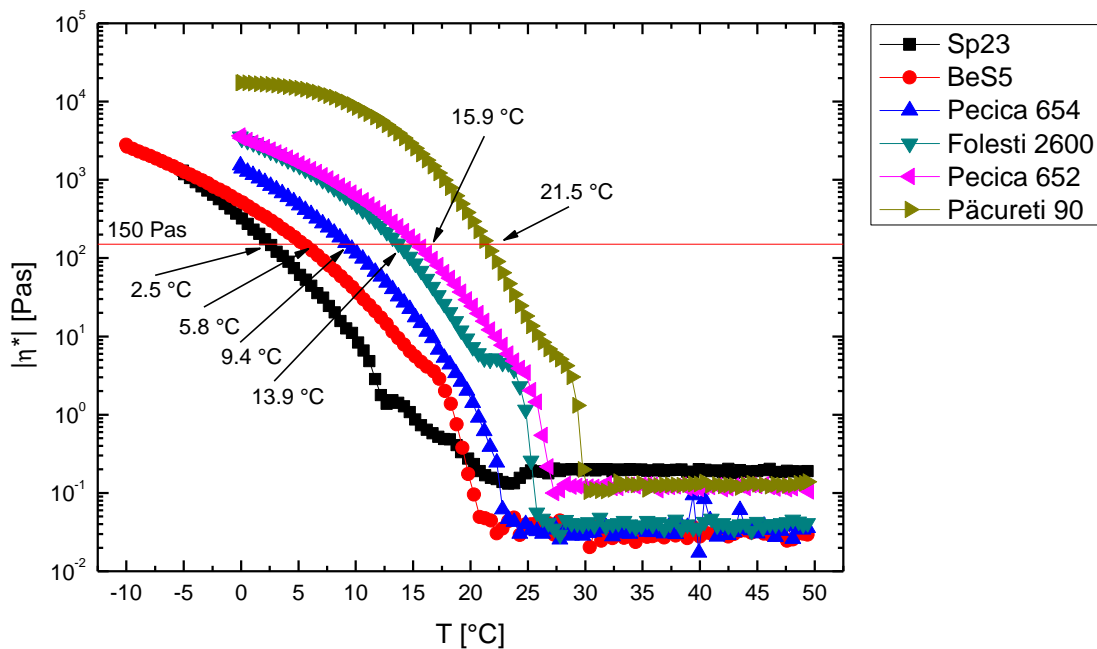


Fig. 10.3: Absolute value of the complex viscosity over temperature of 6 different crude oils, determined using the parameters cooling rate 1 °C/min,  $\omega = 112$  rad/s and  $\gamma_A = 0.05\%$ ; the red horizontal line at 150 Pas shows when the PP of the crude oils is reached

	Sp23	BeS5	Pecica 654	Folesti 2600	Pecica 652	Păcureti 90
PP [°C]	2.5	5.8	9.4	13.9	15.9	21.5

Tab. 10.2: PP values from Fig. 10.3 determined by a rheometer using a cooling rate of 1 °C/min, a deformation of 0.05 % and an angular frequency of 112 rad/s

Comparison between Tab. 10.1 and Tab. 10.2 yields that the maximum deviation of the PP values determined using the PPT from the PP values determined by the rheometer is 4.4 °C which is not too bad since the PPT has an error of up to  $\pm 1.7$  °C. The error of the oscillation tests in the area around the PP (150 Pas) was calculated for Sp23 with three and for Folesti 2600 with four independent measurements. The deviation of  $|\eta^*|$  does not exceed 5 % for Sp23 and 5.1 % for Folesti 2600. It should be mentioned that very low viscous crude oils might partly flow away from the measuring gap during the heating process and light components might vaporize even with the evaporation blocker, which could lead to a higher deviation than 5 % between the measurements.

Unfortunately not all 6 samples were in the LVE range for 0.05 % deformation and 112 rad/s angular frequency as demonstrated in Fig. 10.4 for BeS5.

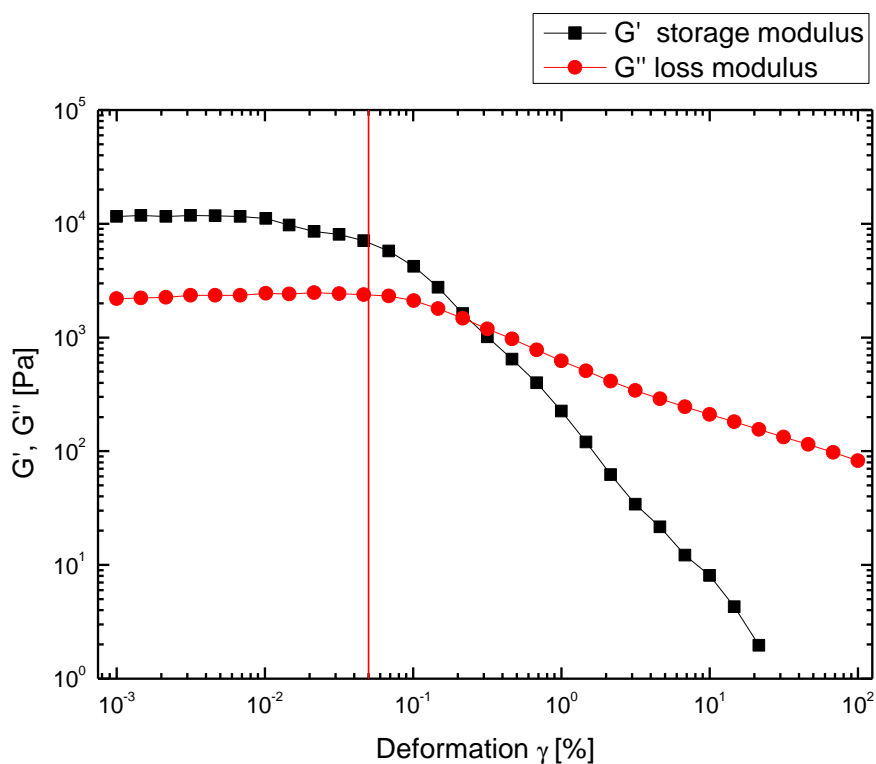


**Fig. 10.4:** Amplitude sweep of BeS5 at 112 rad/s, the vertical red line indicates 0.05 % deformation, which is not in the LVE range for this sample

To achieve more precise PP measurements with the rheometer, other frequencies were tested to see if a frequency exists for which the deformation that is calculated with the shear rate of 0.056 /s lies in the LVE range. Equation (10.3) shows that an increasing  $\omega$ , results in a decreasing  $\gamma_A$  for a constant shear rate. It was found, that the needed deformations for higher angular frequencies are nearer to or in the LVE range. Therefore  $\omega = 600$  rad/s, which is just below the maximum frequency of the rheometer (100 Hz or ca. 623 rad/s), was used for the next amplitude sweep. For this angular frequency the calculated deformation  $\gamma_A = 0.0093$  % lies within the LVE range or very close to it for all of the 6 samples e.g. for BeS5 in Fig. 10.5.



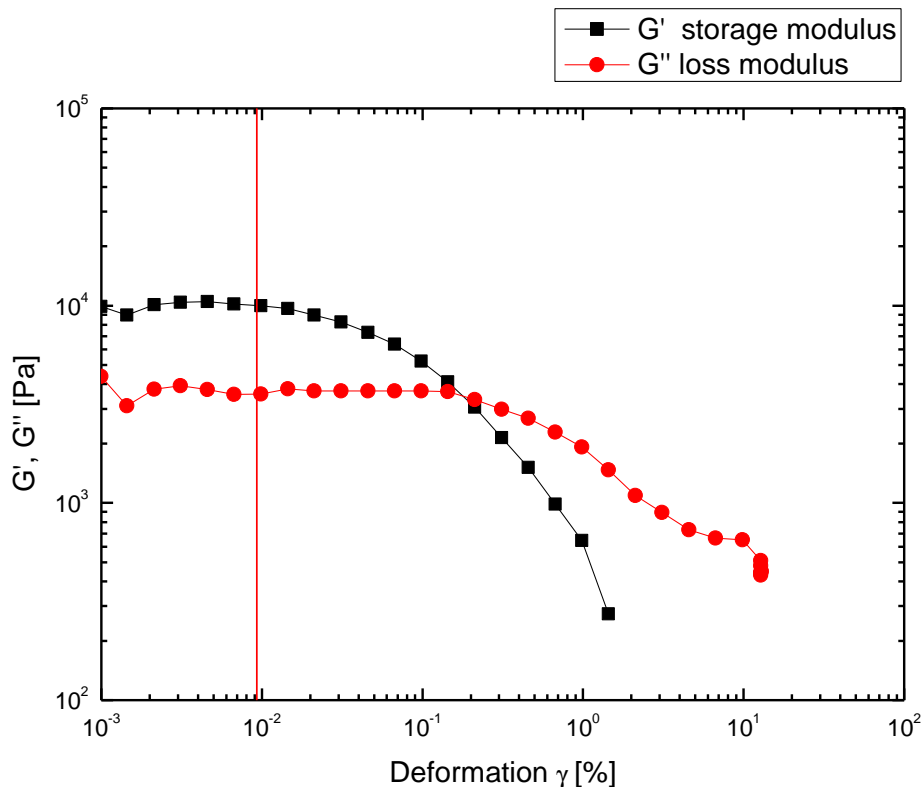


**Fig. 10.5:** Amplitude sweep of BeS5 at 600 rad/s, the vertical red line indicates 0.0093 % deformation, which is barely in the LVE range for this sample

To see if it really improves the accuracy of the PP measurements when the deformation lies in the LVE range, the PPs of all 6 crude oils were measured again with the rheometer. The results in Fig. 10.6 and Tab. 10.3 show, that the PP values are closer to the ones of the PPT because the maximum deviation between the PP values determined by the PPT and by the rheometer is 3.5 °C. But the error calculated for three independent measurements of Folesti 2600 was up to 6.5 % which is higher than the 5 % of the measurements with  $\omega = 112$  rad/s and  $\gamma_A = 0.05$  %. With increasing frequency the  $|\eta^*|$  value which is related to the PP is not the same anymore, for an angular frequency of 600 rad/s it is  $|\eta^*| = 35$  Pa·s. Only one problem occurred while using these parameters, at several measuring points the rheometer software displayed automatic adjusting timeouts which means that the automatic adjust process was aborted. This means that the ideal angular frequency has to be somewhere between 112 rad/s and 600 rad/s.

Two cooling rate experiments were performed with  $\omega = 112$  rad/s, one using a cooling rate of 0.33 °C/min (or 20 °C/h), the results of this measurement are shown in Fig. 10.7 and Tab. 10.4. The other cooling rate was 0.5 °C/min but these measurement results should not be compared with the other ones since the measurements were performed without evaporation blocker, nevertheless except for Pecica 654 the PP values fit between the results if the other two measurements.

A comparison between Fig. 10.3 and Fig. 10.7 shows that the two crude oils Pecica 652 and Pecica 654 are not affected by the lower cooling rate while the PPs of the other 4 crude oils are about 2 °C higher.

Altogether this means that it is possible to measure PPs by performing oscillation tests using a rheometer and hence to investigate the influence of different cooling rates on the PP. The results of the cooling rate experiment in this section show, that the PP being higher when determined using a lower cooling rate fits perfectly to the fact that at low cooling rates more crystals can be observed in crude oil as mentioned in the theoretical part in section 5.2.

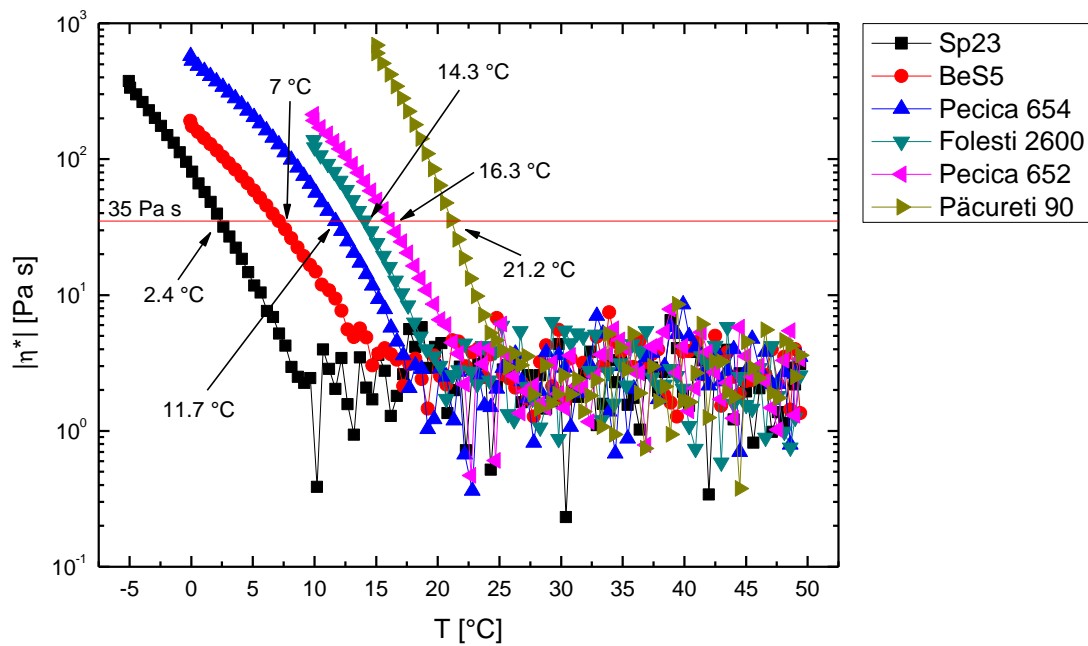


**Fig. 10.6:** Absolute value of the complex viscosity over temperature of 6 different crude oils, determined using the parameters cooling rate 1 °C/min,  $\omega = 600$  rad/s and  $\gamma_A = 0.0093$  %; the red horizontal line at 35 Pa s shows when the PP of the crude oils is reached

	Sp23	BeS5	Pecica 654	Folesti 2600	Pecica 652	Păcureti 90
PP [°C]	2.4	7	11.7	14.3	16.3	21.2

**Tab. 10.3:** PP values from Fig. 10.6 determined by a rheometer using a cooling rate of 1 °C/min, a deformation of 0.0093 % and an angular frequency of 600 rad/s

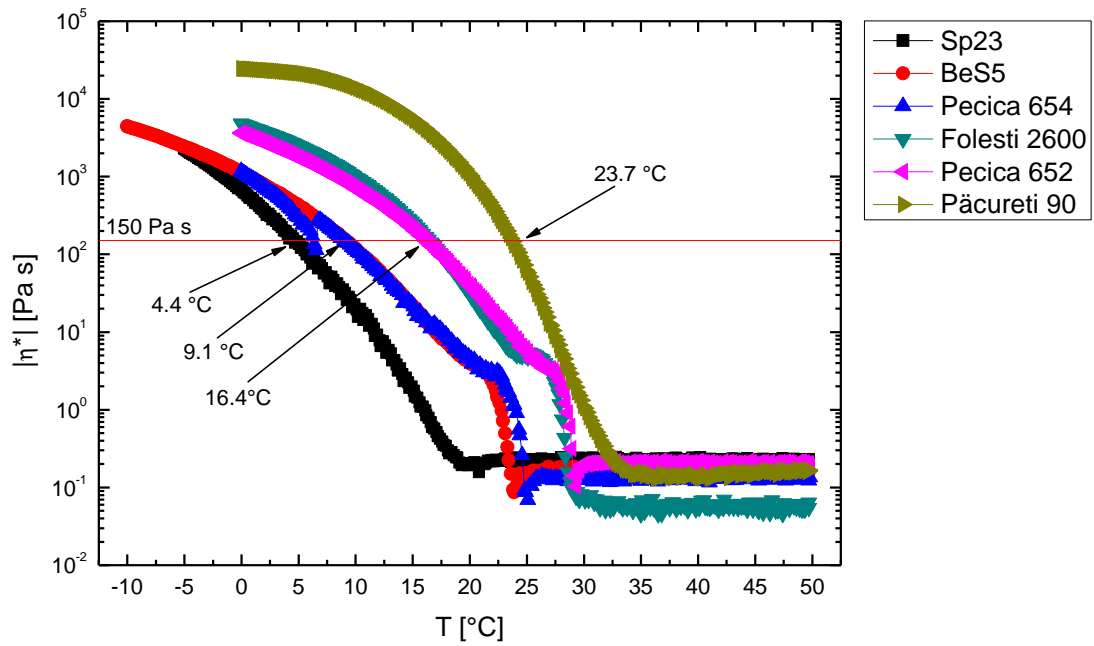


**Fig. 10.7:** Absolute value of the complex viscosity over temperature of 6 different crude oils, determined using the parameters cooling rate  $0.33 \text{ }^\circ\text{C}/\text{min}$ ,  $\omega = 112 \text{ rad/s}$  and  $\gamma_A = 0.05 \%$ ; the red horizontal line at  $150 \text{ Pa s}$  shows when the PP of the crude oils is reached

	Sp23	BeS5	Pecica 654	Folesti 2600	Pecica 652	Păcureti 90
PP [°C]	4.4	9.1	9.1	16.4	16.4	23.7

**Tab. 10.4:** PP values from Fig. 10.7 determined by a rheometer using a cooling rate of  $0.33 \text{ }^\circ\text{C}/\text{min}$ , a deformation of  $0.05 \%$  and an angular frequency of  $112 \text{ rad/s}$

## 11 Conclusion and Recommendations

Experience shows that all crude oils behave differently because of their varying composition, thus it is not possible to formulate a simple generic pretreatment and measuring procedure to classify all crude oils that exist. But it can be said that most crude oils have a maximum pour point value when preheated to a temperature between 45 °C and 65 °C and many crude oils have a minimum pour point when preheated to a temperature around 70 °C (of course there are exceptions possible as mentioned in section 9.1.3). Therefore a crude oil sample should be tested in a lab using a pour point tester at least without heat pretreatment, preheated to a temperature around 50 °C for 12 h and preheated to about 70 °C for at least 20 min.

Before a crude oil is heated in a storage tank to get a lower pour point and less paraffin wax precipitation during the transport to the refinery, a sample of this crude oil should be tested in the lab, at more than the three recommended preheating temperatures to ensure which one exactly is the lowest pour point. The findings gained in such lab tests can help to reduce costs originating from maintenance jobs like pigging or from the heating of the storage tanks to a wrong or unnecessary temperature.

Since the paraffin crystals, agglomerations and crystal lattices are responsible for the pour point it is clear that different preheating procedures influence them as well. The pretreatment changes the amount of crystal material and the shape of the crystals themselves.

When observing crude oil samples under a microscope it is not needed to use a polarization filter all the time, because in a simple transmission microscope the paraffin crystals can be seen very well but it is recommended to use the polarization filter to check if all structures in the observation area are paraffin crystals or if other materials are in between.

To see how exactly the crystals look in detail they can be observed using a scanning electron microscope, but here the sample preparation is time-consuming and many crystal accumulations form which of course look different than the crystals in a drop of crude oil, because until now no really good method exists to get the crystals from the liquid oil on a specimen holder without the oil.

When using a pour point tester it is not possible to measure the pour point of a crude oil at various cooling rates until now. Thus a method to determine the pour point of crude oils via oscillation tests with a rheometer had been developed in this work and since a rheometer is suited excellent to perform measurements at various cooling rates it is possible to determine the pour point of crude oils at different cooling rates with this method.

The pour point of most crude oils is influenced by cooling rates, in general a high cooling rate leads to a lower pour point and a low cooling rate results in a higher pour point, this fact is very interesting for pipelines in colder regions especially during winter.

Crude oils at temperatures below their wax appearance temperatures are viscoelastic-fluids and at the pour point they are viscoelastic-solids, even though the crude oils are still able to flow at sufficient high shear rates, which is due to the shear thinning behavior of crude oils. Therefore crude oils below their wax appearance temperature cannot be described by the viscosity because viscoelastic substances are defined by the storage modulus and the loss modulus or by a combination of both of them in the form of the complex shear modulus or the complex viscosity.

## 12 Future Prospects

One follow-up project of this work could be an investigation of the crystal structure of several different crude oils using a transmission microscope with a hot/cold stage. Hence heat up and cool down processes could be observed with a precise temperature control. With such an experimental setup the pour points of the crude oils could be determined after different preheat treatments and with various cooling rates, which would give further information about the influence of the various preheat temperatures and holding times at these temperatures and about the influence of different cooling rates on the amount of crystal material and on the crystal structure of crude oils.

An additional investigation, which could lead to interesting results, concerns the time it takes until a crude oil sample with a lowered pour point due to a preheat treatment, which is left at room temperature, regains the pour point it had before the heat treatment. Of course the amount of time such a process takes is different for each crude oil but maybe a correlation between this value and the crystal structure or the composition of the measured crude oils exists.

Another future prospect could be the development of a better sample preparation method for the scanning electron microscope, because a transmission microscope has a low depth of focus which makes it difficult to focus on all crystal material in the image section. But a scanning electron microscope has a very high depth of focus which makes it easy to see all crystal material in the image section.

The main difficulty of such a project would not be the problem to get the paraffin crystals from the crude oil on the specimen holder but to clean the crystals without washing them off the specimen holder.

A very interesting follow-up project would be the enhancement of the pour point measurements with the rheometer. At first an angular frequency and the corresponding amplitude have to be found, at which as much crude oils as possible are in the linear viscoelastic range. Then several crude oils have to be measured and the method has to be calibrated, which is achieved, as done in this thesis, by searching a value of the absolute value of the complex viscosity at which the temperatures of the crude oils are closest to their pour points which were determined with a pour point tester earlier. This measuring method would not only increase the precision of the repeatability of the pour point measurements but also the repeatability itself. And of course it is an automatic method with the possibility to perform measurements using various cooling rates.

## Nomenclature

$A$	constant dependent on the entropy of activation of flow (Arrhenius equation)/ geometric constant depending on the nucleus morphology (empiric nucleation enthalpy equation)/ area of a plate
$c$	constant
$C_N$	damper constant
$C_H$	spring constant
$E_a$	activation energy of viscous flow
$\Delta G$	free enthalpy
$\Delta mH_i$	molar melting heat for a given n-alkane $i$
$\Delta P$	pressure drop
$f$	frequency
$F$	force
$G$	shear modulus
$G^*$	complex shear modulus
$G'$	storage modulus
$G''$	loss modulus
$G_{sol}$	free enthalpy of the chemical deposition
$G_{vol}$	free enthalpy of the solution
$h$	height (gap between two plates)
$I$	intensity/ current strength or flow rate
$k$	Boltzmann constant
$L$	length
$M_i$	molecular weight of a given n-alkane $i$
$n$	number of particles/ number of statistically allocated measuring values/ number of rotations per minute
$n^*$	critical number of molecules in the nucleus
$N$	number of particles
$p$	pressure
$r$	radius
$R$	universal gas constant/ radius
$s$	displacement
$t$	time
$T$	temperature
$T_{m,i}$	melting temperature
$v$	velocity
$V$	volume
$\bar{x}$	average value

## Nomenclature

---

$x_i$	single measuring value
$X_s$	molar fraction of solute in the saturated solution at the saturation temperature
$X_c$	molar fraction of solute at the crystallization temperature
$\beta$	supersaturation = $X_s/X_c$
$\gamma$	deformation
$\dot{\gamma}$	shear rate
$\delta$	phase displacement angle
$\varepsilon$	porosity (Carman-Kozeny equation)
$\eta$	viscosity
$\eta^*$	complex viscosity
$\theta$	contact angle defined by interface energies $\sigma_{AA}$ and $\sigma_{AB}$
$\lambda$	wavelength
$\mu$	Newtonian dynamic viscosity
$\nu$	kinematic viscosity
$\rho$	density
$\sigma$	cross section/ specific energy of the crystal-solution interfacial surface/ standard deviation of a single measuring value
$\sigma_{AA}$	interface energy
$\sigma_{AB}$	interface energy
$\sigma_m$	standard deviation of the average value
$\tau$	shear stress
$\varphi$	displacement angle
$\phi$	angle of the cone (cone-plate system)
$\omega$	angular velocity/ angular frequency
$\omega_s$	solids concentration (Carman-Kozeny equation)



## Glossary

BeS5old	Crude Oil from Bernhardsthal Süd 5 (Austria)
BeS5	Crude Oil from Bernhardsthal Süd 5 (Austria)
CHE	Chemical Number
CPM	Cross Polarized Microscopy
CSD	Controlled Shear Deformation
CSR	Controlled Shear Rate
CSS	Controlled Shear Stress
CWDT	Critical Wax Deposition Temperature
DSC	Differential Scanning Calorimetry
Folesti 2600	Crude Oil from Folesti Well 2600 (Romania)
IR	Infrared
LVE	Linear Viscoelastic
NIR	Near Infrared
NSO	Nitrogen, Sulfur, Oxygen
OD	Optical Density
OWCT	Onset Wax Crystallization Temperature
Păcureti 90	Crude Oil from Păcureti Well 90 (Romania)
Pecica 652	Crude Oil from Pecica Well 652 (Romania)
Pecica 654	Crude Oil from Pecica Well 654 (Romania)
PP	Pour Point
PPT	Pout Point Tester
PTL	Power of Transmitted Light
PVT	Pressure, Volume, Temperature
SDS	Solid Detection System
SEM	Scanning Electron Microscope
Sp23	Crude Oil from Spannberg 23 (Austria)
TM	Transmission Microscope
VE	Viscoelastic
WAT	Wax Appearance Temperature
WPT	Wax Precipitation Temperature

## List of Figures

Fig. 2.1:	<i>Structure formulas of examples of alkanes [4]</i> .....	10
Fig. 2.2:	<i>Structure formula of a cycloalkane [4]</i> .....	11
Fig. 2.3:	<i>Structure formula of an aromatic hydrocarbon [4]</i> .....	11
Fig. 2.4:	<i>Composition Diagram for Crude Oils (facsimile) [5]</i> .....	12
Fig. 2.5:	<i>Classification scheme of crude oils [1]</i> .....	13
Fig. 3.1:	<i>CPM schematic drawing [11]</i> .....	15
Fig. 3.2:	<i>A crude oil sample observed at different temperatures with a CPM [11]</i> ..	15
Fig. 3.3:	<i>Typical DSC curve (heat power vs. time) [13]</i> .....	16
Fig. 3.4:	<i>SDS Configuration [11]</i> .....	17
Fig. 3.5:	<i>Typical PTL curve [11]</i> .....	18
Fig. 3.6:	<i>Left: NIR spectra of a waxy gas condensate; right: changes in optical density of an oil at a wavelength of 1100 nm, the WAT is <math>33\pm 1</math> °C [14]</i> ....	19
Fig. 3.7:	<i>Pressure drop across a filter plugged by several oils [10]</i> .....	20
Fig. 3.8:	<i>Determination of the WAT from a viscosity-temperature curve via Arrhenius fit: (a) linear viscosity-temperature plot, (b) logarithmic viscosity-reciprocal temperature plot showing the deviation of the viscosity from linearity [13] (c) viscosity-reciprocal temperature, close-up of the deviation from linearity [9]</i> .....	21
Fig. 3.9:	<i>Formation of a chemical disposition in a mixture of two components, A (bright) and B (dark). (a) Disordered allocation of the two components. (b) Formation of a disposition of the minority component B [16]</i> .....	23
Fig. 3.10:	<i>Free enthalpy of a spherical chemical disposition [16]</i> .....	24
Fig. 3.11:	<i>Definition critical nucleus (facsimile) [16]</i> .....	24
Fig. 3.12:	<i>Heterogeneous nucleation of a disposition consisting of the component B between two crystallites of the component A (facsimile) [16]</i> .....	25
Fig. 3.13:	<i>Disposition density over time (normalized to the saturation disposition density) [16]</i> .....	26
Fig. 3.14:	<i>Crystal growth in stacked layers [15]</i> .....	27
Fig. 3.15:	<i>Crystal growth in spirals [15]</i> .....	27
Fig. 3.16:	<i>Wax disposition within laminar and turbulent flow [11]</i> .....	28
Fig. 3.17:	<i>Typical curve WAT vs. pressure [17]</i> .....	30
Fig. 3.18:	<i>Drawing of the heat exchanger to measure the amount of wax disposition in a flowing system [20]</i> .....	31
Fig. 3.19:	<i>Asymptotic behavior of the wax deposition over the time [20]</i> .....	31
Fig. 4.1:	<i>Pour point test apparatus setup (all dimensions are stated in millimeters) [21]</i> .....	34
Fig. 4.2:	<i>Pressure vessel [21]</i> .....	35
Fig. 4.3:	<i>Pour Point Tester principle; 1 light barrier, 2 temperature sensor, 3 test specimen, 4 motor (ca. 0.1 rpm) [26]</i> .....	36
Fig. 5.1:	<i>Effect of temperature on wax precipitation determined by a CPM during a static cooling process of 2 °C/min. At 45 °C (a), 28 °C (b), 24 °C (c) and 20 °C (d) [27]</i> .....	38
Fig. 5.2:	<i>Effect of cooling rate on wax precipitation. All three pictures were taken at the same temperature which was below the pour point, just the cooling rates were different: 2 °C/min (a), 1 °C/min (b) and 0.5 °C/min (c) [27]</i> ....	39
Fig. 6.1:	<i>Reduced effective pipe diameter due to wax depositions [7]</i> .....	41

## List of Figures

---

Fig. 6.2:	<i>Pressure loss in a pipe with a certain length for laminar flow conditions [4]</i>	42
Fig. 7.1:	<i>Wax crystallization with and without paraffin inhibitors or PPDs; left: uninhibited paraffin crystallization, right: paraffin inhibitor molecule and paraffin crystallization with inhibitor [5]</i>	44
Fig. 7.2:	<i>Wax crystallization; top: uninhibited paraffin crystallization, right: inhibited paraffin crystallization [29]</i>	44
Fig. 7.3:	<i>Paraffin crystals before (left) and after (right) magnetic treatment [5]</i>	46
Fig. 7.4:	<i>Hydraulically activated power pig HAPP (uses high pressure fluid jets to remove dispositions) [32]</i>	47
Fig. 7.5:	<i>Scrapers mounted on a sucker rod [5]</i>	47
Fig. 7.6:	<i>Hot oiling [5]</i>	49
Fig. 7.7:	<i>Downhole heater [5]</i>	50
Fig. 8.1:	<i>Two plates model, two plates with the sample between them</i>	53
Fig. 8.2:	<i>(a) viscosity over shear rate; (b) shear stress over shear rate</i>	55
Fig. 8.3:	<i>Viscosity over time: (a) thixotropic behavior 1) region of constant shear rate 2) recovery; (b) rheopectic behavior 1) region of constant shear rate, 2) recovery</i>	56
Fig. 8.4:	<i>(a) Newtonian model (damper), (b) Hookean model (spring)</i>	57
Fig. 8.5:	<i>Two plates model for ideal elastic behavior</i>	57
Fig. 8.6:	<i>(a) Maxwell model, (b) Kelvin/Voigt model</i>	59
Fig. 8.7:	<i>Sketch of the cone plate measuring system [4]</i>	61
Fig. 8.8:	<i>Measuring systems: (a) plate-plate, (b) cone-plate, (c) cylinder, (d) double gap [4]</i>	61
Fig. 8.9:	<i>(a) complex shear modulus, (b) complex viscosity</i>	63
Fig. 8.10:	<i>LVE range: (a) sample with VE-solid behavior, (b) sample with VE-fluid behavior</i>	65
Fig. 9.1:	<i>PPT Setup</i>	68
Fig. 9.2:	<i>PPT: measuring arm and measuring cup with sample</i>	68
Fig. 9.3:	<i>WinPPT: measured curve of CHE20105147 Bernhardsthal Süd 5</i>	69
Fig. 9.4:	<i>BeS5old: three different preheat temperatures</i>	71
Fig. 9.5:	<i>Pour points of BeS5old with two different heat pretreatments and 70 °C PPT start temp.</i>	72
Fig. 9.6:	<i>Pour points of BeS5old with two different heat pretreatments and 50 °C PPT start temp.</i>	72
Fig. 9.7:	<i>BeS5old untreated tested with different PPT start temperatures</i>	73
Fig. 9.8:	<i>Measuring curve of Sp23 with 9 PP cycles</i>	74
Fig. 9.9:	<i>9 PP cycles at 13 different preheating temperatures of the sample BeS5</i>	76
Fig. 9.10:	<i>BeS5: the first value of the 9 cycles for each pretreatment temperature with the error of the single measuring values</i>	76
Fig. 9.11:	<i>BeS5: average value and error of the PP cycles for 13 different Preheat Temperatures</i>	78
Fig. 9.12:	<i>Sp23: average value and error of the PP cycles for 13 different Preheat Temperatures</i>	79
Fig. 9.13:	<i>Folesti 2600: average value and error of the PP cycles for 13 different Preheat Temperatures</i>	79
Fig. 9.14:	<i>Pecica 652: average value and error of the PP cycles for 13 different Preheat Temperatures</i>	80
Fig. 9.15:	<i>PP of inhibited Akshabulak crude oil over Preheat Temperature [30]</i>	80

Fig. 9.16: <i>Pecica 652 without thermal pretreatment, needle- and rod-shaped crystals: (a) the yellow bar scales 50 <math>\mu\text{m}</math>; (b) higher magnification, the yellow bar scales 20 <math>\mu\text{m}</math> .....</i>	83
Fig. 9.17: <i>Cool down process of Pecica 652 preheated to 55 <math>^{\circ}\text{C}</math>, the yellow bar scales 50 <math>\mu\text{m}</math> in all 4 pictures, the dots and the bent rods are paraffin crystals: (a) photograph taken directly after application, small dots are visible; (b) 1 min 23 sec after application, the crystals are bigger and some have agglomerated to rods; (c) 3 min 29 sec after application, the crystals have grown a lot and many rod shaped agglomerations have formed, afterwards not much change could be observed even after one hour; (d) this picture was taken 1 min after (c) using a polarization filter.....</i>	83
Fig. 9.18: <i>Cool down process of Pecica 652 preheated to 85 <math>^{\circ}\text{C}</math>, the yellow bar in the 4 pictures scale 50 <math>\mu\text{m}</math> each: (a) directly after application, very few crystals are visible; (b) 1 min 48 sec after application, more crystals (small white dots) but still the same size as in (a); (c) 2 min 18 sec after application, the crystals have grown but not many new ones have formed; (d) several min after application, the crystals have grown bigger but no agglomerations have formed.....</i>	84
Fig. 9.19: <i>Pecica 652 preheated to 85 <math>^{\circ}\text{C}</math>, the sample had room temperature for several minutes before it was observed: (a) higher magnification (yellow bar scales 50 <math>\mu\text{m}</math>), (b) even higher magnification (grey bar scales 10 <math>\mu\text{m}</math>); the spherical crystals from Fig. 9.18 are in fact little hook-shaped crystals which entrap liquid crude oil.....</i>	84
Fig. 9.20: <i>BeS5 cooled before viewed under the microscope, the yellow bar scales 50 <math>\mu\text{m}</math> in all three photographs: (a) without pretreatment, needle-shaped crystals; (b) preheated to 55 <math>^{\circ}\text{C}</math>, dots and needles or rods; (c) preheated to 85 <math>^{\circ}\text{C}</math>; hook-shaped crystals like in Fig. 9.19 (a) and (b) .....</i>	85
Fig. 9.21: <i>Pecica 652 without heat pretreatment: (a) paraffin crystal accumulations consisting mainly of needle-shaped crystals, (b) paraffin crystal accumulations and NaCl crystals covered with paraffin crystals, (c) and (d) needle-shaped crystals with different lengths .....</i>	87
Fig. 9.22: <i>Pecica 652 preheated to 55 <math>^{\circ}\text{C}</math>: (a) and (b) big paraffin crystal accumulations, (c) much more crystal material than in Fig. 9.21 an Fig. 9.23, (d) many paraffin covered NaCl crystals, which show the heterogeneous nucleation .....</i>	88
Fig. 9.23: <i>Pecica 652 preheated to 85 <math>^{\circ}\text{C}</math>: (a) not very much crystal material compared to Fig. 9.21, (b)-(d) big structures consisting of a mixture of short needles- and small hook-shaped crystals.....</i>	89
Fig. 9.24: <i>Pecica 652 without thermal pretreatment: comparison between TM and SEM pictures .....</i>	90
Fig. 9.25: <i>Pecica 652 preheated to 55 <math>^{\circ}\text{C}</math>: comparison between TM and SEM pictures .....</i>	90
Fig. 9.26: <i>Pecica 652 preheated to 85 <math>^{\circ}\text{C}</math>: comparison between TM and SEM pictures .....</i>	91
Fig. 10.1: <i>Rheometer with plate-plate measuring system and Peltier hood.....</i>	93
Fig. 10.2: <i>Sketch of the PPT measuring cup with the sensor to determine the PP (small circle); length unit [mm].....</i>	94
Fig. 10.3: <i>Absolute value of the complex viscosity over temperature of 6 different crude oils, determined using the parameters cooling rate 1 <math>^{\circ}\text{C}/\text{min}</math>, <math>\omega = 112 \text{ rad/s}</math> and <math>\gamma_A = 0.05 \%</math>; the red horizontal line at 150 Pa s shows when the PP of the crude oils is reached .....</i>	95

Fig. 10.4: Amplitude sweep of BeS5 at 112 rad/s, the vertical red line indicates 0.05 % deformation, which is not in the LVE range for this sample .....	96
Fig. 10.5: Amplitude sweep of BeS5 at 600 rad/s, the vertical red line indicates 0.0093 % deformation, which is barely in the LVE range for this sample .	97
Fig. 10.6: Absolute value of the complex viscosity over temperature of 6 different crude oils, determined using the parameters cooling rate 1 °C/min, $\omega = 600$ rad/s and $\gamma_A = 0.0093$ %; the red horizontal line at 35 Pa s shows when the PP of the crude oils is reached.....	98
Fig. 10.7: Absolute value of the complex viscosity over temperature of 6 different crude oils, determined using the parameters cooling rate 0.33 °C/min, $\omega = 112$ rad/s and $\gamma_A = 0.05$ %; the red horizontal line at 150 Pa s shows when the PP of the crude oils is reached.....	99
Fig. A1.1: 9 PP cycles at 13 different preheating temperatures of the sample Sp23.....	114
Fig. A1.2: Sp23: the first value of the 9 cycles for each pretreatment temperature with the error of the single measuring values.....	115
Fig. A1.3: 9 PP cycles at 13 different preheating temperatures of the sample Folesti 2600.....	116
Fig. A1.4: Folesti 2600: the first value of the 9 cycles for each pretreatment temperature with the error of the single measuring values .....	116
Fig. A1.5: 9 PP cycles at 13 different preheating temperatures of the sample Pecica 652.....	117
Fig. A1.6: Pecica 652: the first value of the 9 cycles for each pretreatment temperature with the error of the single measuring values .....	118
Fig. A2.1: Folesti 2600 cooled before viewed under the microscope: (a) and (b) without pretreatment, needle-shaped crystals, yellow bar scales 50 $\mu\text{m}$ ; (c) preheated to 55 °C, bent rods, yellow bar scales 25 $\mu\text{m}$ .....	119
Fig. A2.2: Sp23 cooled before viewed under the microscope, the yellow bars in all three photographs scale 50 $\mu\text{m}$ , needle-shaped crystals in all three pictures, (a) without pretreatment; (b) preheated to 55 °C; (c) preheated to 85 °C.....	120
Fig. A2.3: Pecica 652 cooled before viewed under the microscope, the photographs on the right side were always taken a few minutes later than the left ones; (a) and (b) without heat pretreatment, bars scale 20 $\mu\text{m}$ , needle-shaped crystals; (c) and (d) preheated to 55 °C, yellow bars scale 50 $\mu\text{m}$ , spherical and rod-shaped crystals; (e) and (f) preheated to 85 °C, yellow bars scale 50 $\mu\text{m}$ , spherical agglomerations consisting of hook-shaped crystals ....	121
Fig. A3.1: Pecica 652 without thermal pretreatment, accumulations of needle-shaped paraffin crystals and paraffin covered NaCl crystals.....	122
Fig. A3.2: Pecica 652 preheated to 55 °C, accumulations of needle-shaped paraffin crystals and paraffin covered NaCl crystals.....	123
Fig. A3.3: Pecica 652 preheated to 85 °C, accumulations of hook-shaped paraffin crystals and a paraffin covered NaCl crystal.....	124

## References

- [1] Killops, S. D. and Killops V.J.: "Einführung in die organische Geochemie", 1997 (Ferdinand Enke, Stuttgart)
- [2] Bartholomé, E. et al.: "Ullmanns Encyklopädie der technischen Chemie", 1976 (Verlag Chemie, Weinheim, New York)
- [3] Neumüller, O.-A.: "Römpps Chemie –Lexikon", 1988 (Frankh, Stuttgart)
- [4] Mayrhofer, E.: Diploma Thesis, "Influence of Pressure on Paraffin Inhibitor Performance", 2011
- [5] Kainz, A.: Diploma Thesis, "Paraffin Inhibitor Screening on Vienna Basin Crude Oils", 2007
- [6] Misra, S. et al.: "Paraffin Problems in Crude Oil Production And Transportation: A Review", SPE 28181, 1994, 50-54
- [7] Mansoori, G.A.: "Paraffin/ Wax and Waxy Crude Oil", University of Illinois at Chicago, [http://tigger.uic.edu/~mansoori/Wax.and.Waxy.Crude\\_html](http://tigger.uic.edu/~mansoori/Wax.and.Waxy.Crude_html), downloaded during January 2011
- [8] Kök, M. V. et al.: "Comparative Methods in the Determinations of Wax Content and Pour Points of Crude Oils", Journal of Thermal Analysis and Calorimetry, 2007, 90, 827-831
- [9] Rønningsen, H. P. et al.: "Wax Precipitation from North Sea Crude Oils. 1. Crystallization and Dissolution Temperatures, and Newtonian and Non-Newtonian flow Properties ", Energy & Fuels, 1991, 5, 895-908
- [10] Coutinho, J. A. P. and Daridon, J.-L.: "The Limitations of the Cloud Point Measurement Techniques and the Influence of the Oil Composition on Its Detection", Petroleum Science and Technology, 2005, 23, 1113-1128
- [11] Hammami, A. and Raines, M. A.: "Paraffin Deposition From Crude Oils: Comparison of Laboratory Results With Field Data", SPE 54021, 1998, 4, 9-18
- [12] Martos, C. et al.: "Characterization of Brazilian Crude Oil Samples To Improve the Prediction of Wax Precipitation in Flow Assurance Problems", Energy & Fuels, 2010, 24, 2221-2226

## References

---

- [13] Abdul Aziz, A. K. and Issham, I.: "Determination of the Crystallization of Waxy Crude and the Influence of Diluents", Department of Petroleum Engineering, Faculty of Chemical and Natural Resources Engineering, Universiti Teknologi Malaysia, 1997, 316-325
- [14] Kaso, P. et al.: "Measurement of Wax Appearance Temperature Using Near-Infrared (NIR) Scattering", *Energy & Fuels*, 2009, 23, 4988-4994
- [15] Denis, J. and Durand, J.-P.: "Modification of Wax Crystallization in Petroleum Products", *Revue de l'Institut Français du Pétrole*, 1991, 46, 637-649
- [16] Bauer, E. et al.: "Materialwissenschaften", lecture scriptum for technical physics, Institute of Solid-State Physics, Vienna University of Technology, academic year 2005/2006
- [17] Brown, T.S. et al.: "The Effects of Light Ends and High Pressure on Paraffin Formation", *SPE 28505*, 1994, 415-429
- [18] Huanquan, P. and Abbas, F.: "Pressure and Composition Effect on Wax Precipitation: Experimental Data and Model Results", *SPE 36740*, Reservoir Engineering Research Institute, 1996, 579-592
- [19] Vieira, L.C. et al.: "Effect of Pressure on the Crystallization of Crude Oil Waxes. II. Evaluation of Crude Oils and Condensate", *Energy & Fuels*, 2010, 24, 2213-2220
- [20] Bott, T.R. and Gudmundsson, J.S.: "Deposition of Paraffin Wax from Flowing Systems", Institute of Petroleum, IP 77 – 007, University of Birmingham, Department of Chemical Engineering
- [21] ASTM Standard D 5853, 1995 (2006): "Standard Test Method for Pour Point of Crude Oils", ASTM International, West Conshohocken, PA
- [22] Dobbs, J. B.: "A Unique Method of Paraffin Control in Production Operations", *SPE 55647*, 1999, 1-6
- [23] Pedersen, K.S. and Rønningsen, H.P.: "Influence of Wax Inhibitors on Wax Appearance Temperature, Pour Point, and Viscosity of Waxy Crude Oils", *Energy & Fuels* 2003, 17, 321-328
- [24] ASTM Standard D 97, 1965 (2006): "Standard Test Method for Pour Point of Petroleum Products", ASTM International, West Conshohocken, PA

- [25] ASTM Standard D 5985, 1996 (2002): "Standard Test Method for Pour Point of Petroleum Products (Rotational Method)", ASTM International, West Conshohocken, PA
- [26] PSL Systemtechnik Germany, <http://www.psl-systemtechnik.de>, downloaded during March 2011
- [27] Chang, C. and Boger, D.V.: "Influence of Thermal History on the Waxy Structure of Statically Cooled Waxy Crude Oil", SPE 57959, 2000, 5, 148-157
- [28] Demtröder, W.: "Experimentalphysik 1", 3<sup>rd</sup> edition, corrected reprint 2004 (Springer, Berlin, Heidelberg, New York)
- [29] Bilderback, C.A. and McDougall, L.A.: "Complete Paraffin Control in Petroleum Production", Journal of Petroleum Technology, 1969, 1151-1156
- [30] Zettlitzer, M.: "Successful field application of chemical flow improvers in pipeline transportation of highly paraffinic oil in Kazakhstan", SPE 65168, 2000, 1-12
- [31] <http://www.magtekinc.com/services1.htm>, "Study of Paraffin Crystallization Process Under the Influence of Magnetic Fields and Chemicals", SPE paper, 1997, 1-6
- [32] Stoltze, B.: "A new Pipeline Cleaning Technology: Hydraulically Activated Power Pigging (HAPP)", Pigging Products and Services Association, 2007, <http://www.ppsa-online.com/papers/2007-8-Stoltze.pdf>, downloaded during March 2011
- [33] <http://www.paraffincleaner.com>, downloaded during March 2011
- [34] Yousif, M.H. et al.: "Control Paraffin with Well Bore Insulating Gelled Fluids", Petroleum Engineer International, 1994, 26-28
- [35] Towler, B. F.: "System and Method for the Mitigation of Paraffin Wax Deposition from Crude Oil by using Ultrasonic Waves", Patent, University of Wyoming, 2004, <http://uwadmnweb.uwyo.edu/rpc/Patents%20PDF/WO04024309A21.pdf>, downloaded during March 2011
- [36] Mezger, T.G.: "Das Rheologie Handbuch", 2<sup>nd</sup> edition, revised version, 2006 (Vincentz, Hannover)
- [37] Lopes da Silva, J. and Coutinho, J. A. P.: "Dynamic rheological analysis of the gelation behaviour of waxy crude oils", Rheol Acta, 2004, 43, 433-441



## **Acknowledgements**

I would like to thank Ao. Univ. Prof. Dr. Martin Gröschl from IAP (TU Wien) as well as Mag. Clemens Zaach, Dipl. Ing. Milan Dardalic, Othmar Neubauer, Wolfgang Hujer and the whole OMV E&P Team in Gänserndorf for their excellent advice and help which made this thesis possible.

Special thanks go to my family and my friends who always supported me during my studies and while working on this thesis.

# Appendix

## A1 Results of the Thermal History Measurements

Pre heat T [°C]	PP cycles									$\bar{x}$	$\sigma_m$	$\sigma$
	1	2	3	4	5	6	7	8	9			
	PP [°C]									[°C]		
25	1.9	1.2	3.0	1.7	2.0	1.9	1.4	2.2	3.5	2.09	0.25	0.74
30	1.3	2.5	3.1	3.4	1.5	2.8	2.7	1.5	1.7	2.28	0.26	0.79
35	3.6	2.3	1.4	3.2	1.2	2.6	2.7	3.7	2.8	2.61	0.29	0.87
40	2.8	3.1	2.7	3.2	3.7	3.4	4.0	3.5	3.3	3.30	0.14	0.41
45	4.3	4.1	4.1	4.3	4.2	3.9	4.4	4.6	4.5	4.27	0.07	0.22
50	4.3	4.8	4.5	4.8	4.8	4.9	4.9	4.8	4.8	4.73	0.07	0.20
55	4.1	5.0	4.5	4.8	5.0	4.8	4.8	4.8	4.6	4.71	0.09	0.28
60	3.5	3.9	4.0	4.2	4.3	4.3	4.4	4.3	4.0	4.10	0.09	0.28
65	3.5	3.7	3.9	3.7	3.7	3.6	3.8	3.7	3.5	3.68	0.04	0.13
70	4.4	4.6	4.7	4.8	4.5	4.7	4.8	4.6	4.6	4.63	0.04	0.13
75	4.8	5.2	5.0	5.0	5.2	5.0	4.9	5.1	5.1	5.03	0.04	0.13
80	5.1	5.1	5.3	5.2	5.3	5.4	5.4	5.2	5.4	5.27	0.04	0.12
85	4.6	5.7	5.9	5.5	5.9	5.8	6.0	6.0	6.1	5.72	0.15	0.46

Tab. A1.1: PP cycles, average value and error for Sp23 at 13 different temperatures

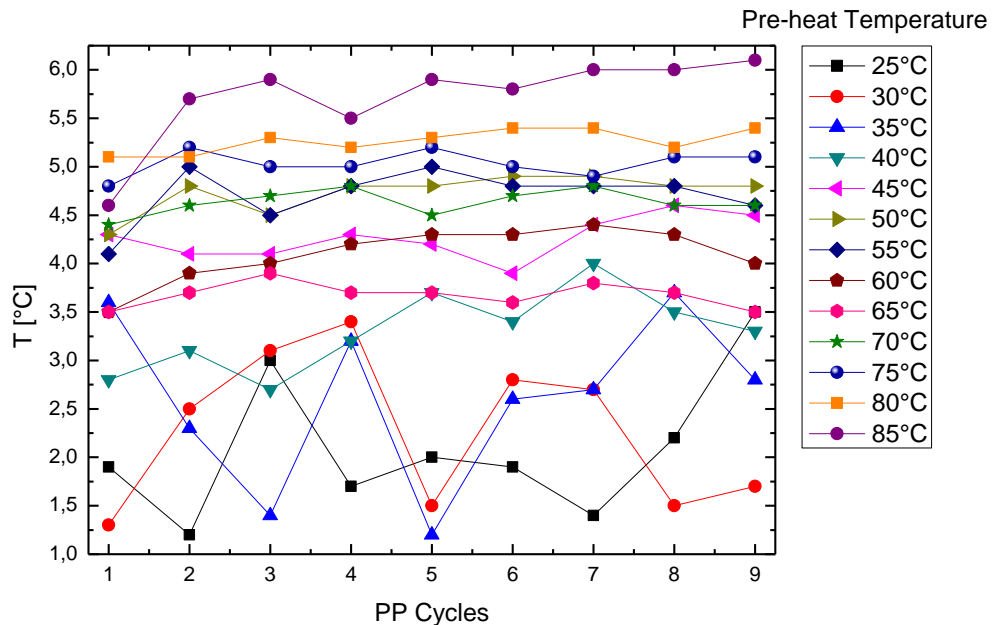


Fig. A1.1: 9 PP cycles at 13 different preheating temperatures of the sample Sp23

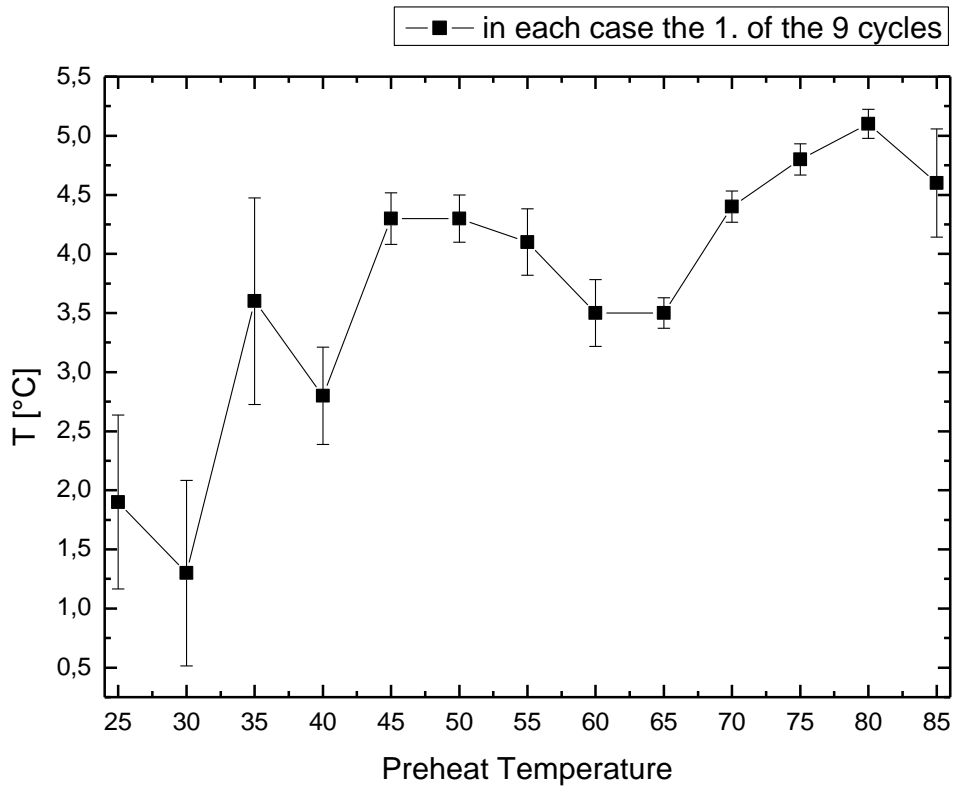


Fig. A1.2: Sp23: the first value of the 9 cycles for each pretreatment temperature with the error of the single measuring values

Pre heat T [°C]	PP cycles									$\bar{x}$	$\sigma_m$	$\sigma$
	1	2	3	4	5	6	7	8	9			
	PP [°C]									[°C]		
25	13.5	13.8	14.0	14.0	14.3	14.4	14.6	14.7	14.8	14.23	0.15	0.44
30	13.8	13.8	14.0	14.0	14.0	13.8	13.9	14.0	14.2	13.94	0.04	0.13
35	14.1	14.4	14.6	14.6	14.8	14.8	15.0	15.2	15.2	14.74	0.12	0.36
40	13.9	14.0	13.8	14.0	13.8	13.8	14.0	14.0	14.1	13.93	0.04	0.11
45	14.1	13.9	13.7	14.2	14.0	13.9	13.9	14.0	13.9	13.96	0.05	0.14
50	14.6	14.4	14.6	14.7	14.9	14.5	14.0	14.0	14.0	14.41	0.11	0.34
55	14.2	14.3	14.8	14.2	14.8	14.6	14.3	15.0	14.6	14.53	0.10	0.30
60	13.9	14.1	14.2	14.3	14.3	14.3	14.3	14.3	14.6	14.26	0.06	0.19
65	13.4	13.6	13.7	14.0	14.0	14.1	14.2	14.5	14.3	13.98	0.12	0.35
70	9.2	9.6	9.8	10.0	10.1	10.3	10.3	10.4	10.6	10.03	0.15	0.44
75	3.2	7.2	7.0	8.3	7.8	7.2	8.3	8.6	8.3	7.32	0.55	1.65
80	8.5	7.1	7.1	8.2	8.6	8.6	8.3	8.5	9.2	8.23	0.23	0.70
85	7.3	7.6	7.4	7.3	8.3	8.9	9.0	8.5	8.1	8.04	0.22	0.67

Tab. A1.2: PP cycles, average value and error for Folesti 2600 at 13 different temperatures

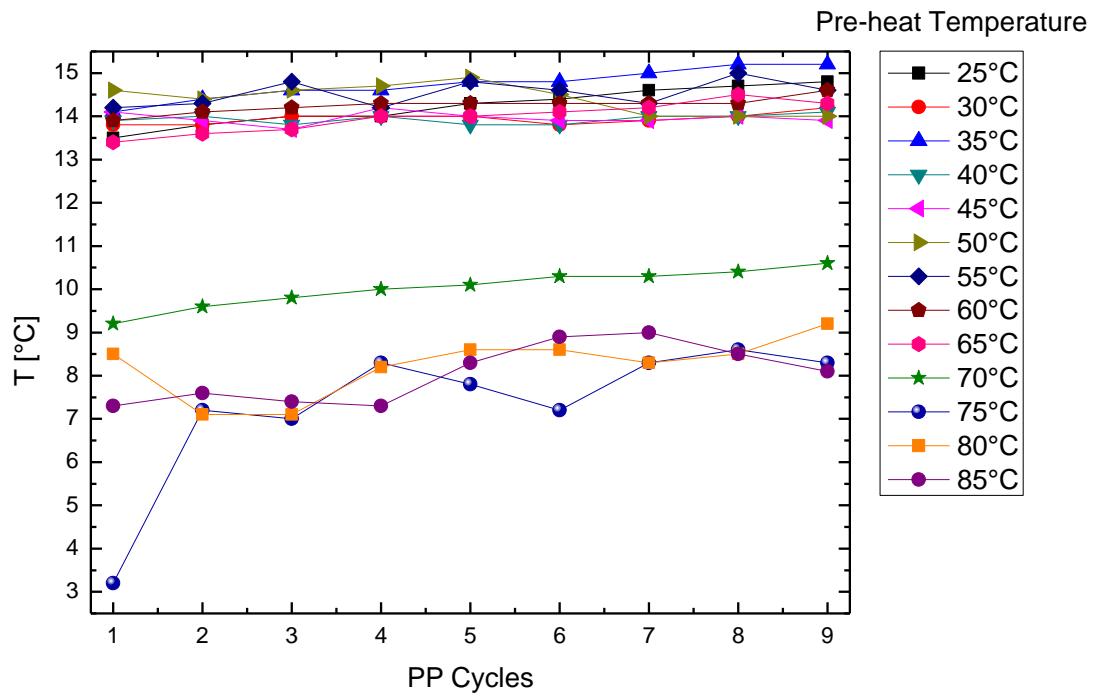


Fig. A1.3: 9 PP cycles at 13 different preheating temperatures of the sample Folesti 2600

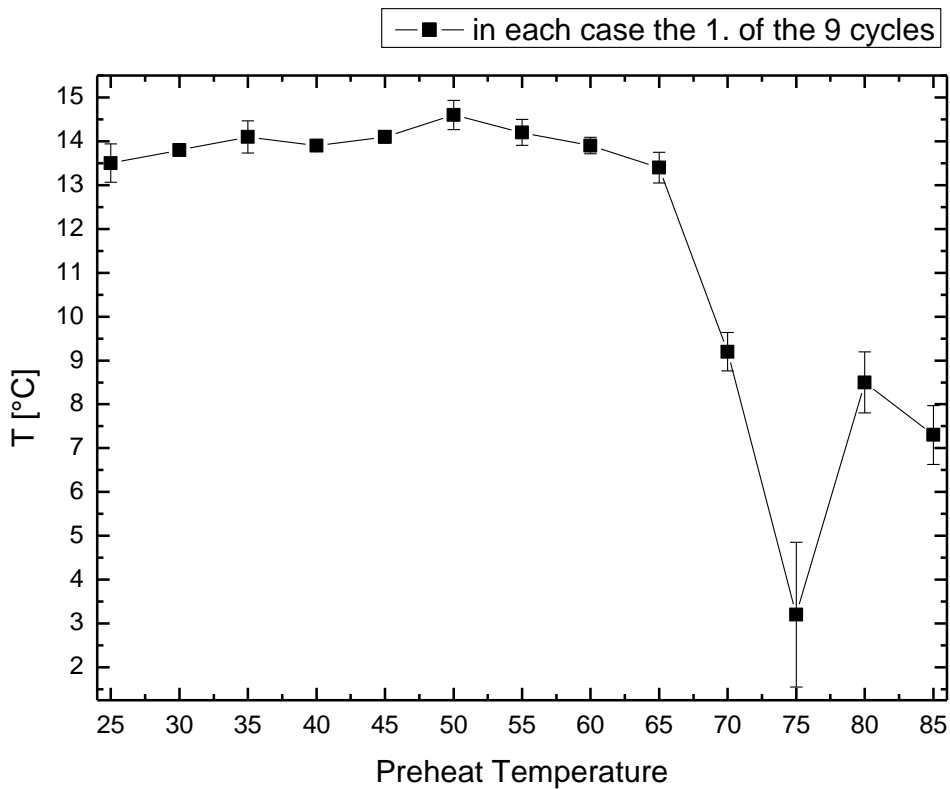


Fig. A1.4: Folesti 2600: the first value of the 9 cycles for each pretreatment temperature with the error of the single measuring values

Pre heat T [°C]	PP cycles									$\bar{x}$	$\sigma_m$	$\sigma$
	1	2	3	4	5	6	7	8	9			
	PP [°C]									[°C]		
25	14.8	16.1	16.4	16.6	16.5	16.6	16.8	17.4	17.0	16.47	0.24	0.73
30	15.4	16.0	16.1	16.3	16.6	16.9	16.7	16.8	16.9	16.41	0.17	0.51
35	15.4	16.2	16.4	17.1	16.7	16.9	16.7	16.8	17.4	16.62	0.19	0.58
40	19.6	18.4	18.1	17.8	17.8	17.4	17.2	17.3	16.9	17.83	0.27	0.81
45	19.4	19.5	19.2	18.7	17.9	17.8	17.8	17.6	17.3	18.36	0.28	0.85
50	20.4	20.2	20.2	20.2	20.1	19.7	19.4	19.5	19.4	19.90	0.13	0.40
55	21.0	20.9	20.9	20.8	20.8	20.9	20.9	20.9	20.7	20.87	0.03	0.09
60	21.2	20.8	20.8	20.9	20.9	20.9	20.9	20.8	20.9	20.90	0.04	0.12
65	19.3	18.7	18.3	18.3	19.6	18.5	19.0	18.7	19.0	18.82	0.15	0.44
70	10.9	13.6	14.7	15.3	16.1	16.3	16.3	15.9	16.1	15.02	0.60	1.79
75	12.8	15.5	16.1	16.0	16.1	15.9	16.0	16.3	16.4	15.68	0.37	1.11
80	15.4	14.9	16.2	15.9	16.1	16.4	16.3	16.5	16.4	16.01	0.18	0.53
85	15.4	16.0	16.3	16.6	16.8	16.5	16.8	16.7	17.0	16.46	0.17	0.50

Tab. A1.3: PP cycles, average value and error for Pecica 652 at 13 different temperatures

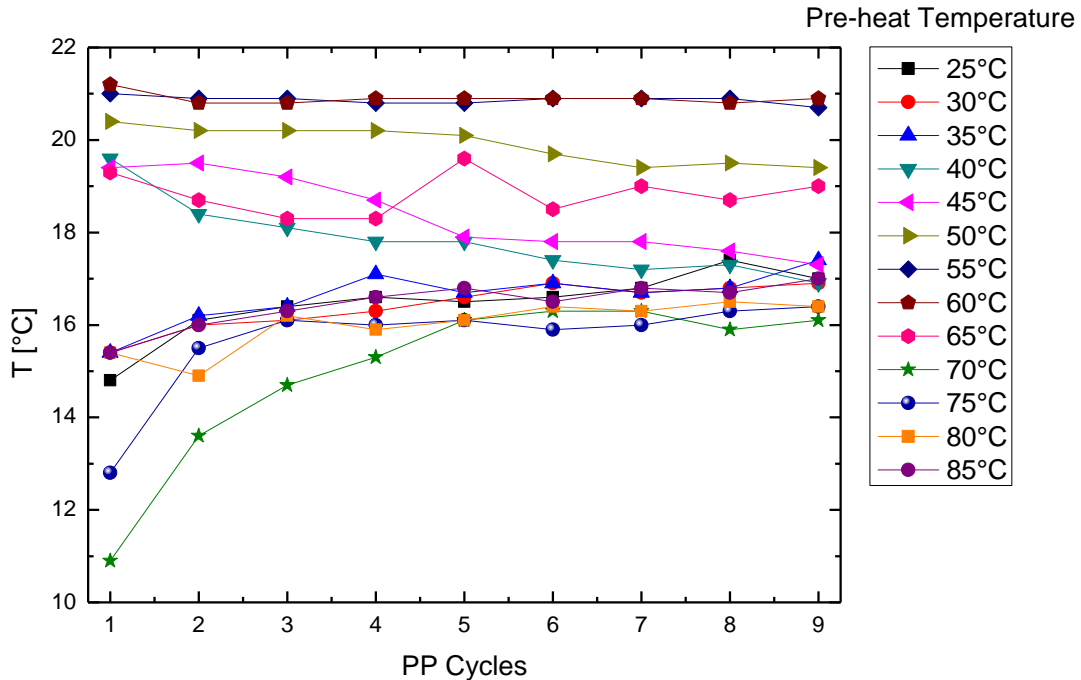
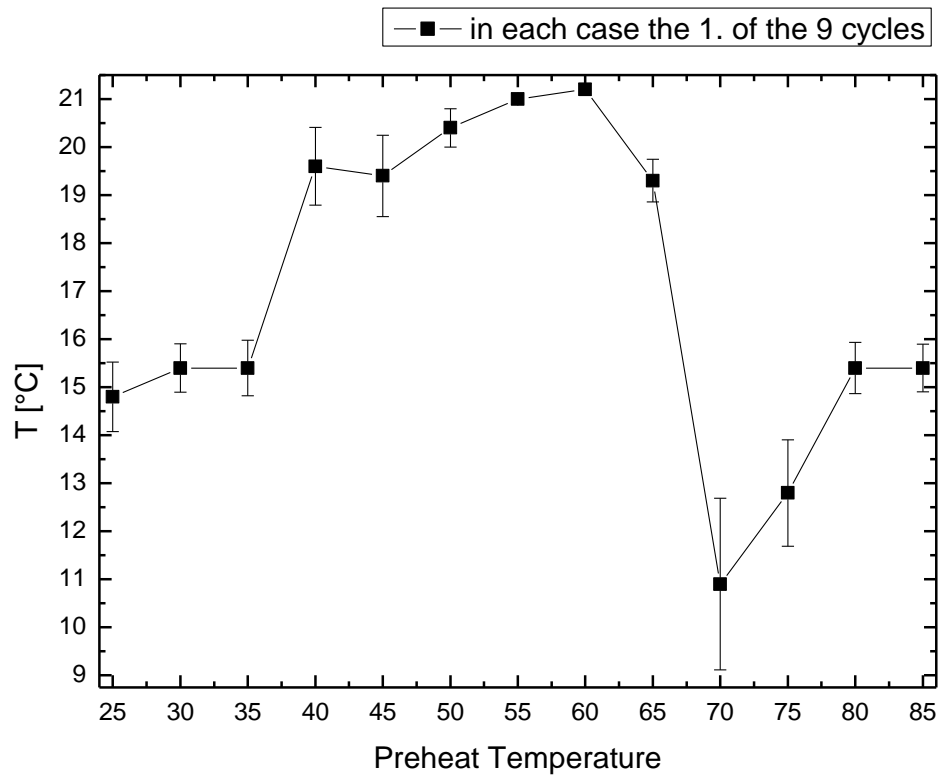
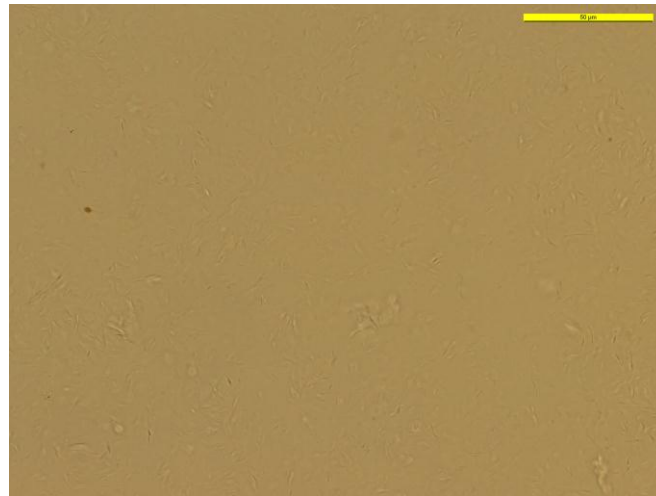


Fig. A1.5: 9 PP cycles at 13 different preheating temperatures of the sample Pecica 652

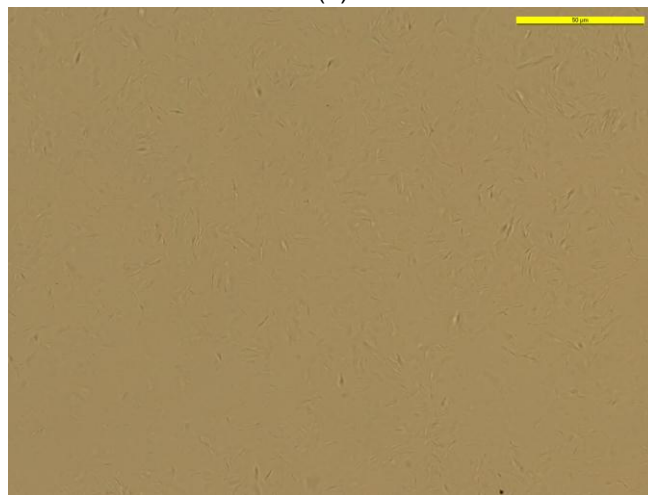


**Fig. A1.6:** *Pecica 652: the first value of the 9 cycles for each pretreatment temperature with the error of the single measuring values*

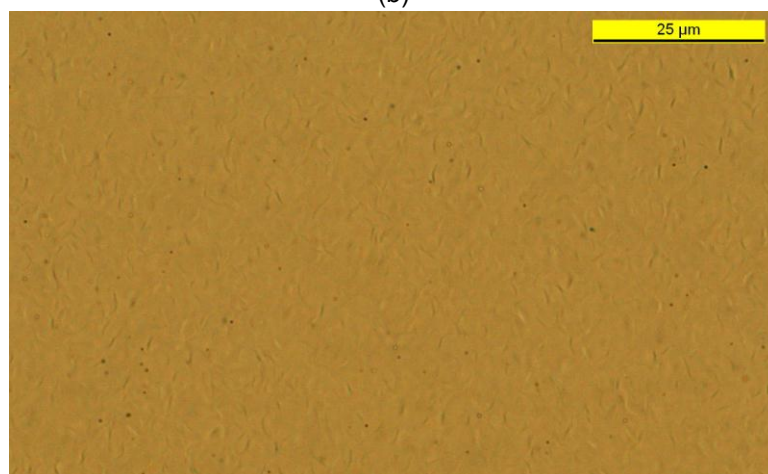
## A2 Transmission Microscope Photographs



(a)

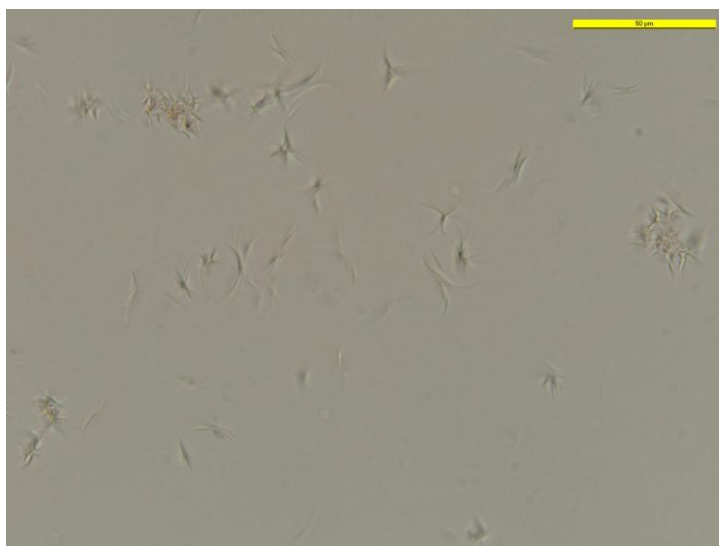


(b)

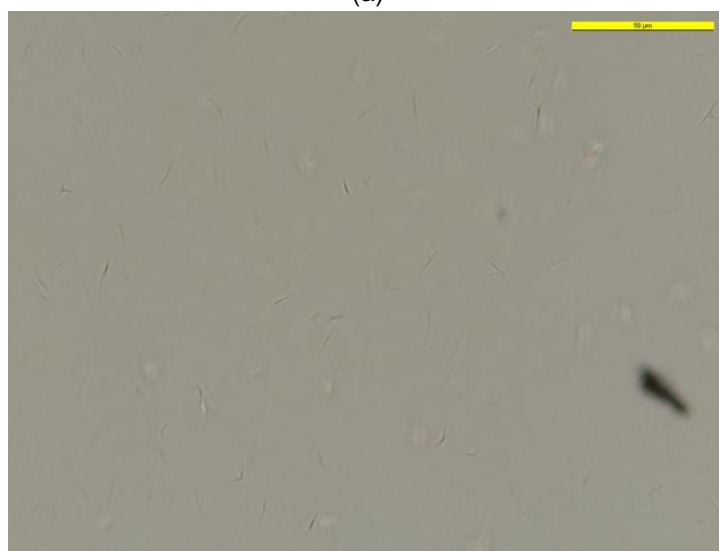


(c)

**Fig. A2.1:** *Folesti 2600 cooled before viewed under the microscope: (a) and (b) without pretreatment, needle-shaped crystals, yellow bar scales 50 μm; (c) preheated to 55 °C, bent rods, yellow bar scales 25 μm*



(a)



(b)

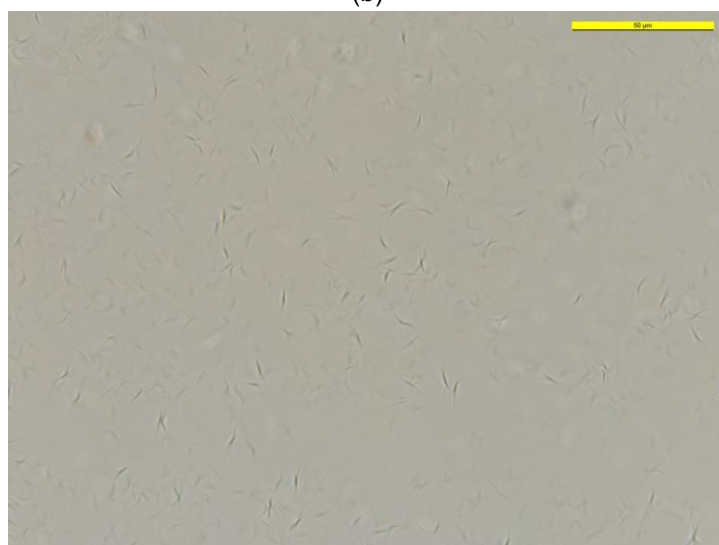


**Fig. A2.2:** *Sp23 cooled before viewed under the microscope, the yellow bars in all three photographs scale 50  $\mu\text{m}$ , needle-shaped crystals in all three pictures, (a) without pretreatment; (b) preheated to 55  $^{\circ}\text{C}$ ; (c) preheated to 85  $^{\circ}\text{C}$*



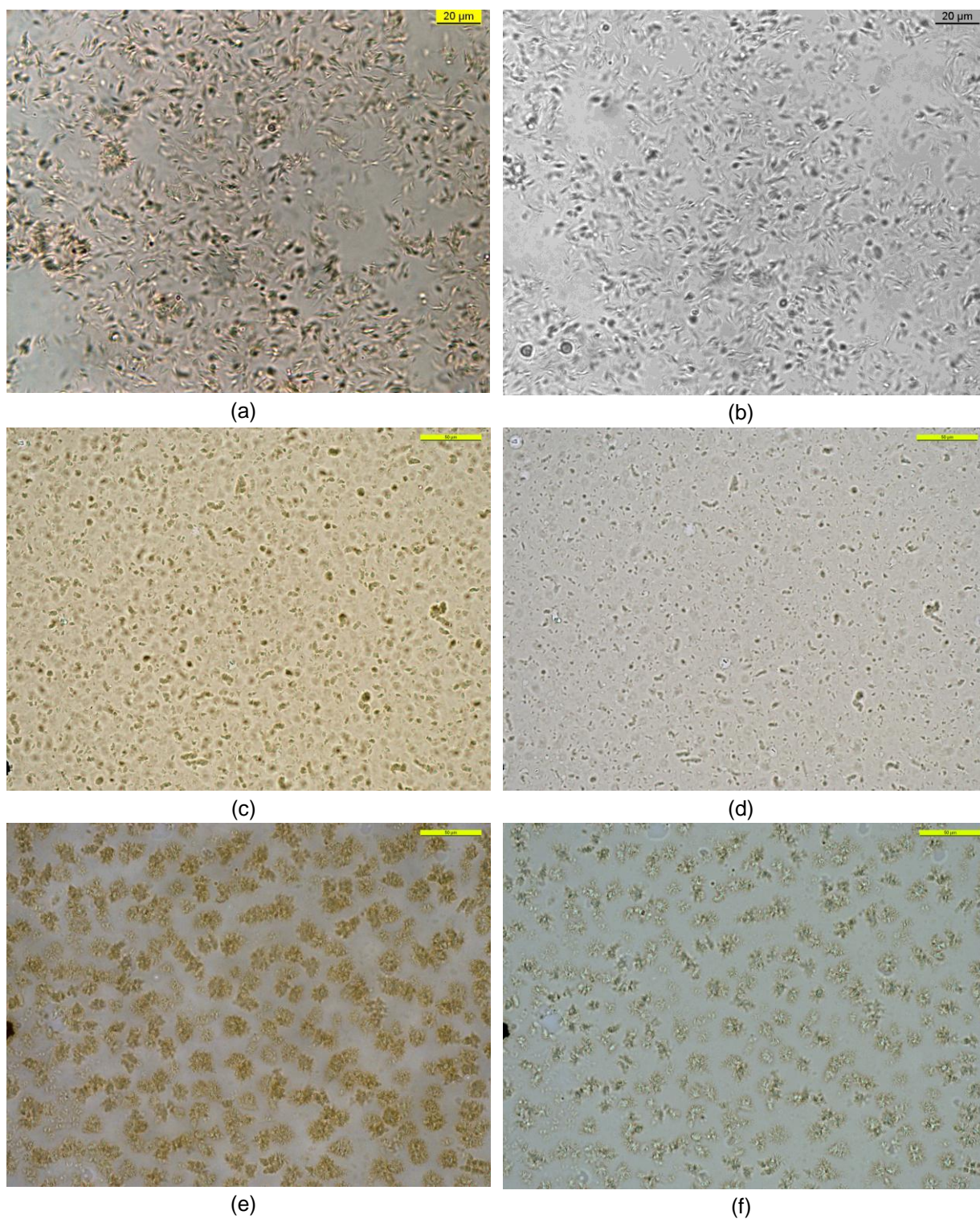


**Fig. A2.3:** *Pecica 652* cooled before viewed under the microscope, the photographs on the right side were always taken a few minutes later than the left ones; (a) and (b) without heat pretreatment, bars scale 20  $\mu\text{m}$ , needle-shaped crystals; (c) and (d) preheated to 55  $^{\circ}\text{C}$ , yellow bars scale 50  $\mu\text{m}$ , spherical and rod-shaped crystals; (e) and (f) preheated to 85  $^{\circ}\text{C}$ , yellow bars scale 50  $\mu\text{m}$ , spherical agglomerations consisting of hook-shaped crystals

### A3 Scanning Electron Microscope Pictures

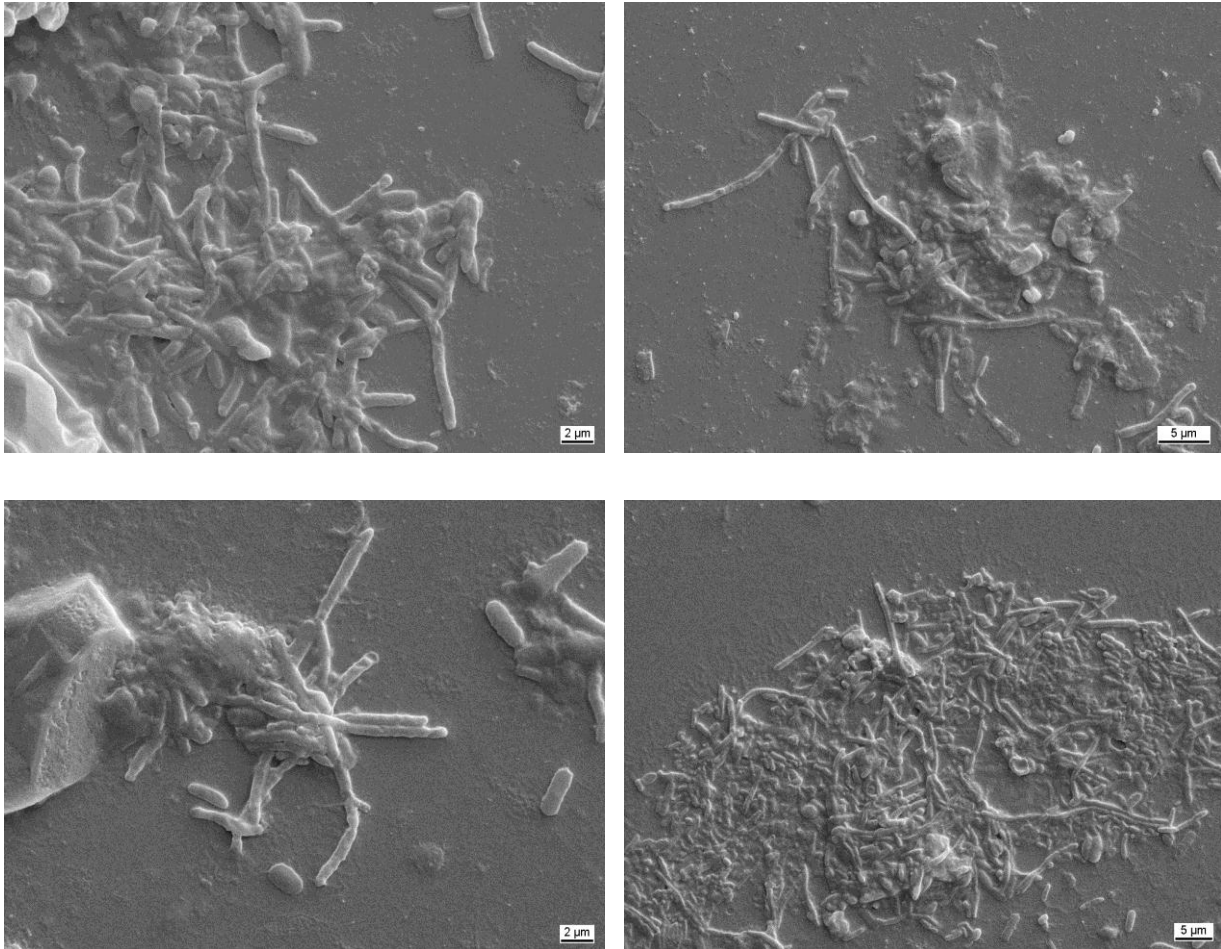


**Fig. A3.1:** *Pecica 652 without thermal pretreatment, accumulations of needle-shaped paraffin crystals and paraffin covered NaCl crystals*

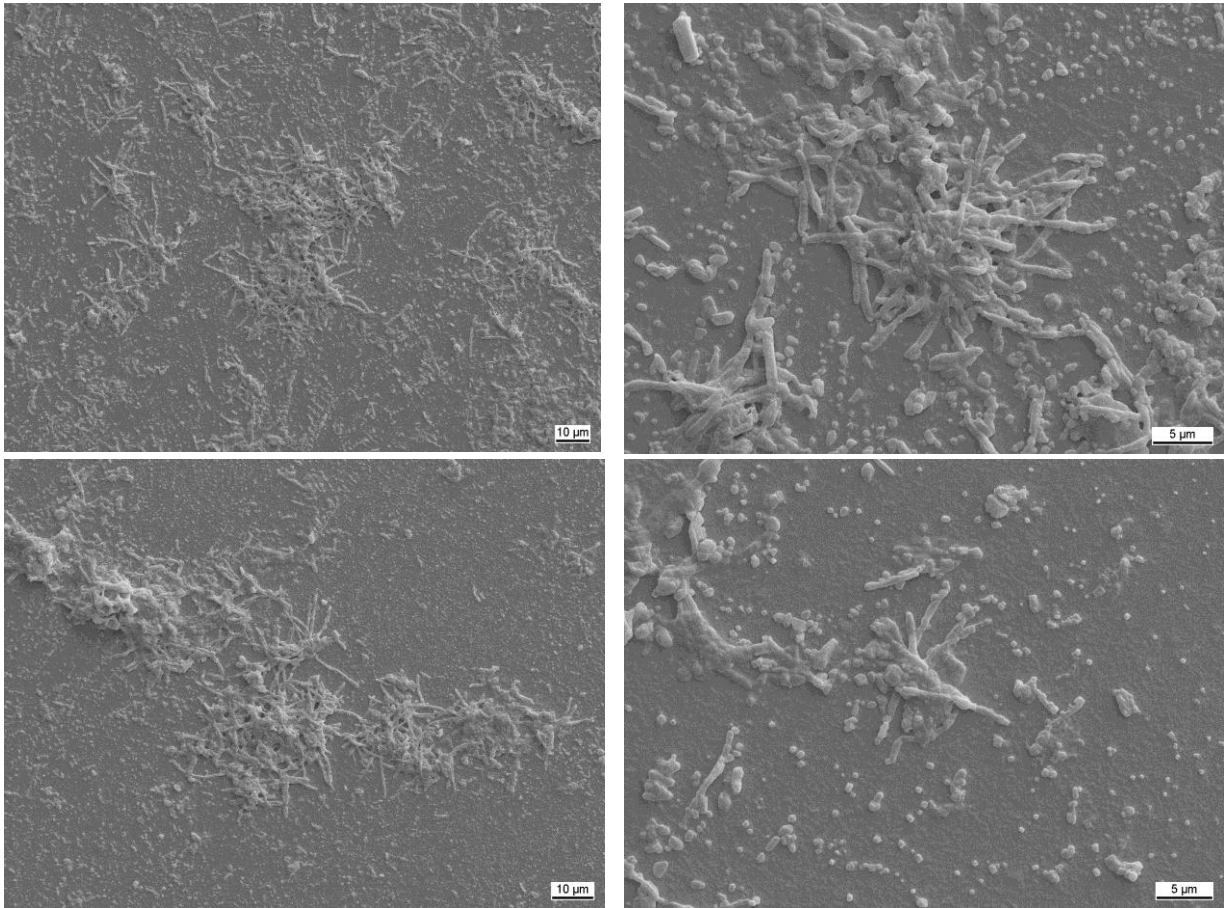


**Fig. A3.2:** *Pecica 652 preheated to 55 °C, accumulations of needle-shaped paraffin crystals and paraffin covered NaCl crystals*



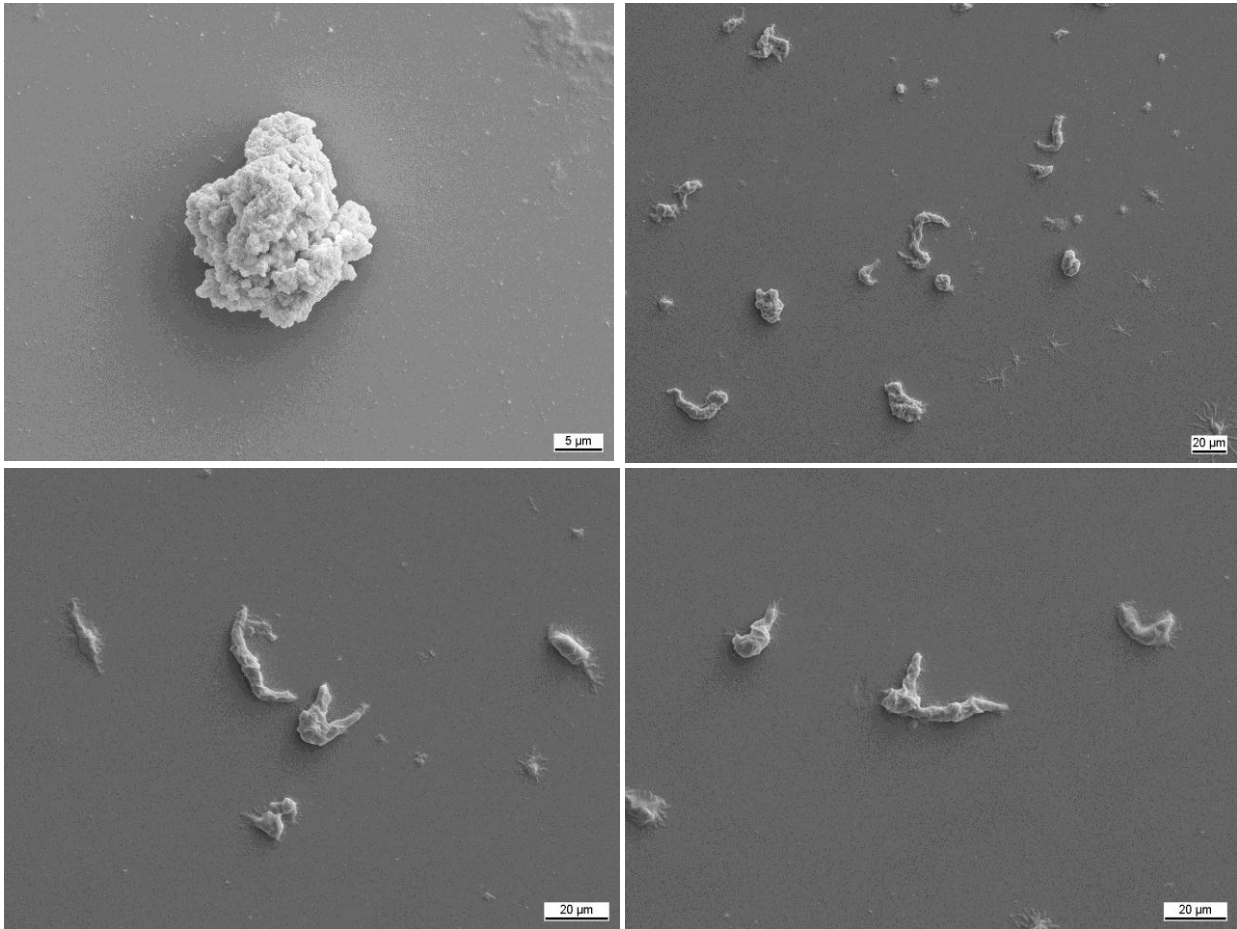
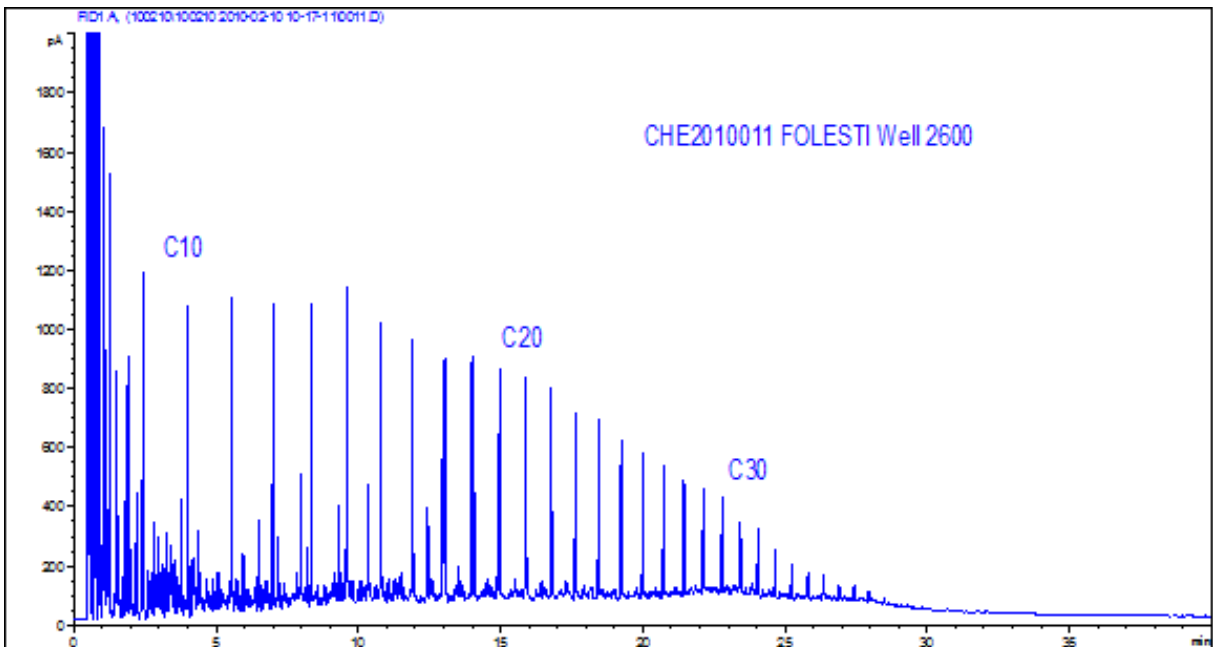
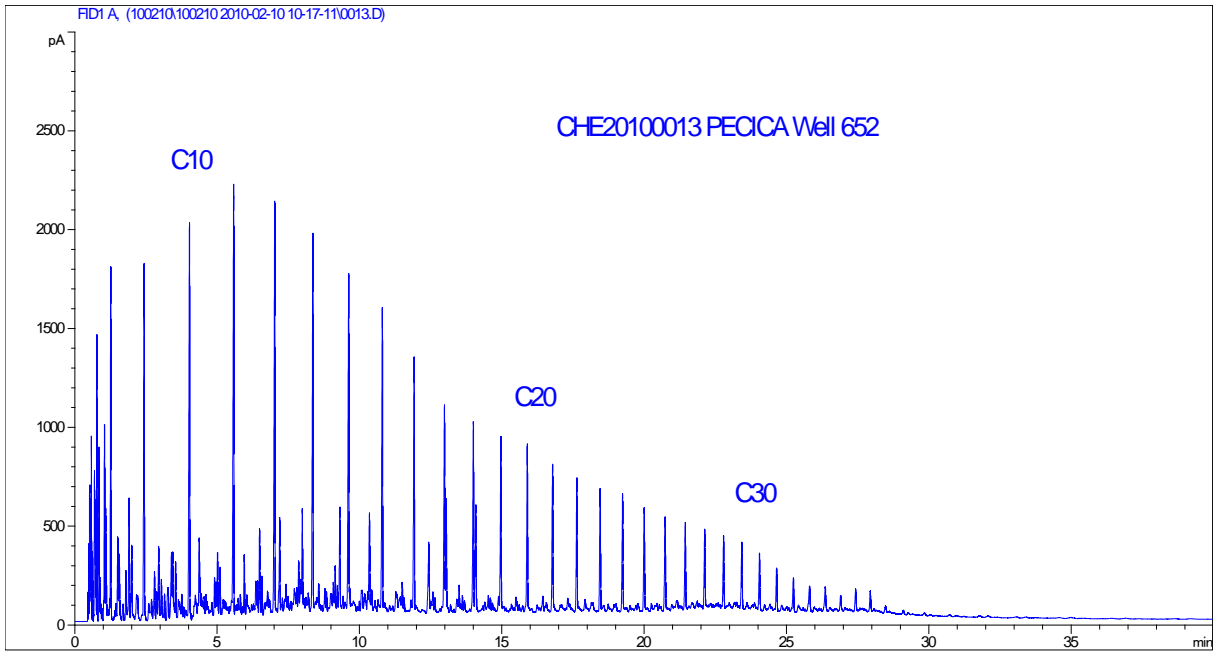
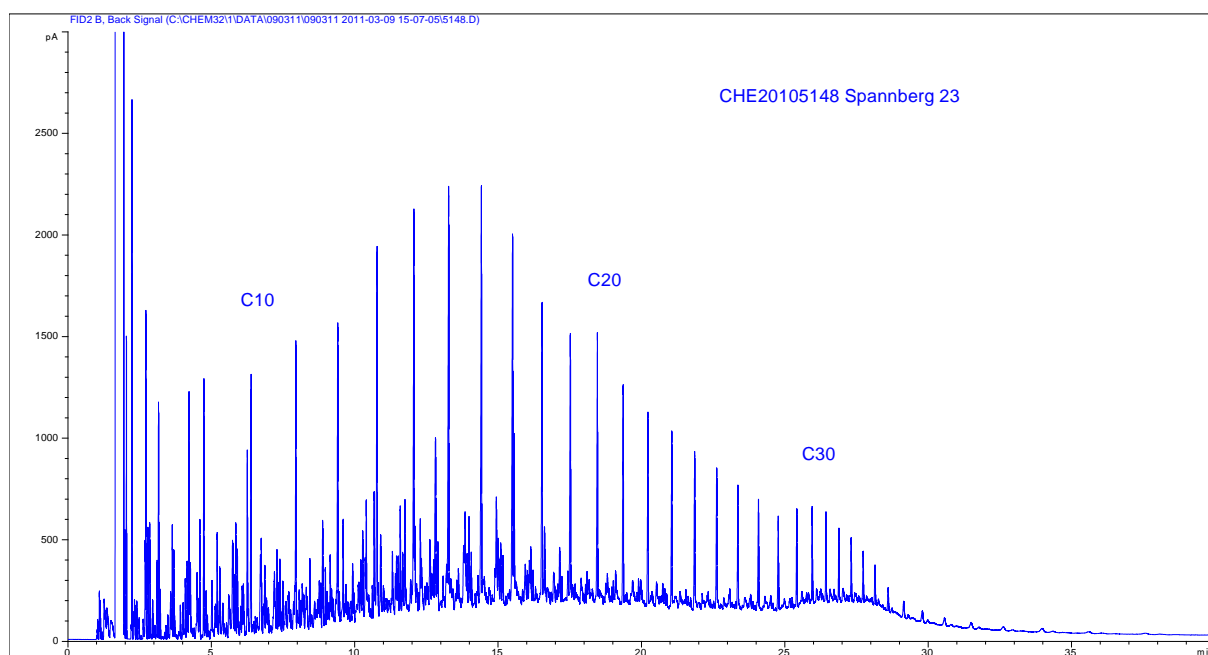
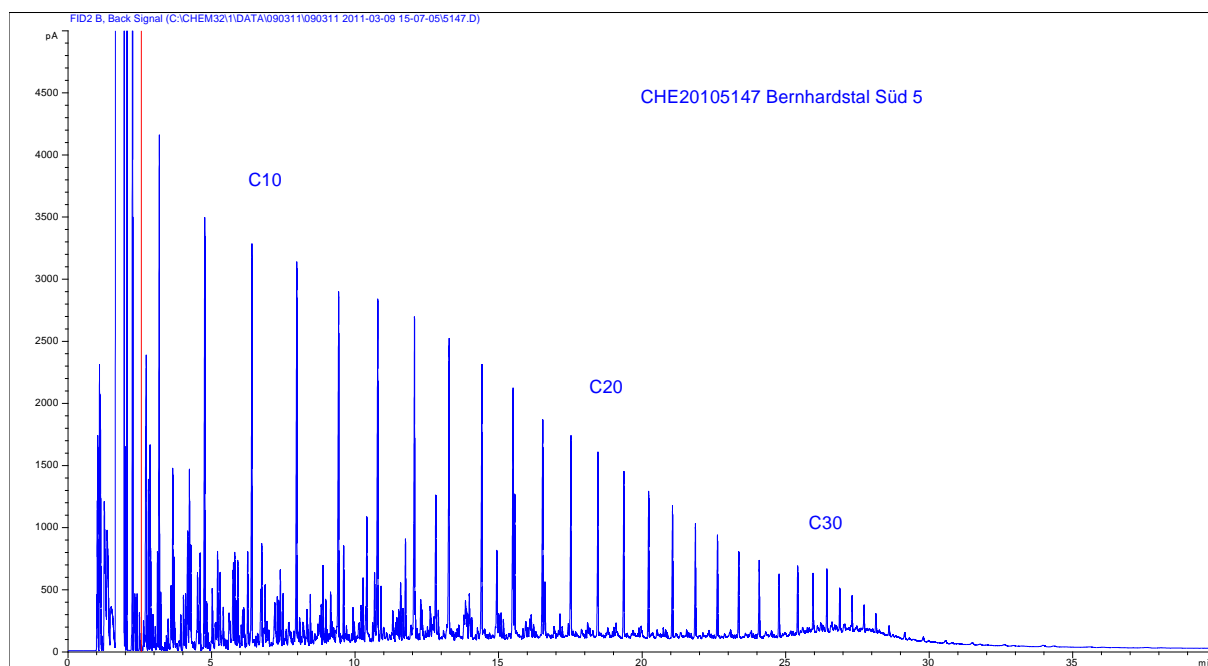


**Fig. A3.3:** *Pecica 652* preheated to 85 °C, accumulations of hook-shaped paraffin crystals and a paraffin covered NaCl crystal

## A4 Gas Chromatography Diagrams



# Appendix



## A5 Data Sheet Rheometer

### 9 Technical Specifications

## 9 Technical Specifications

### 9.1 Measuring Drive

Drive principle	permanent magnet synchronous drive
Minimum torque	0.1 $\mu\text{Nm}$ (Physica MCR 301 / 501) (0.02 $\mu\text{Nm}$ with DSO) 0.5 $\mu\text{Nm}$ (Physica MCR 101 / Smartpave) 250 $\mu\text{Nm}$ (Physica MCR 51)
Maximum torque	125 mNm (Physica MCR 51 / 101 / Smartpave) 200 mNm (Physica MCR 301) 230 mNm (Physica MCR 501)
Torque resolution	< 0.1 $\mu\text{Nm}$ (Physica MCR 51) 0.002 $\mu\text{Nm}$ (Physica MCR 101 / Smartpave) 0.001 $\mu\text{Nm}$ (Physica MCR 301 and 501)
Torque accuracy	max. ( 0.2 $\mu\text{Nm}$ ; 0.5%)
Maximum rise of torque	1500 Nm/s
Speed range CSS	$10^{-6} \text{ min}^{-1}$ - 3000 $\text{min}^{-1}$ (Physica MCR 51) $10^{-6} \text{ min}^{-1}$ - 3000 $\text{min}^{-1}$ (Physica MCR 101) $10^{-7} \text{ min}^{-1}$ - 3000 $\text{min}^{-1}$ (Physica MCR 301 and 501)
Speed range CSR	$10^{-3} \text{ min}^{-1}$ - 3000 $\text{min}^{-1}$ (Physica MCR 51) $10^{-4} \text{ min}^{-1}$ - 3000 $\text{min}^{-1}$ (Physica MCR 101 / Smartpave) $10^{-6} \text{ min}^{-1}$ - 3000 $\text{min}^{-1}$ (Physica MCR 301 / 501)
Typical adjustment time:	to a speed of 1000 $\text{min}^{-1}$ : 150 ms to an angle of 20 mrad: 200 ms
Frequency range	$10^{-4} \text{ Hz}$ -100 Hz $10^{-6} \text{ Hz}$ -100 Hz

### 9.2 Encoder

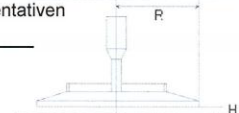
Measuring principle	optical incremental encoder
Internal digital resolution	0.012 $\mu\text{rad}$ (no oversampling)
Real resolution	< 1 $\mu\text{rad}$ within the range of measurement accuracy

# A6 Data Sheet Measuring System PP50

## Measuring System Data Sheet Messsystem-Datenblatt PP50



Geometry Data	Geometrie-Daten	Unit
Serialnumber	Seriennummer	18362
Plate-Diameter, external, D	Plattendurchmesser, außen, D	49.965 mm

Parallel & Plate measuring system	Platte-Platte Messsystem	
This calculation refers to the plate radius $R_{\max}$ according to DIN53018	Diese Berechnung bezieht sich auf den Außenradius $R_{\max}$ nach DIN53018	$1 \text{ rad} = \frac{360^\circ}{2\pi}$ $\omega = 2\pi \cdot n$
$\dot{\gamma}_{\max} = \frac{\omega \cdot R}{H}$	$\tau_{\max} = \frac{2 \cdot M}{\pi \cdot R^3}$	$\gamma_{\max} = \frac{R \cdot \varphi}{H}$
Calculation based on the representative shear rate and shear stress	Berechnungen basierend auf der repräsentativen Scherrate und Schubspannung	
$\dot{\gamma}_{\text{rep}} = \frac{2}{3} \cdot \frac{\omega \cdot R}{H}$	$\tau_{\text{rep}} = \frac{4}{3} \cdot \frac{M}{\pi \cdot R^3}$	$\gamma_{\text{rep}} = \frac{2}{3} \cdot \frac{R \cdot \varphi}{H}$

Variable	Variable	SI-Unit
$\tau$ ...shear stress	$\tau$ ...Schubspannung	Pa
M...torque	M...Moment	Nm
$\gamma$ ...strain	$\gamma$ ...Deformation	1
$\varphi$ ...deflection angle	$\varphi$ ...Auslenkwinkel	rad
$\dot{\gamma}$ ...shear rate	$\dot{\gamma}$ ...Scherrate	$\text{s}^{-1}$
n...speed	n...Geschwindigkeit	$\text{s}^{-1}$
H...gap	H...Spalt	m
R...plate radius	R...Plattenradius	m
$\omega$ ...angular velocity	$\omega$ ...Winkelgeschwindigkeit	rad/s

Dimensions	Abmessungen	Unit
Plate, Radius	Platte, Radius	24.983 mm
Gap, Standard	Spalt, Standard	1.000 mm

Geometry Data	Geometriedaten	Unit
Appr. Sample Volume, at 1mm gap	Probenmenge, circa, bei 1mm Spalt	1.96 ml
Active Length	Aktive Länge	100.0 mm
Positioning Length	Positionierungslänge	100.0 mm

Conversion Factors, max	Umrechnungsfaktoren, max	Unit
Conversion Factor $C_{SS,\max}^{(1)}$	Umrechnungsfaktor $C_{SS,\max}^{(1)}$	40.8293 Pa / mNm
Conversion Factor $C_{SR,\max}^{(1)}$	Umrechnungsfaktor $C_{SR,\max}^{(1)}$	2.6162 $\text{s}^{-1}$ / $\text{min}^{-1}$

(1) calculated according to DIN53018

(1) method used for Toolmaster

(1) berechnet nach DIN53018

(1) Methode verwendet für den Toolmaster

Representative Conversion Factors	Repräsentative Umrechnungsfaktoren	Unit
Conversion Factor $C_{SS,\text{rep}}^{(2)}$	Umrechnungsfaktor $C_{SS,\text{rep}}^{(2)}$	27.2196 Pa / mNm
Conversion Factor $C_{SR,\text{rep}}^{(2)}$	Umrechnungsfaktor $C_{SR,\text{rep}}^{(2)}$	1.7441 $\text{s}^{-1}$ / $\text{min}^{-1}$

(2) calculated representative factors

(2) alternative method comparable to cone-plate

(2) berechnete Repräsentativwerte

(2) alternative Methode vergleichbar mit Kegel-Platte



## Measuring System Data Sheet

### Messsystem-Datenblatt

#### PP50



...Additional Data	...Zusätzliche Daten	Unit
Conversion Factor $C_{SD}$	Umrechnungsfaktor $C_{SD}$	2.498 % / mrad
Conversion Factor $C_{SD}$ [SI-Unit]	Umrechnungsfaktor $C_{SD}$ [SI-Einheit]	24.98 1 / rad
Conversion Factor $C_{SS}$ [SI-Unit]	Umrechnungsfaktor $C_{SS}$ [SI-Einheit]	40829.35 Pa / Nm
Conversion Factor $C_{SR}$ [SI-Unit]	Umrechnungsfaktor $C_{SR}$ [SI-Einheit]	156.97 s <sup>-1</sup> / s <sup>-1</sup>
-> calculated values according to (1)		
-> berechnete Werte nach (1)		
Conversion Factor $C_{SS}$ [SI-Unit]	Umrechnungsfaktor $C_{SS}$ [SI-Einheit]	27219.56 Pa / Nm
Conversion Factor $C_{SR}$ [SI-Unit]	Umrechnungsfaktor $C_{SR}$ [SI-Einheit]	104.65 s <sup>-1</sup> / s <sup>-1</sup>
-> calculated values according to (2)		
-> berechnete Werte nach (2)		

Calculation / Conversion Factors	Berechnung / Umrechnungsfaktoren
$C_{SS}$	$\tau = C_{SS} \cdot M$
$C_{SD}$	$\gamma = C_{SD} \cdot \varphi$
$C_{SR}$	$\dot{\gamma} = C_{SR} \cdot \dot{n}$

Remark	Bemerkung
Standard Parallel Plate	Standard Platte-Platte

ISO 6721-10	ISO 6721-10
<u>International Standards:</u> The PP geometry complies with the international standard <b>ISO6721-10</b> if used in combination with a MCR series rheometer MCR10x,30x,50x and an actively heated oven, e.g. - CTDxxx - P-ETDxxx+H-ETDxxx - P-PTDxxx+H-PTDxxx	<u>Internationale Standards:</u> Die PP Geometrie in Kombination mit einem MCR Serien Rheometer MCR10x,30x,50x und einer aktiven Heizung, z.B. - CTDxxx - P-ETDxxx+H-ETDxxx - P-PTDxxx+H-PTDxxx ist kompatibel mit dem internationalen Standard <b>ISO6721-10</b> .

© Anton Paar Germany GmbH - Änderungen vorbehalten / subject to alteration  
D-73760 Ostfildern, Helmuth-Hirth-Str. 6  
Tel: +49 (0)711 720 91-0, E-mail: info.de@anton-paar.com